DISTRIBUTED SPACE-TIME BLOCK CODES IN WIRELESS COOPERATIVE NETWORKS

by

Zhihang Yi

A thesis submitted to the
Department of Electrical and Computer Engineering
in conformity with the requirements for
the degree of Doctor of Philosophy

Queen's University
Kingston, Ontario, Canada
June 2009

Abstract

In cooperative networks, relays cooperate and form a distributed multi-antenna system to provide spatial diversity. In order to achieve high bandwidth efficiency, distributed space-time block codes (DSTBCs) are proposed and have been studied extensively. Among all DSTBCs, this thesis focuses on the codes which are single-symbol maximum likelihood (ML) decodable and can achieve the full diversity order.

This thesis presents four works on single-symbol ML decodable DSTBCs. The first work proposes the row-monomial distributed orthogonal space-time block codes (DOSTBCs). We find an upper bound of the data-rate of the row-monomial DOSTBC and construct the codes achieving this upper bound. In the second work, we first study the general DOSTBCs and derive an upper bound of the data-rate of the DOSTBC. Secondly, we propose the row-monomial DOSTBCs with channel phase information (DOSTBCs-CPI) and derive an upper bound of the data-rate of those codes. Furthermore, we find the actual row-monomial DOSTBCs-CPI which achieve the upper bound of the data-rate.

In the third and fourth works of this thesis, we focus on error performance analysis of single-symbol ML decodable DSTBCs. Specifically, we study the distributed Alamouti's code in dissimilar cooperative networks. In the third work, we assume that the relays are blind relays and we derive two very accurate approximate bit error rate (BER) expressions

of the distributed Alamouti's code. In the fourth work, we assume that the relays are CSI-assisted relays. When those CSI-assisted relays adopt the amplifying coefficients that was proposed in [33] and widely used in many previous publications, upper and lower bounds of the BER of the distributed Alamouti's code are derived. Very surprisingly, the lower bound indicates that the code cannot achieve the full diversity order when the CSI-assisted relays adopt the amplifying coefficients proposed in [33]. Therefore, we propose a new threshold-based amplifying coefficient and it makes the code achieve the full diversity order two. Moreover, three optimum and one suboptimum schemes are developed to calculate the threshold used in this new amplifying coefficient.

Acknowledgments

I would like to express my gratitude to my supervisor, Dr. Il-Min Kim, who has helped me reach many academic milestones and prepared me to reach many more. I want to thank him for his expertise, insights, and inspiration. I have also benefited tremendously from his enthusiasm, understanding, and patience.

I would also like to thank the other members of my committee, Dr. Jinho Choi from Swansea University, Dr. Steven D. Blostein, Dr. Fady Alajaji, Dr. Mohamed Ibnkahla, and Dr. Thomas J. Harris for their insightful comments and for contributing their broad perspectives to this thesis.

Of my many colleagues and friends, I want to thank my lab colleagues, MinChul Ju, Vincent Perreira, and Mamoun Markawi, for all the technical and non-technical discussions. Thanks also go to my dear friends, Neng Wang, Minhua Ding, Zheng Chen, Liang Wei, Yu Cao, and Wei Sheng, for their help, friendship, and all the wonderful time we share.

I would especially like to thank my mother, Xiaorong Fu, and my father, Guangmo Yi, for their support, understanding, and love, which mean much more than I can express. As their only child, I regret that I can not be with them for most of the time. The only thing I can do is to work harder and make them feel proud of me.

Contents

List of Figures

Acronyms

AF	Amplify-and-Forward
BER	Bit Error Rate
CDF	Cumulative Distribution Function
CPI	Channel Phase Information
CRC	Cyclic Redundancy Check
CSI	Channel State Information
DF	Decode-and-Forward
DOSTBC	Distributed Orthogonal Space-Time Block Code
DSTBC	Distributed Space-Time Block Code
MGF	Moment Generating Function
ML	Maximum Likelihood
PEP	Pairwise Error Probability
PDF	Probability Density Function
PSK	Phase Shift Keying
QAM	Quadrature Amplitude Modulation
SER	Symbol Error Rate
SISO	Single Input Single Output
SIMO	Single Input Multiple Output
SNR	Signal-to-Noise Ratio

STBC	Space-Time Block Code

List of Important Symbols

K	Number of relays
N	Number of information-bearing symbols
T	Number of times slots used by the relays
M	Size of constellation
P_b	Average bit error rate
h_k	Fading coefficient of the channel from the source to the k-th relay
f_k	Fading coefficient of the channel from the k-th relay to the destination
ρ_k	Amplifying coefficient at the k-th relay
$\boldsymbol{R}$	Covariance matrix of the noises at the destination
$\mathscr{R}$	Data-rate of a distributed space-time code
Ω_x	Variance of a random variable x
$\boldsymbol{X}$	Code matrix of distributed space-time block code
ϕ	Null set
E_s	Transmission power of the source
E_{rk}	Transmission power of the k-th relay
$\mathscr{CN}(0,1)$	Circularly symmetric complex Gaussian distribution with zero mean and unit variance
$\mathscr{M}(s)$	Moment generating function
$\mathrm{diag}[x_1,\cdots,x_k]$	$k \times k$ diagonal matrix with $x_1,\cdots,x_k$ on its main diagonal

$\boldsymbol{0}_{k_1 \times k_2}$	$k_1 \times k_2$ all-zero matrix
$\boldsymbol{I}_{k \times k}$	$k \times k$ identity matrix
$\boldsymbol{X}(:, k_1 : k_2)$	Matrix formed by the $k_1, \cdots, k_2$ columns of $\boldsymbol{X}$
$[\cdot]_k$	k-th entry of a vector
$[\cdot]_{k_1,k_2}$	(k_1, k_2)-th entry of a matrix
$(\cdot)^*$	Complex conjugate
$(\cdot)^H$	Hermitian
$(\cdot)^T$	Transpose
$\lvert \cdot \rvert$	Absolute value of a complex number
$\lceil \cdot \rceil$	Ceiling function
$\lfloor \cdot \rfloor$	Floor function
$\mathrm{mod}(\cdot, \cdot)$	Modulo operation
$\Re\{\cdot\}$	Real part of a complex number
$\lambda_{\max}(\cdot)$	Largest eigenvalue of a matrix
$d(\cdot)$	Spectral radius of a matrix
$I(\cdot, \cdot)$	Mutual information
$(\cdot)^{-1}$	Matrix inverse
$\det(\cdot)$	Determinant of a matrix
$\mathrm{rank}(\cdot)$	Rank of a matrix
$Q(\cdot)$	Q-function
$\mathbb{E}[\cdot]$	Expectation of a random variable
$\mathscr{C}(\cdot, \cdot)$	Correlation coefficient of two random variables
$\mathscr{O}(\cdot)$	Asymptotic notation
$\mathrm{Cov}(\cdot, \cdot)$	Covariance of two random variables
$\mathrm{Var}(\cdot)$	Variance of a random variable

$\mathrm{Ei}(\cdot)$	Exponential integral function
$\mathrm{Pr}(\cdot)$	Probability of an event
$\bigtriangledown(\cdot)$	Gradient of a function
$\doteq$	Asymptotic exponential equality
$\dot{\geq}$	Asymptotic exponential inequality

Chapter 1

Introduction

1.1 Introduction

1.1.1 Cooperative Networks

Radio-wave propagation through wireless channels is a complicated phenomenon characterized by various effects, such as multipath, fading, and shadowing. Due to the irregularities of ground and typical wave propagation phenomena such as diffraction, scattering, and reflection, when a signal is transmitted over wireless channels, it arrives at the receiver along a number of distinct paths, a phenomenon referred to as multipath. These paths have distinct and time-varying amplitudes, phases, and direction of arrivals and they add up constructively or destructively at the receiver. These variations are collectively referred to as *fading*. Fading is one of the major impairments of wireless channels and it is usually seen as an obstacle to reliable data transmission. Considerable efforts have been devoted to combat fading and guarantee the quality of service over wireless channels.

One effective method to mitigate fading is to implement *diversity* techniques in wireless communication systems. The fundamental idea of diversity techniques is to transmit multiple independent replicas of the same information-bearing symbols to the receiver. By

doing so, the probability that all the replicas suffer severe fading simultaneously is reduced considerably. There are several ways in which one implement diversity techniques. For example, one can employ *frequency diversity* by transmitting the same symbols on multiple carriers [30] or employ *time diversity* by transmitting the same symbols at multiple time slots [9].

More attentions are given to *spatial diversity* [17,18,57,62]. Spatial diversity is achieved by transmitting the same information-bearing symbols by multiple antennas, which can be deployed at the transmitter, or the receiver, or both ends. As an example, we consider uncoded binary phase shift keying (PSK) signals over a single-input single output (SISO) system and over a single-input multiple-output system (SIMO). For the SISO system, it is well-known that the average symbol error rate (SER) P_s at the high average signal-to-noise ratio (SNR) range is approximated by [42]

$$P_s \approx \frac{1}{E}, \tag{1.1}$$

where E is the transmission power. In contrast, for a SIMO system which has K receiving antennas and uses maximum ratio combining to detect the signals, the average SER becomes

$$P_s \approx \frac{1}{E^K}, \tag{1.2}$$

We observe that, by employing extra receiving antennas, the average SER decays with the transmission power at a faster speed. Since the performance gain at the high SNR range is dictated by the exponent of the transmission power in the average SER expression, the exponent is called the *diversity order.*

In order to achieve spatial diversity in multiple antenna systems, the antennas need to be spaced sufficiently far apart. Usually, a separation of a few wavelengths is required between two antennas in order to ensure that the symbols fade independently [42]. However, in

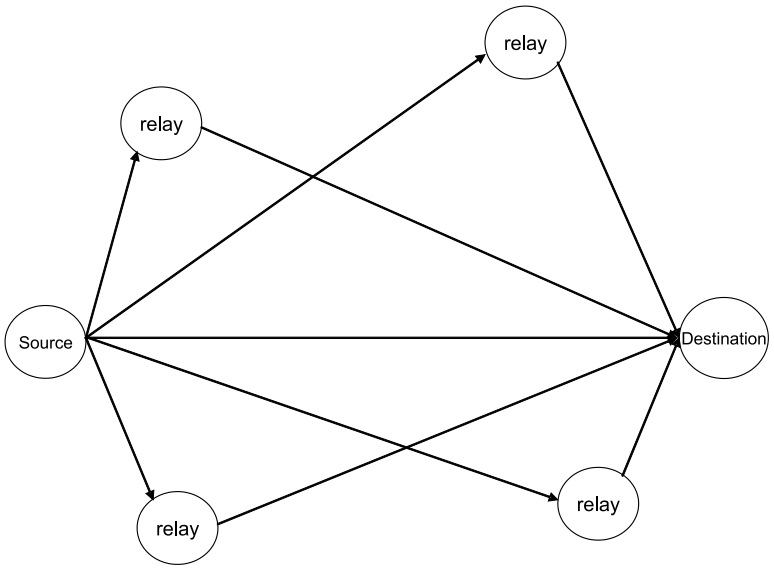

Figure 1.1. System model of a cooperative network.

some scenarios, such as in cellular, ad hoc, and sensor networks, there are strict size and complexity limitations on the wireless terminals, and hence, it may not be practical to implement multiple antennas and space them sufficiently far apart.

In order to cope with this difficulty, *cooperative diversity* has been proposed recently [49, 50]. Cooperative diversity exploits the broadcast nature and the inherent spatial diversity of wireless channels. The fundamental idea of cooperative diversity is that several single-antenna terminals cooperate and achieve spatial diversity by forming a distributed multi-antenna system. Specifically, a source, several relays, and a destination constitute a cooperative network as shown in Fig. 1.1, where the relays help the source transmit information-bearing symbols to the destination. The same information-bearing symbols are transmitted along several independent channels, including the channel from the source to the destination and the channels from the relays to the destination. As a result, the system can exploit spatial diversity and achieve better performance. The wireless networks exploiting cooperative diversity are usually called *cooperative networks*.

In order to coordinate the transmissions from different relays, Laneman *et al.* proposed *repetition-based cooperative strategy* [33]. In this strategy, the source broadcasted one information bearing symbol at the first time slot. Then every relay was assigned one time slot to transmit this symbol to the destination. Furthermore, depending on how the relays processed the signals received from the source, two cooperative protocols, the amplify-and-forward (AF) protocol and the decode-and-forward (DF) protocol, were proposed in [33]. The authors analyzed the outage probabilities of both protocols in a cooperative network using the repetition-based strategy [33]. The results showed that the repetition-based strategy could achieve full diversity order in the number of cooperating terminals, i.e. $K+1$ diversity order could be achieved if there were one source and K relays. Due to its simplicity and ability to achieve full diversity order, the repetition-based cooperative strategy was used and studied in many literatures [2, 6, 21, 24, 34, 45, 59, 60].

Recently, researchers conclude that the repetition-based cooperative network has very poor bandwidth efficiency. This is because only one relay is allowed to transmit the signals at each time slot. As a result, many works are devoted to improve the bandwidth efficiency of the cooperative networks, including cooperative beamforming [20, 64], relay selection scheme [4, 66, 69], and DSTBCs [35, 41, 63, 68]. All those schemes let more than one relay transmit the signals simultaneously to the destination, and hence, the bandwidth efficiency is improved.

The principle of cooperative beamforming is to assign a proper weight coefficient to every relay in order to make the signals from different relays add up constructively at the destination. Some channel state information (CSI) of the channels from the relays to the destination is needed at the relays in order to compute the weight coefficients. In fact, cooperative beamforming can achieve the full diversity order only when full CSI is at the relays [20, 64]. This is hard to achieve even in a slow fading environment. On the other

hand, relay selection scheme always selects the relay with the best channel condition to transmit the signals [4, 66, 69]. Relay selection is accomplished at the destination, because the destination is usually assumed to have full CSI. Thus, the selection result must be fed back from the destination to the relays, which requires a much smaller amount of feedback overhead than the cooperative beamforming. However, relay selection usually does not have good performance at low SNR range, although it can achieve full diversity order.

1.1.2 Distributed Space-Time Block Codes

Unlike the cooperative beamforming and the relay selection scheme, the DSTBCs do not need any feedback overhead, which makes the DSTBCs more attractive especially in a fast fading environment. Furthermore, the DSTBCs can considerably improve the bandwidth efficiency without losing any diversity order. In [35,41,63], for example, the authors proved that the DSTBCs had higher bandwidth efficiency than the repetition-based cooperative strategy from the information theory aspect. After then, many works have been devoted to the design of practical DSTBCs. In particular, special attentions have been given to the codes which are single-symbol maximum likelihood (ML) decodable at the destination, because such codes have very low decoding complexity and they are very attractive for practical implementation. A code is called single-symbol ML decodable if the joint decoding of all the information-bearing symbols can be decoupled into several scalar decoding problems, each of which contains only one information-bearing symbol. The most well-known example is the Alamouti code [1], where the receiver can decode the information-bearing symbols s_1 and s_2 individually. A precise definition of the single-symbol ML decodability has been given in [31], where a code is single-symbol ML decodable if its ML decoding metric can be written as a sum of multiple terms and every term depends on at most one information-bearing symbol.

In the context of the DF protocol, it is usually assumed that a cyclic redundancy check (CRC) is performed at the relays [68]. The relays that correctly decode the information-bearing symbols form a decoding set and only the relays in this set can participate in the transmissions to the destination. Since the relays in the decoding set have perfect copies of the information-bearing symbols, the transmissions from the relays to the destination can be seen as a classic co-located multiple-antenna system, and hence, existing space-time block codes (STBCs) can be used without any modification. When there are K relays, for example, one can choose an orthogonal space-time code $\boldsymbol{X}$ with K rows and assign each row to a specific relay. Once the relay can correctly decode the information-bearing symbols, it transmits those symbols to the destination in the form of the pre-assigned row. This ensures that the decoding at the destination is still single-symbol ML decodable and full diversity order is maintained as well. Other STBCs, such as quasi-orthogonal STBCs and linear dispersion codes can be used in a DF cooperative network as well by following a similar manner.

Recently, many researchers have considered the construction of DSTBCs by addressing the distributed nature of the cooperative networks. In [46, 53], for example, the authors developed randomized DSTBCs, where each relay determines the code in a random and independent fashion. The randomized DSTBCs have the advantage that they could be used in a cooperative network where no centralized control terminal exists and the number of relays in the network were random. Furthermore, in [11, 36, 51], the authors considered asynchronous cooperative networks. The proposed DSTBCs could achieve the full diversity order even when the transmissions from the relays to the destination were not symbol aligned.

On the other hand, the AF protocol has a lower complexity than the DF protocol, since the relays working in the AF mode only require amplifying the received signals from the

source instead of decoding them. Due to the same reason, however, the relays cannot perform CRC when they are working in the AF mode. This makes the analysis and construction of the DSTBCs in the AF cooperative networks much harder than in the DF cooperative networks. In [27], Jing *et al.* applied the linear dispersion codes in the AF cooperative networks and studied the diversity order by deriving the average pairwise error probability (PEP). It was shown that the diversity order of the codes was $K(1-\log\log E/\log E)$, where K was the number of relays and E was the transmission power. The authors noticed that the construction of the linear dispersion codes in the AF cooperative networks had different criteria compared to that in the classic co-located multiple-antenna systems. Motivated by this proposition, many researchers have tried to design the optimum linear dispersion codes for the AF cooperative networks by minimizing the average PEP or outage probability [13, 37]. Recently, Mheidat *et al.* considered the non-coherent detection of the DSTBCs in the AF cooperative networks in [39].

1.2 Motivation and Thesis Overview

Although extensive works have been accomplished to design DSTBCs for the AF cooperative networks, very little of them address the problem of finding orthogonal DSTBCs, which are single-symbol ML decodable at the destination. In [25], Hua *et al.* investigated the use of generalized orthogonal designs in cooperative networks. It is well-known that the generalized orthogonal designs can achieve the single-symbol ML decodability and full diversity [1, 56] in co-located multiple-antenna systems. However, when they were directly used in cooperative networks, the orthogonality of the codes was lost, and hence, the codes were not single-symbol ML decodable any more [25]. Jing *et al.* used the existing orthogonal and quasi-orthogonal designs in cooperative networks [28]. But, the codes

proposed in [28] were not single-symbol ML decodable neither. In [43, 54], the authors constructed DSTBCs based on generalized coordinate interleaved orthogonal designs. Although the proposed codes were single-symbol ML decodable, they could not achieve the full diversity order in an arbitrary constellation. This has motivated us to design and analysis DSTBCs which are single-symbol ML decodable and can achieve full diversity order in an arbitrary constellation.

In Chapter 2 of this thesis, we propose the *distributed orthogonal space-time block codes* (DOSTBCs), and we show that the DOSTBCs achieve the single-symbol ML decodability and the full diversity order in an arbitrary constellation. Then further analysis is given to some special DOSTBCs, namely the *row-monomial DOSTBCs*, which generate uncorrelated noises at the destination. Specifically, an upper bound of the data-rate of the row-monomial DOSTBC is derived. The codes achieving this upper bound are systematically constructed as well.

However, we impose two limitations on the row-monomial DOSTBCs, in order to simplify the analysis. The first one is that the associated matrices of the codes must be row-monomialwhich ensure uncorrelated noises at the destination. The other is the assumption that the relays do not have any CSI of the channels from the source to the relays, i.e. the channels of the first hop. In Chapter 3 of this thesis, we first abandon the row-monomial limitation; but keep the CSI limitation. That is, we consider the DOSTBCs where the noises at the destination are possibly correlated and the relays do not have any CSI of the first-hop channels. By deriving an upper bound of the data-rate of the DOSTBC, we show that the data-rate cannot be substantially improved from the row-monomial DOSTBCs by removing the row-monomial limitation. Secondly, we remove the CSI limitation; but keep the row-monomial limitation. Specifically, the relays know the channel phase information (CPI) of the first-hop channels and use this information in the code construction. Those

codes are referred to as *row-monomial DOSTBCs with CPI* (DOSTBCs-CPI). We derive an upper bound of the data-rate of the row-monomial DOSTBC-CPI and also find the actual codes achieving this upper bound.

In Chapters 4 and 5 of this thesis, we focus on error performance analysis of single-symbol ML decodable DSTBCs in dissimilar cooperative networks where wireless channels possibly have different variances. In order to make the analysis possible, we consider distributed Alamouti's code which is used in a cooperative networks with two relays. In Chapter 4, we assume that the relays are *blind relays*, i.e. the relays have no CSI. Under this assumption, two closed-form approximate expressions of the exact BER of the distributed Alamouti's code are derived. Irrespective of the values of the channel variances, we can always use one of the two proposed closed-form approximate BER expressions and accurately evaluate the BER of the distributed Alamouti's code. Furthermore, those approximate BER expressions show that the distributed Alamouti's code achieve the full diversity order two in a cooperative network with two blind relays.

In Chapter 5 of this thesis, we assume that the relays are *CSI-assisted relays*. That is, the relays have full CSI of the first-hop channels. We first assume that the relays adopt the amplifying coefficient proposed in [33]. A tight lower and an upper bounds of the average BER of the distributed Alamouti's code are derived. Then we show that the distributed Alamouti's code only achieves diversity order one when the relays use the amplifying coefficient proposed in [33]. Furthermore, in a general cooperative network with more than two relays, we show that the DSTBCs proposed in [27] only achieve diversity order one as well when the amplifying coefficient proposed in [33] is used at the relays. To resolve this problem, we propose a new threshold-based amplifying coefficient for the distributed Alamouti's code. This new amplifying coefficient makes the code achieve the full diversity

order two. Moreover, based on three different criteria, three optimum and one suboptimum schemes are developed in order to choose the value of the threshold used in the new amplifying coefficient.

1.3 Thesis Contribution

The primary contributions of this thesis are briefly summarized as follows.

- For the first time, single-symbol ML decodable DSTBCs are designed for AF cooperative networks. Specifically, we design three different types of codes, row-monomial DOSTBCs, DOSTBCs, and row-monomial DOSTBCs-CPI. All those codes are single-symbol ML decodable in AF cooperative networks and achieve full diversity order in arbitrary constellations. Moreover, upper bounds of the data-rates of the proposed codes are found and the codes achieving the upper bounds are constructed. In particular, the row-monomial DOSTBCs-CPI are very attractive for practical implementations, because they have very low decoding complexity and very high bandwidth efficiency even when the number of relays is large.

- Error performance of the distributed Alamouti's code is analyzed when the relays are blind relays. Two approximate BER expressions of the distributed Alamouti's code are derived. Irrespective of the values of channel variances, we can always use one of those two approximate expressions in order to accurately evaluate the error performance of the distributed Alamouti's code. Those two approximate BER expressions also show that the distributed Alamouti's code indeed achieve full diversity order two when the relays are blind relays.

- When the relays are CSI-assisted relays, error performance of the distributed Alamouti's code is analyzed as well. When the relays use conventional amplifying coefficient, we derive very tight lower and upper bounds of the average BER. The lower bound shows that the code only achieves diversity order one when conventional amplifying coefficient is used at the relays. Then we propose a new threshold-based amplifying coefficient for the CSI-assisted relays. This new amplifying coefficient makes the distributed Alamouti's code achieve full diversity order two. Moreover, we propose several schemes to optimize the value of the threshold used in the new amplifying coefficient. All of those schemes can improve the performance greatly.

Chapter 2

Single-Symbol ML Decodable Distributed STBCs for Cooperative Networks

In this chapter, distributed orthogonal space-time block codes (DOSTBCs), which achieve single-symbol maximum likelihood decodability and full diversity order, are first considered. However, analysis and systematic construction of the DOSTBCs is very hard, since the noise covariance matrix is not diagonal in general. Thus, some special DOSTBCs, which have diagonal noise covariance matrices at the destination, are investigated. These codes are referred to as the row-monomial DOSTBCs. An upper bound of the data-rate of the row-monomial DOSTBC is derived and it is approximately twice as high as that of the repetition-based cooperative strategy. Furthermore, systematic construction methods of the row-monomial DOSTBCs achieving the upper-bound of the data-rate are developed.

2.1 Introduction

It is well-known that relay cooperation can improve the performance of a wireless network considerably [33, 34, 49, 50]. A source, several relays, and a destination constitute a cooperative network, where the relays forward the signals from the source to the destination.

Because the destination may receive different signals from several relays simultaneously, some mechanism is needed to prevent or cancel the interference among these signals.

A simple solution is the so-called *repetition-based cooperative strategy*, which was proposed in [33]. In this strategy, only one relay is allowed to transmit signals at every time slot. Consequently, no interference exists at the destination, and hence, the decoding process is single-symbol maximum likelihood (ML) decodable. Furthermore, it has been shown that the repetition-based cooperative strategy could achieve the full diversity order K, where K is the number of relays. Due to its single-symbol ML decodability and full diversity order, the repetition-based cooperative strategy was used and studied in many papers [2,6,21,22,35,45]. However, the repetition-based cooperative strategy has very poor bandwidth efficiency. It is easy to see that the data-rate[1] of the repetition-based cooperative strategy is $1/K$.

Recently, many researchers noticed that the use of *distributed space-time block codes* (DSTBCs) could improve the bandwidth efficiency of cooperative networks [35, 41, 63] and many practical DSTBCs were proposed [16, 27, 36, 68]. However, none of those codes were single-symbol ML decodable in general.[2] In [25], Hua *et al.* investigated the use of generalized orthogonal designs in cooperative networks. It is well-known that the generalized orthogonal designs can achieve the single-symbol ML decodability and full diversity [1, 56]. However, when the generalized orthogonal designs were directly used in

[1] In this chapter, the data-rate of a cooperative strategy or a distributed space-time block code is defined as the average number of symbols transmitted by the relays per time slot, i.e. its value is equal to the ratio of the number of transmitted symbols to the number of time slots used by the relays to transmit all these symbols.

[2] The schemes proposed in [68] would be single-symbol ML decodable only if the space-time code it used was single-symbol ML decodable. The fundamental difference between [68] and this chapter is that the decode-and-forward protocol is considered in [68]; while, we consider the amplify-and-forward protocol in this chapter.

cooperative networks, the orthogonality of the codes was lost, and hence, the codes were not single-symbol ML decodable any more [25]. Very recently, Jing *et al.* used existing orthogonal and quasi-orthogonal designs in cooperative networks [28]. The codes proposed in [28] were not single-symbol ML decodable in general neither. To the best of our knowledge, DSTBCs which simultaneously achieve the single-symbol ML decodability and the full diversity order have never been designed. This motivated our work.

In this chapter, we first consider the *distributed orthogonal space-time block codes* (DOSTBCs) in the amplify-and-forward cooperative networks. The DOSTBCs achieve the single-symbol ML decodability and the full diversity order. However, analysis and systematic construction of the DOSTBCs is very hard due to the fact that the covariance matrix of the noise at the destination is non-diagonal in general. Therefore, we restrict our interests to a subset of the DOSTBCs, which result in a diagonal noise covariance matrix at the destination. We refer to the codes in this subset as the *row-monomial DOSTBCs* and derive an upper bound of the data-rate of the row-monomial DOSTBC. Compared to the repetition-based cooperative strategy, the row-monomial DOSTBCs achieve approximately twice higher data-rate, while having the same decoding complexity and diversity order. Furthermore, systematic construction methods of the row-monomial DOSTBCs are developed. We prove that the codes generated by the systematic construction methods achieve the upper-bound of the data-rate when the number K of relays and/or the number N of information-bearing symbols are even.

The rest of this chapter is organized as follows. Section 2.2 describes the cooperative network considered in this chapter. In Section 2.3, we define the DOSTBCs and show that they achieve the single-symbol ML decodability and the full diversity order. In Section 2.4, the row-monomial DOSTBCs are first defined and an upper bound of the data-rate of the row-monomial DOSTBC is then derived. Section 2.5 presents the systematic construction

methods of the row-monomial DOSTBCs. We present some numerical results in Section 2.6 and then conclude this chapter in Section 2.7.

Notations: Bold upper and lower letters denote matrices and row vectors, respectively. Also, diag$[x_1,\cdots,x_K]$ denotes the $K\times K$ diagonal matrix with $x_1,\cdots,x_K$ on its main diagonal; $\boldsymbol{0}_{k_1\times k_2}$ the $k_1\times k_2$ all-zero matrix; $\boldsymbol{I}_{T\times T}$ the $T\times T$ identity matrix; $[\cdot]_k$ the k-th entry of a vector; $[\cdot]_{k_1,k_2}$ the (k_1,k_2)-th entry of a matrix; $(\cdot)^*$ the complex conjugate; $(\cdot)^H$ the Hermitian; $(\cdot)^T$ the transpose. For two real numbers a and b, $\lceil a\rceil$ denotes the ceiling function of a; $\lfloor a\rfloor$ the floor function of a; $\mod(a,b)$ the modulo operation. For two sets $\mathscr{S}_1$ and $\mathscr{S}_2$, $\mathscr{S}_1-\mathscr{S}_2$ denotes the set whose elements are in $\mathscr{S}_1$ but not in $\mathscr{S}_2$.

2.2 System Model

Consider a cooperative network with one source, K relays, and one destination. Every terminal has only one antenna and is half-duplex. Denote the channel from the source to the k-th relay by h_k and the channel from the k-th relay to the destination by f_k. h_k and f_k are spatially uncorrelated complex Gaussian random variables with zero mean and unit variance. We assume that the destination knows the instantaneous values of the channel coefficients h_k and f_k by using training sequences; while the source and relays have no knowledge of the instantaneous channel coefficients. Note that we assume that there is no direct link between the source and destination terminals. The same assumption has been made in many previous publications [16, 27, 36, 68].

At the beginning, the source transmits N complex-valued symbols over N consecutive time slots.[3] Let $\boldsymbol{s}=[s_1,\cdots,s_N]$ denote the symbol vector transmitted from the source,

[3]If the transmitted symbols are real-valued, it is easy to show that rate-one generalized real orthogonal design proposed in [56] can be used in cooperative networks without any changes, while achieving the single-symbol ML decodability and full diversity order [25]. Therefore, we focus on the complex-valued symbols

where the power of s_n is E_s. Assume the coherence time of h_k is larger than N; then the received signal vector $\boldsymbol{y}_k$ at the k-th relay is $\boldsymbol{y}_k = h_k\boldsymbol{s} + \boldsymbol{n}_k$, where $\boldsymbol{n}_k = [n_{k,1}, \cdots, n_{k,N}]$ is the additive noise at the k-th relay and it is uncorrelated complex Gaussian with zero mean and identity covariance matrix. All the relays are working in the amplify-and-forward mode and the amplifying coefficient ρ is $\sqrt{E_r/(1+E_s)}$ for every relay, where E_r is the transmission power at every relay. In many previous papers such as [27, 41], the same choice of $\rho = \sqrt{E_r/(1+E_s)}$ has been made. This amplifying coefficient ensures the average transmission power of every relay is E_r in the long term. Moreover, every relay uses the same transmission power E_r. Optimum power allocation across the relays can certainly improve the performance further, but it can only be achieved when the relays have knowledge of the instantaneous channel coefficients.

In order to construct a distributed space-time block code, every relay multiplies $\boldsymbol{y}_k$ and $\boldsymbol{y}_k^*$ with $\boldsymbol{A}_k$ and $\boldsymbol{B}_k$, respectively, and then sum up these two products. The dimension of $\boldsymbol{A}_k$ and $\boldsymbol{B}_k$ is $N \times T$. Thus, the transmitted signal vector $\boldsymbol{x}_k$ from the k-th relay is

$$\begin{aligned} \boldsymbol{x}_k &= \rho(\boldsymbol{y}_k\boldsymbol{A}_k + \boldsymbol{y}_k^*\boldsymbol{B}_k) \\ &= \rho h_k\boldsymbol{s}\boldsymbol{A}_k + \rho h_k^*\boldsymbol{s}^*\boldsymbol{B}_k + \rho\boldsymbol{n}_k\boldsymbol{A}_k + \rho\boldsymbol{n}_k^*\boldsymbol{B}_k. \end{aligned} \tag{2.1}$$

This construction method originates from the construction of a space-time code for co-located multiple-antenna systems, where the transmitted signal vector from the k-th antenna is $\boldsymbol{s}\boldsymbol{A}_k + \boldsymbol{s}^*\boldsymbol{B}_k$ [61]. Since we consider the amplify-and-forward cooperative networks, the relays do not have the estimate of $\boldsymbol{s}$. Therefore, they use $\boldsymbol{y}_k$ and $\boldsymbol{y}_k^*$, which contain the information of $\boldsymbol{s}$, to construct the transmitted signal vector.

Assume the coherence time of f_k is larger than T; then the received signal vector $\boldsymbol{y}_D$ at

in this chapter.

the destination is given by

$$\begin{aligned} \boldsymbol{y}_D &= \sum_{k=1}^{K} f_k \boldsymbol{x}_k + \boldsymbol{n}_D \\ &= \sum_{k=1}^{K} (\rho\, f_k h_k \boldsymbol{s}\boldsymbol{A}_k + \rho\, f_k h_k^* \boldsymbol{s}^* \boldsymbol{B}_k) + \sum_{k=1}^{K} (\rho\, f_k \boldsymbol{n}_k \boldsymbol{A}_k + \rho\, f_k \boldsymbol{n}_k^* \boldsymbol{B}_k) + \boldsymbol{n}_D, \end{aligned} \tag{2.2}$$

where $\boldsymbol{n}_D = [n_{D,1}, \cdots, n_{D,T}]$ is the additive noise at the destination and is uncorrelated complex Gaussian with zero mean and identity covariance matrix. We assume perfect synchronization among the relays as in [16, 25, 27, 34–36, 68]. Synchronization is a critical issue for the practical implementation of cooperative networks; but it is beyond the scope of this chapter. Define $\boldsymbol{w}$, $\boldsymbol{X}$, and $\boldsymbol{n}$ as follows:

$$\boldsymbol{w} = [\rho\, f_1, \cdots, \rho\, f_K] \tag{2.3}$$

$$\boldsymbol{X} = [h_1 \boldsymbol{s}\boldsymbol{A}_1 + h_1^* \boldsymbol{s}^* \boldsymbol{B}_1; \cdots; h_K \boldsymbol{s}\boldsymbol{A}_K + h_K^* \boldsymbol{s}^* \boldsymbol{B}_K] \tag{2.4}$$

$$\boldsymbol{n} = \sum_{k=1}^{K} (\rho\, f_k \boldsymbol{n}_k \boldsymbol{A}_k + \rho\, f_k \boldsymbol{n}_k^* \boldsymbol{B}_k) + \boldsymbol{n}_D; \tag{2.5}$$

then we can rewrite (2.2) in the following way

$$\boldsymbol{y}_D = \boldsymbol{w}\boldsymbol{X} + \boldsymbol{n}. \tag{2.6}$$

Because the matrix $\boldsymbol{X}$ contains N information-bearing symbols, $s_1, \cdots, s_N$, and it lasts for T time slots, the data-rate of $\boldsymbol{X}$ is equal to N/T.[4] From (2.5), it is easy to see that the mean of $\boldsymbol{n}$ is zero and the covariance matrix $\boldsymbol{R}$ of $\boldsymbol{n}$ is given by

$$\boldsymbol{R} = \sum_{k=1}^{K} \left(|\rho\, f_k|^2 \left(\boldsymbol{A}_k^H \boldsymbol{A}_k + \boldsymbol{B}_k^H \boldsymbol{B}_k \right) \right) + \boldsymbol{I}_{T \times T}. \tag{2.7}$$

[4]Considering the N time slots used by the source to transmit the symbol vector $\boldsymbol{s}$, the overall data-rate of the entire transmission scheme is $N/(N+T)$. In this chapter, because we focus on the design of $\boldsymbol{X}$, we will use the data-rate N/T of $\boldsymbol{X}$ as the metric to evaluate the bandwidth efficiency, as we have mentioned in Section 2.1.

2.3 Distributed Orthogonal Space-Time Block Codes

In this section, we will first define the DOSTBCs. Then, in order to evaluate the diversity order of the DOSTBCs, some properties of $\boldsymbol{A}_k$ and $\boldsymbol{B}_k$ are presented. Lastly, we show that the DOSTBCs can achieve the full diversity order.

From (2.6), the ML estimate $\hat{\boldsymbol{s}}$ of $\boldsymbol{s}$ is given by

$$\begin{aligned}\hat{\boldsymbol{s}} &= \arg\min_{\boldsymbol{s}\in\mathscr{C}} (\boldsymbol{y}_D - \boldsymbol{w}\boldsymbol{X})\boldsymbol{R}^{-1}(\boldsymbol{y}_D - \boldsymbol{w}\boldsymbol{X})^H \\ &= \arg\min_{\boldsymbol{s}\in\mathscr{C}} \left(-2\Re\left(\boldsymbol{w}\boldsymbol{X}\boldsymbol{R}^{-1}\boldsymbol{y}_D^H\right) + \boldsymbol{w}\boldsymbol{X}\boldsymbol{R}^{-1}\boldsymbol{X}^H\boldsymbol{w}^H\right), \end{aligned} \tag{2.8}$$

where $\mathscr{C}$ is the set containing all the possible symbol vector $\boldsymbol{s}$. Inspired by the definition of the generalized orthogonal designs [56, 61], we define the DOSTBCs in the following way.

Definition 2.1: A $K \times T$ matrix $\boldsymbol{X}$ is called a distributed orthogonal space-time block code (DOSTBC) in variables $s_1, \cdots, s_N$ if the following two conditions are satisfied:

D2.1.1) The entries of $\boldsymbol{X}$ are 0, $\pm h_k s_n$, $\pm h_k^* s_n^*$, or multiples of these indeterminates by $\mathbf{j}$, where $\mathbf{j} = \sqrt{-1}$.

D2.1.2) The matrix $\boldsymbol{X}$ satisfies the following equality

$$\boldsymbol{X}\boldsymbol{R}^{-1}\boldsymbol{X}^H = |s_1|^2\boldsymbol{D}_1 + \cdots + |s_N|^2\boldsymbol{D}_N, \tag{2.9}$$

where $\boldsymbol{D}_n = \mathrm{diag}[|h_1|^2 D_{n,1}, \cdots, |h_K|^2 D_{n,K}]$ and $D_{n,k}$ are non-zero for $k = 1, \cdots, K$.

Substituting (2.9) into (2.8), it is easy to show that the DOSTBCs are single-symbol ML decodable. The first term in (2.8) can be written as $-\Re\{\sum_{n=1}^{N}(\alpha_n s_n + \beta_n s_n^*)\}$, where α_n and β_n are independent of s_n. By (2.9), the second term in (2.8) can be decomposed into a sum of terms that only depend on $|s_n|^2$. Therefore, (2.8) does not contain the terms $s_{n_1}s_{n_2}$, $s_{n_1}s_{n_2}^*$, $s_{n_1}^*s_{n_2}$, or $s_{n_1}^*s_{n_2}^*$, $n_1 \neq n_2$, which implies the single-symbol ML decodability [31, 56].

Furthermore, the DOSTBCs can also achieve the full diversity order K. Before presenting the proof, we first derive some fundamental properties on $\boldsymbol{A}_k$ and $\boldsymbol{B}_k$, which will be used throughout this chapter. For convenience, we define that a matrix is *column-monomial (row-monomial)* if there is at most one non-zero entry on every column (row) of it.

Lemma 2.1. *If a DOSTBC $\boldsymbol{X}$ in variables $s_1, \cdots, s_N$ exists, its associated matrices $\boldsymbol{A}_k$ and $\boldsymbol{B}_k$, $1 \leq k \leq K$, have the following properties:*

1. *$\boldsymbol{A}_k$ and $\boldsymbol{B}_k$ cannot have non-zero entries at the same position.*

2. *$\boldsymbol{A}_k$, $\boldsymbol{B}_k$, and $\boldsymbol{A}_k + \boldsymbol{B}_k$ are column-monomial.*

3. *$\boldsymbol{A}_{k_1}\boldsymbol{R}^{-1}\boldsymbol{A}_{k_2}^H = \boldsymbol{B}_{k_1}\boldsymbol{R}^{-1}\boldsymbol{B}_{k_2}^H = \boldsymbol{0}_{N\times N}$, for $1 \leq k_1 \neq k_2 \leq K$.*

4. *$\boldsymbol{A}_k\boldsymbol{R}^{-1}\boldsymbol{A}_k^H + \boldsymbol{B}_k^*\boldsymbol{R}^{-1}\boldsymbol{B}_k^T = \mathrm{diag}[D_{1,k}, \cdots, D_{N,k}]$, for $1 \leq k \leq K$.*

Proof: The proof of the first two properties is similar to the proof of Property 3.2 in [55]. The proof of the fourth property is similar to the proof of Proposition 1 in [61]. The proof of the third property is given in the following. When $k_1 \neq k_2$, according to (2.9), $[\boldsymbol{X}\boldsymbol{R}^{-1}\boldsymbol{X}^H]_{k_1,k_2}$ is given by

$$\begin{aligned}[\boldsymbol{X}\boldsymbol{R}^{-1}\boldsymbol{X}^H]_{k_1,k_2} &= h_{k_1}h_{k_2}^*\boldsymbol{s}\boldsymbol{A}_{k_1}\boldsymbol{R}^{-1}\boldsymbol{A}_{k_2}^H\boldsymbol{s}^H + h_{k_1}^*h_{k_2}^*\boldsymbol{s}^*\boldsymbol{B}_{k_1}\boldsymbol{R}^{-1}\boldsymbol{A}_{k_2}^H\boldsymbol{s}^H \\ &\quad + h_{k_1}h_{k_2}\boldsymbol{s}\boldsymbol{A}_{k_1}\boldsymbol{R}^{-1}\boldsymbol{B}_{k_2}^H\boldsymbol{s}^T + h_{k_1}^*h_{k_2}\boldsymbol{s}^*\boldsymbol{B}_{k_1}\boldsymbol{R}^{-1}\boldsymbol{B}_{k_2}^H\boldsymbol{s}^T \\ &= 0. \end{aligned} \tag{2.10}$$

Note that h_{k_1} and h_{k_2} can be any complex numbers. Thus, in order to make (2.10) hold for every possible value of h_{k_1} and h_{k_2}, the following equalities must hold

$$\boldsymbol{s}\boldsymbol{A}_{k_1}\boldsymbol{R}^{-1}\boldsymbol{A}_{k_2}^H\boldsymbol{s}^H = \boldsymbol{s}^*\boldsymbol{B}_{k_1}\boldsymbol{R}^{-1}\boldsymbol{B}_{k_2}^H\boldsymbol{s}^T = 0 \tag{2.11}$$

By using Lemma 1 of [38], we have the third property. ■

The diversity order of the DOSTBCs is given in the following lemma.

Lemma 2.2. *Assume $T \geq K$, $E_r = c_r E$, and $E_s = c_s E$, where c_r and c_s are positive constants. The DOSTBCs can achieve the full diversity order K.*

Proof: See Appendix 2-A. ■

After evaluating the diversity order of the DOSTBCs, a natural question is how to systematically construct the DOSTBCs. Unfortunately, systematic construction method has not yet been found. We note that the major hindrance comes from the fact that the noise covariance matrix $\boldsymbol{R}$ in (2.7) is not diagonal in general. In the next section, thus, we will consider a subset of the DOSTBCs, whose codes result in a diagonal $\boldsymbol{R}$.

2.4 Row-Monomial Distributed Orthogonal Space-Time Block Codes

In this section, we first show that, if $\boldsymbol{A}_k$ and $\boldsymbol{B}_k$ are row-monomial, the covariance matrix $\boldsymbol{R}$ becomes diagonal. Then we define a subset of the DOSTBCs, whose associated matrices $\boldsymbol{A}_k$ and $\boldsymbol{B}_k$ are row-monomial, and hence, we refer to the codes in this subset as the row-monomial DOSTBCs. Lastly, an upper bound of the data-rate of the row-monomial DOSTBC is derived.

As we stated in Section 2.3, the non-diagonality of $\boldsymbol{R}$ makes the systematic construction of the DOSTBCs very hard. Thus, we restrict our interests to a special subset of the DOSTBCs, where $\boldsymbol{R}$ is diagonal. In the following, we show that the diagonality of $\boldsymbol{R}$ is equivalent to the row-monomial condition of $\boldsymbol{A}_k$ and $\boldsymbol{B}_k$.

Theorem 2.1. *The matrix $\boldsymbol{R}$ in (2.7) is a diagonal matrix if and only if $\boldsymbol{A}_k$ and $\boldsymbol{B}_k$ are row-monomial.*

Proof: See Appendix 2-B. ■

Based on Theorem 2.1, we define the row-monomial DOSTBCs in the following way.

Definition 2.2: A $K \times T$ matrix $\boldsymbol{X}$ is called a row-monomial DOSTBC in variables $s_1, \cdots, s_N$ if it satisfies D2.1.1 and D2.1.2 in Definition 2.1 and its associated matrices $\boldsymbol{A}_k$ and $\boldsymbol{B}_k$, $1 \leq k \leq K$, are all row-monomial.

Obviously, the row-monomial DOSTBCs are single-symbol ML decodable and they achieve the full diversity order K, because they represent a subset of the DOSTBCs. For the same reason, all the results in Section 2.3 are still valid for the row-monomial DOSTBCs. In order to evaluate bandwidth efficiency, we drive an upper-bound of the data-rate of the row-monomial DOSTBC. To this end, we present several conditions on $\boldsymbol{A}_k$ and $\boldsymbol{B}_k$ at first. In this chapter, two matrices $\boldsymbol{A}$ and $\boldsymbol{B}$ are said to be *column-disjoint*, if $\boldsymbol{A}$ and $\boldsymbol{B}$ cannot contain non-zero entries on the same column simultaneously, i.e. if a column in $\boldsymbol{A}$ contains a non-zero entry at any row, then all the entries of the same column in $\boldsymbol{B}$ must be zero; conversely, if a column in $\boldsymbol{B}$ contains a non-zero entry at any row, then all the entries of the same column in $\boldsymbol{A}$ must be zero.

Lemma 2.3. *If a row-monomial DOSTBC $\boldsymbol{X}$ in variables $s_1, \cdots, s_N$ exists, its associated matrices $\boldsymbol{A}_k$ and $\boldsymbol{B}_k$, $1 \leq k \leq K$, satisfy the following two conditions:*

1) $\boldsymbol{A}_{k_1}$ and $\boldsymbol{A}_{k_2}$ are column-disjoint for $k_1 \neq k_2$.

2) $\boldsymbol{B}_{k_1}$ and $\boldsymbol{B}_{k_2}$ are column-disjoint for $k_1 \neq k_2$.

Proof: See Appendix 2-C. ■

Lemma 2.3 is crucial to find the upper bound of the data-rate of the row-monomial DOSTBC. According to Definition 2.2, if $\boldsymbol{X}$ is a row-monomial DOSTBC, there are two types of non-zero entries in it: 1) the entries containing $\pm h_k s_n$ or the multiples of it by $\mathbf{j}$; 2) the entries containing $\pm h_k^* s_n^*$ or the multiples of it by $\mathbf{j}$. In the following, we will refer to

the first type of entries as the *non-conjugate* entries and refer to the second type of entries as the *conjugate* entries. Lemma 2.3 implies that any column in $\boldsymbol{X}$ cannot contain more than one non-conjugate entry or more than one conjugate entry. However, one column in $\boldsymbol{X}$ can contain one non-conjugate entry and one conjugate entry at the same time. Therefore, the columns in $\boldsymbol{X}$ can be partitioned into two types: 1) the columns containing one non-conjugate entry or one conjugate entry; 2) the columns containing one non-conjugate entry and one conjugate entry. In the following, we will refer to the first type of columns as the Type-I columns and refer to the second type of columns as the Type-II columns. For the Type-II columns, we have the following lemma.

Lemma 2.4. *If a row-monomial DOSTBC $\boldsymbol{X}$ in variables $s_1, \cdots, s_N$ exists, the Type-II columns in $\boldsymbol{X}$ have the following properties:*

1. *The total number of the Type-II columns in $\boldsymbol{X}$ is even.*

2. *In all the Type-II columns of $\boldsymbol{X}$, the total number of the entries containing s_n or s_n^*, $1 \leq n \leq N$, is even.*

Proof: See Appendix 2-D. ■

Since the data-rate of $\boldsymbol{X}$ is defined as N/T, improving the data-rate of $\boldsymbol{X}$ is equivalent to reducing the length T of $\boldsymbol{X}$, when N is fixed. Furthermore, we note that a Type-II column contains two non-zero entries; while a Type-I column contains only one non-zero entry. Therefore, if all the non-zero entries in $\boldsymbol{X}$ are contained in the Type-II columns, the data-rate of $\boldsymbol{X}$ achieves the maximum value. Unfortunately, in some circumstances, not all the non-zero entries in $\boldsymbol{X}$ can be contained in the Type-II columns. In those circumstances, in order to reduce T, we need to make $\boldsymbol{X}$ contain as many non-zero entries in the Type-II columns as possible. Based on this and Lemmas 2.3 and 2.4, we derive an upper bound of the data-rate of the row-monomial DOSTBC and the result is given in the following

theorem.

Theorem 2.2. *If a row-monomial DOSTBC* $\boldsymbol{X}$ *in variables* $s_1, \cdots, s_N$ *exists, its data-rate* $\mathscr{R}_R$ *satisfies the following inequality:*

$$\mathscr{R}_R = \frac{N}{T} \leq \begin{cases} \frac{1}{m}, & \text{when} \quad N = 2l, K = 2m \\ \frac{2l+1}{2lm+2m}, & \text{when} \quad N = 2l+1, K = 2m \\ \frac{1}{m+1}, & \text{when} \quad N = 2l, K = 2m+1 \\ \min\left(\frac{2l+1}{2lm+2m+l+1}, \frac{2l+1}{2lm+2l+m+1}\right), & \text{when} \quad N = 2l+1, K = 2m+1 \end{cases}, \quad (2.12)$$

where $N \geq 1$ *and* $K \geq 1$.

Proof: See Appendix 2-E. ■

Because the data-rate of the repetition-based cooperative strategy is just $1/K$, the data-rate of the row-monomial DOSTBC is approximately twice as high as that of the repetition-based cooperative strategy according to (2.12). As we stated before, these are the data-rates of the transmission from the relays to the destination. On the other hand, we can also consider the overall data-rate of the cooperative network, i.e. the data-rate of the entire transmission from the source to the destination. For example, when N and K are both even, it is not hard to see that the overall data-rate of the cooperative networks using the row-monomial DOSTBCs is $2/(2+K)$. On the other hand, the overall data-rate of the repetition-based cooperative strategy is $1/(1+K)$, which is always smaller than $2/(2+K)$ for non-negative K. Thus, we can conclude that the row-monomial DOSTBCs always have better bandwidth efficiency than the repetition-based cooperative strategy. Note that the better bandwidth efficiency of the row-monomial DOSTBCs is achieved without losing the single-symbol ML decodability or the full diversity order.

But we notice that the upper bounds of the data-rates of the row-monomial DOSTBCs decrease when K increases. For a large cooperative network, the row-monomial DOSTBCs

will not have good bandwidth efficiency. Therefore, although the row-monomial DOST-BCs are designed for a cooperative network with an arbitrary K, it may be preferable to implement them only for a cooperative network with a small K. When K is large, we may improve the bandwidth efficiency by relaxing the constraint of single-symbol ML decodability.

2.5 Systematic Construction of the Row-Monomial DOST-BCs Achieving the Upper Bound of the Data-Rate

In this section, we present the systematic construction methods of the row-monomial DOST-BCs. For given N and K, we use $\boldsymbol{X}(N,K)$ to denote the code generated by the systematic construction method. There are four different cases depending on the values of N and K.

2.5.1 $N = 2l$ and $K = 2m$

For convenience, we will use $\boldsymbol{A}_k(:,t_1:t_2)$ to denote the submatrix consisting of the t_1-th, t_1+1-th, $\cdots$, t_2-th columns of $\boldsymbol{A}_k$. Similarly, $\boldsymbol{B}_k(:,t_1:t_2)$ denotes the submatrix consisting of the t_1-th, t_1+1-th, $\cdots$, t_2-th columns of $\boldsymbol{B}_k$. Furthermore, define $\boldsymbol{G}_s$ as follows:

$$\boldsymbol{G}_s = \begin{bmatrix} 0 & 1 \\ 1 & 0 \end{bmatrix}. \tag{2.13}$$

Based on $\boldsymbol{G}_s$, two matrices $\boldsymbol{G}_A$ and $\boldsymbol{G}_B$ with dimension $N \times N$ are defined:

$$\boldsymbol{G}_A = \mathrm{diag}[1,-1,1,-1,\cdots,1,-1] \tag{2.14}$$

$$\boldsymbol{G}_B = \mathrm{diag}\left[\boldsymbol{G}_s,\cdots,\boldsymbol{G}_s\right]. \tag{2.15}$$

The proposed systematic construction method of the row-monomial DOSTBCs achieving the upper bound of (2.12) is as follows:

Construction I:

Initialization: Set $p = 1$. Set $\boldsymbol{A}_k = \boldsymbol{B}_k = \boldsymbol{0}_{N\times\infty}$, $1 \le k \le K$, where ∞ means that the length of the matrices is not decided yet.

Step 1: Set $\boldsymbol{A}_{2p-1}(:,(p-1)N+1:pN) = \boldsymbol{G}_A$ and $\boldsymbol{B}_{2p}(:,(p-1)N+1:pN) = \boldsymbol{G}_B$.

Step 2: Set $p = p+1$. If $p \le m$, go to *Step 1*; otherwise, go to *Step 3*.

Step 3: Discard the all-zero columns at the tail of $\boldsymbol{A}_{K-1}$ and $\boldsymbol{B}_K$. Set the length of $\boldsymbol{A}_k$ and $\boldsymbol{B}_k$, $1 \le k \le K$, equal to that of $\boldsymbol{A}_{K-1}$ and $\boldsymbol{B}_K$.

Step 4: Calculate $\boldsymbol{X}(N,K)$ through (2.4) by using the matrices $\boldsymbol{A}_k$ and $\boldsymbol{B}_k$ obtained in *Steps 1–3*, and end the construction.

The following lemma shows that Construction I generates the row-monomial DOST-BCs achieving the upper bound of (2.12) for any even N and K.

Lemma 2.5. *For any even $N = 2l$ and $K = 2m$, the codes generated by Construction I achieve the data-rate $1/m$.*

Proof: In Construction I, the length of $\boldsymbol{A}_k$ and $\boldsymbol{B}_k$, $1 \le k \le K$, is decided by the length of $\boldsymbol{A}_{K-1}$ and $\boldsymbol{B}_K$. Because $\boldsymbol{A}_{K-1}(:,(m-1)N+1:mN)$ and $\boldsymbol{B}_K(:,(m-1)N+1:mN)$ are set to be $\boldsymbol{G}_A$ and $\boldsymbol{G}_B$, respectively, when $p = m$, the length of $\boldsymbol{A}_{K-1}$ and $\boldsymbol{B}_K$ is mN. Consequently, the length of $\boldsymbol{A}_k$ and $\boldsymbol{B}_k$, $1 \le k \le K$ is mN. By (2.4), the length of $\boldsymbol{X}(N,K)$ is T and it is the same as that of $\boldsymbol{A}_k$ and $\boldsymbol{B}_k$. Therefore, the value of T is mN, and hence, the data-rate of $\boldsymbol{X}(N,K)$ is $1/m$. ■

For example, when $N = 4$ and $K = 4$, the code constructed by Construction I is given by

$$\boldsymbol{X}(4,4) = \begin{bmatrix} h_1s_1 & -h_1s_2 & h_1s_3 & -h_1s_4 & 0 & 0 & 0 & 0 \\ h_2^*s_2^* & h_2^*s_1^* & h_2^*s_4^* & h_2s_3^* & 0 & 0 & 0 & 0 \\ 0 & 0 & 0 & 0 & h_3s_1 & -h_3s_2 & h_3s_3 & -h_3s_4 \\ 0 & 0 & 0 & 0 & h_4^*s_2^* & h_4^*s_1^* & h_4^*s_4^* & h_4s_3^* \end{bmatrix}, \quad (2.16)$$

and it achieves the upper bound of the data-rate $1/2$.

2.5.2 $N = 2l+1$ and $K = 2m$

This case is equivalent to the case that $N = 2l$ and $K = 2m$ if s_N is not considered. Based on this, the proposed systematic construction method of the row-monomial DOSTBCs achieving the upper bound of (2.12) is as follows:

Construction II:

Step 1: Neglect s_N and construct a $K \times 2lm$ matrix $\boldsymbol{X}_1$ in variables $s_1, \cdots, s_{N-1}$ by Construction I.

Step 2: Form a $K \times K$ diagonal matrix $\boldsymbol{X}_2 = \mathrm{diag}[h_1 s_N, \cdots, h_K s_N]$.

Step 3: Let $\boldsymbol{X}(N,K) = [\boldsymbol{X}_1, \boldsymbol{X}_2]$ and end the construction.

Because the length of $\boldsymbol{X}_1$ and $\boldsymbol{X}_2$ is $2lm$ and K, respectively, the length of $\boldsymbol{X}(N,K)$ is $2lm+K$. Thus, the data-rate of $\boldsymbol{X}(N,K)$ is $(2l+1)/(2lm+K)$, which is exactly the same as the upper-bound of (2.12).

For example, when $N = 5$ and $K = 4$, the code constructed by Construction II is given by

$$\boldsymbol{X}_1 = \begin{bmatrix} h_1 s_1 & -h_1 s_2 & h_1 s_3 & -h_1 s_4 & 0 & 0 & 0 & 0 \\ h_2^* s_2^* & h_2^* s_1^* & h_2^* s_4^* & h_2 s_3^* & 0 & 0 & 0 & 0 \\ 0 & 0 & 0 & 0 & h_3 s_1 & -h_3 s_2 & h_3 s_3 & -h_3 s_4 \\ 0 & 0 & 0 & 0 & h_4^* s_2^* & h_4^* s_1^* & h_4^* s_4^* & h_4 s_3^* \end{bmatrix}, \quad (2.17)$$

$$\boldsymbol{X}_2 = \begin{bmatrix} h_1 s_5 & 0 & 0 & 0 \\ 0 & h_2 s_5 & 0 & 0 \\ 0 & 0 & h_3 s_5 & 0 \\ 0 & 0 & 0 & h_4 s_5 \end{bmatrix}, \quad (2.18)$$

and $\boldsymbol{X}(5,4) = [\boldsymbol{X}_1, \boldsymbol{X}_2]$. The code $\boldsymbol{X}(5,4)$ achieves the upper bound of the data-rate $5/12$.

2.5.3 $N = 2l$ and $K = 2m+1$

This case is equivalent to the case that $N = 2l$ and $K = 2m$ if the K-th relay is not considered. Based on this, the proposed systematic construction method of the row-monomial DOSTBCs achieving the upper bound of (2.12) is as follows:

Construction III:

Step 1: Neglect the K-th relay and construct a $2m \times 2lm$ matrix $\boldsymbol{X}_1$ by Construction I.

Step 2: Form a vector $\boldsymbol{x}_2 = [h_K s_1, \cdots, h_K s_N]$

Step 3: Build a block diagonal matrix $\boldsymbol{X}(N,K) = \mathrm{diag}[\boldsymbol{X}_1, \boldsymbol{x}_2]$ and end the construction.

Because the length of $\boldsymbol{X}_1$ and $\boldsymbol{x}_2$ is $2lm$ and N, respectively, the length of $\boldsymbol{X}(N,K)$ is $2lm+N$. Thus, the data-rate of $\boldsymbol{X}(N,K)$ is $1/(1+m)$, which is exactly the same as the upper-bound of (2.12).

For example, when $N = 4$ and $K = 5$, the code constructed by Construction III is given by

$$\boldsymbol{X}_1 = \begin{bmatrix} h_1 s_1 & -h_1 s_2 & h_1 s_3 & -h_1 s_4 & 0 & 0 & 0 & 0 \\ h_2^* s_2^* & h_2^* s_1^* & h_2^* s_4^* & h_2 s_3^* & 0 & 0 & 0 & 0 \\ 0 & 0 & 0 & 0 & h_3 s_1 & -h_3 s_2 & h_3 s_3 & -h_3 s_4 \\ 0 & 0 & 0 & 0 & h_4^* s_2^* & h_4^* s_1^* & h_4^* s_4^* & h_4 s_3^* \end{bmatrix}, \quad (2.19)$$

$$\boldsymbol{x}_2 = \begin{bmatrix} h_5 s_1 & h_5 s_2 & h_5 s_3 & h_5 s_4 \end{bmatrix}, \quad (2.20)$$

and $\boldsymbol{X}(4,5) = \mathrm{diag}[\boldsymbol{X}_1, \boldsymbol{x}_2]$. The code $\boldsymbol{X}(4,5)$ achieves the upper bound of the data-rate $1/3$.

2.5.4 $N = 2l+1$ and $K = 2m+1$

For this case, the proposed systematic construction method of the row-monomial DOSTBCs is as follows:

Construction IV:

Part I:

Initialization: Set $p = 0$ and $\mathscr{S} = \{s_1, \cdots, s_N\}$.

Step 1: Neglect $s_{1+ \mod(p,N)}$ and construct a $2 \times 2l$ matrix $\boldsymbol{X}^{(p)}$ in variables $\mathscr{S} - \{s_{1+ \mod(p,N)}\}$ by Construction I.

Step 2: Set $p = p+1$. If $p < m$, go to *Step 1*; otherwise, go to *Step 3*.

Step 3: Let $\boldsymbol{X}_1 = \left[\text{diag}[\boldsymbol{X}^{(0)}, \cdots, \boldsymbol{X}^{(m-1)}]; \boldsymbol{0}_{1\times 2lm}\right]$ and proceed to Part II.

Part II:

Initialization: Set $p = 0$, $\mathscr{S}^{(K)} = \mathscr{S}$, and $c = 1$. Construct a $K \times \infty$ matrix $\boldsymbol{X}_2$ with all zero entries, where ∞ means that the length of $\boldsymbol{X}_2$ is not decided yet.

Step 1: Set $[\boldsymbol{X}_2]_{2p+1,c}$ equal to $h^*_{2p+1} s^*_{1+ \mod(p,N)}$.

Step 2: If $\mathscr{S}^{(K)} = \phi$, set $c = c+1$ and go to *Step 4*.

Step 3: Choose the element with the largest subscript from $\mathscr{S}^{(K)}$ and denote it by $s_{\max}$. Let $[\boldsymbol{X}_2]_{K,c}$ equal to $h_K s_{\max}$ and set $c = c+1$. Let $[\boldsymbol{X}_2]_{2p+1,c}$ and $[\boldsymbol{X}_2]_{K,c}$ equal to $h^*_{2p+1} s^*_{\max}$ and $-h_K s_{1+ \mod(p,N)}$, respectively. Set $\mathscr{S}^{(K)} = \mathscr{S}^{(K)} - \{s_{\max}, s_{1+ \mod(p,N)}\}$ and $c = c+1$.

Step 4: Set $p = p+1$. If $p < m$, go to *Step 1*; otherwise, set $p = 0$ and proceed to *Step 5*.

Step 5: Let $[\boldsymbol{X}_2]_{2p+2,c}$ equal to $h_{2p+2} s_{1+ \mod(p,N)}$.

Step 6: If $\mathscr{S}^{(K)} = \phi$, set $c = c+1$ and go to *Step 8*.

Step 7: Choose the element with the largest subscript from $\mathscr{S}^{(K)}$ and denote it by $s_{\max}$. Let $[\boldsymbol{X}_2]_{K,c}$ equal to $h^*_K s^*_{\max}$ and set $c = c+1$. Let $[\boldsymbol{X}_2]_{2p+2,c}$ and $[\boldsymbol{X}_2]_{K,c}$ equal to $-h_{2p+2} s_{\max}$ and $h^*_K s^*_{1+ \mod(p,N)}$, respectively. Set $\mathscr{S}^{(K)} = \mathscr{S}^{(K)} - \{s_{\max}, s_{1+ \mod(p,N)}\}$ and $c = c+1$.

Step 8: Set $p = p+1$. If $p < m$, go to *Step 5*; otherwise, discard the all-zero columns at the tail of $\boldsymbol{X}_2$, build $\boldsymbol{X}(N,K) = [\boldsymbol{X}_1, \boldsymbol{X}_2]$, and end the construction.

For any odd $N \leq 9$ and $K \leq 9$, we have confirmed that the codes generated by Construction IV achieve the upper bound of (2.12) indeed. For example, when $N = 5$ and $K = 5$, the matrices $\boldsymbol{X}_1$ and $\boldsymbol{X}_2$ constructed by Construction IV are given by

$$\boldsymbol{X}_1 = \left[\begin{array}{cccc|cccc} h_1 s_2 & -h_1 s_3 & h_1 s_4 & -h_1 s_5 & 0 & 0 & 0 & 0 \\ h_2^* s_3^* & h_2^* s_2^* & h_2^* s_5^* & h_2 s_4^* & 0 & 0 & 0 & 0 \\ \hline 0 & 0 & 0 & 0 & h_3 s_1 & -h_3 s_3 & h_3 s_4 & -h_3 s_5 \\ 0 & 0 & 0 & 0 & h_4^* s_3^* & h_4^* s_1^* & h_4^* s_5^* & h_4 s_4^* \\ \hline 0 & 0 & 0 & 0 & 0 & 0 & 0 & 0 \end{array}\right] \tag{2.21}$$

and

$$\boldsymbol{X}_2 = \left[\begin{array}{cc|cc|cc|c} h_1^* s_1^* & h_1^* s_5^* & 0 & 0 & 0 & 0 & 0 \\ 0 & 0 & 0 & 0 & h_2 s_1 & -h_2 s_3 & 0 \\ 0 & 0 & h_3^* s_2^* & h_3^* s_4^* & 0 & 0 & 0 \\ 0 & 0 & 0 & 0 & 0 & 0 & h_4 s_2 \\ h_5 s_5 & -h_5 s_1 & h_5 s_4 & -h_5 s_2 & h_3^* s_3^* & h_5^* s_1^* & 0 \end{array}\right], \tag{2.22}$$

respectively, where the solid lines illustrate the construction steps. Therefore, $\boldsymbol{X}(5,5) = [\boldsymbol{X}_1, \boldsymbol{X}_2]$ achieves the upper bound of the data-rate $1/3$. In general, however, it is hard to prove that Construction IV can generate the row-monomial DOSTBCs achieving the upper bound of (2.12) for any odd N and K.

2.6 Numerical Results

In this section, we compare the performance of the proposed code $\boldsymbol{X}(4,4)$, the repetition-based cooperative strategy, the distributed linear dispersion codes in [27], and the quasi-orthogonal DSTBCs in [28]. We assume that wireless channels are uncorrelated Rayleigh fading channels. By computer simulation, we plot the average bit error rate (BER) against

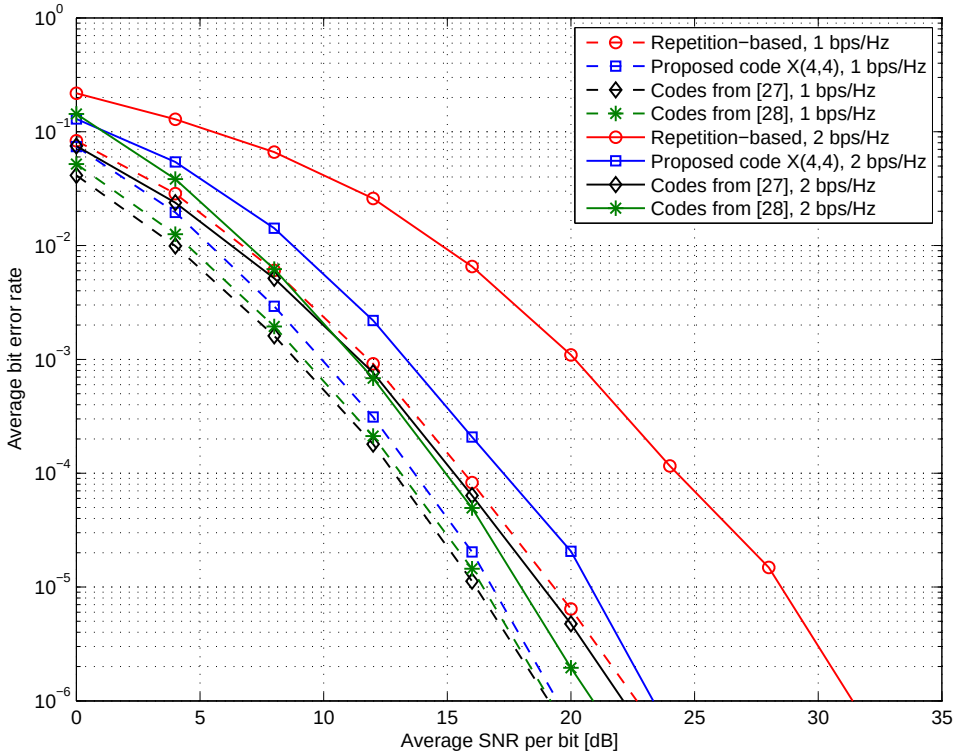

Figure 2.1. Comparison of the row-monomial DOSTBCs, the repetition-based cooperative strategy, the distributed linear dispersion codes in [27], and the quasi-orthogonal distributed space-time block codes in [28], $N = 4$, $K = 4$.

the average signal to noise ratio (SNR) per bit, where the average SNR per bit is equal to the ratio of E_r to the logarithm of the size of the modulation scheme. Optimum power allocation proposed in [27] is adopted, i.e. $E_s = KE_r$. Furthermore, a proper modulation scheme is chose for every code in order to make them achieve the same bandwidth efficiency. For example, since the data-rate of the row-monomial DOSTBC is $1/2$ when $N = 4$ and $K = 4$, 16-QAM is chosen to make the code achieve bandwidth efficiency 2 bps/Hz.

The comparison results are given in Fig. 2.1. It can be seen that the performance of the row-monomial DOSTBCs is much better than that of the repetition-based cooperative strategy in the whole SNR range. The performance gain of the row-monomial DOSTBCs

is more impressive when the bandwidth efficiency is 2 bps/Hz. Furthermore, because the BER curves of the row-monomial DOSTBCs are parallel with those of the repetition-based cooperative strategy, the row-monomial DOSTBCs indeed achieve the full diversity order K. On the other hand, the performance of the row-monomial DOSTBCs is not as good as that of the distributed linear dispersion codes in [27] and the quasi-orthogonal DSTBCs in [28]. However, the row-monomial DOSTBCs have much less decoding complexity, because they are single-symbol ML decodable.

2.7 Conclusion

We have first studied the DOSTBCs and showed that the DOSTBCs are single-symbol ML decodable and have the full diversity order K. Further investigation has been given to the row-monomial DOSTBCs and an upper bound of the data-rate of the row-monomial DOSTBC has been derived. Compared to the repetition-based cooperative strategy, the row-monomial DOSTBCs achieve approximately twice higher data-rate without losing the single-symbol ML decodability or the full diversity order. Furthermore, systematic construction methods of the row-monomial DOSTBCs have been developed. When N and/or K are even, we have proven that the codes generated by the systematic construction methods always achieve the upper-bound of the data-rate. When N and K are both odd, the proof has not been found; but we have confirmed that the codes generated by the systematic construction method achieve the upper-bound of the data-rate for N and K up to 9.

2.8 Appendix 2-A: Proof of Lemma 2.2

In this proof, for a matrix $\boldsymbol{H}$, we use $\lambda_{\max}(\boldsymbol{H})$ to denote its largest eigenvalue; $d(\boldsymbol{H})$ its spectral radius; $|\boldsymbol{H}|$ the matrix containing the absolute value of the entries in $\boldsymbol{H}$. As in [71],

we use $\doteq$ and $\dot{\geq}$ to denote the asymptotic exponential equality and inequality, respectively.

The proof starts by defining $\tilde{\boldsymbol{w}}$ and $\tilde{\boldsymbol{X}}$ as follows:

$$\tilde{\boldsymbol{w}} = [\rho f_1|h_1|, \cdots, \rho f_K|h_K|] \tag{2.A-1}$$

$$\tilde{\boldsymbol{X}} = [\boldsymbol{s}e^{j\phi_1}\boldsymbol{A}_1 + \boldsymbol{s}^* e^{-j\phi_1}\boldsymbol{B}_1; \cdots; \boldsymbol{s}e^{j\phi_K}\boldsymbol{A}_K + \boldsymbol{s}^* e^{-j\phi_K}\boldsymbol{B}_K], \tag{2.A-2}$$

where ϕ_k is the phase of h_k. Consequently, we have $\boldsymbol{y}_D = \tilde{\boldsymbol{w}}\tilde{\boldsymbol{X}} + \boldsymbol{n}$ from (2.6). When $\tilde{\boldsymbol{w}}$ is given, the mutual information between $\boldsymbol{y}_D$ and $\tilde{\boldsymbol{X}}$ is given by

$$I(\tilde{\boldsymbol{X}}; \boldsymbol{y}_D|\tilde{\boldsymbol{w}}) = \log\left(1 + \tilde{\boldsymbol{w}}\tilde{\boldsymbol{X}}\boldsymbol{R}^{-1}\tilde{\boldsymbol{X}}^H\tilde{\boldsymbol{w}}^H\right) \geq \log\left(1 + \frac{1}{\lambda_{\max}(\boldsymbol{R})}\tilde{\boldsymbol{w}}\tilde{\boldsymbol{X}}\tilde{\boldsymbol{X}}^H\tilde{\boldsymbol{w}}^H\right). \tag{2.A-3}$$

In general, $\boldsymbol{R}$ is not a diagonal matrix and we can write $\boldsymbol{R} = \boldsymbol{R}_D + \boldsymbol{R}_O$, where $\boldsymbol{R}_D$ and $\boldsymbol{R}_O$ contain the main diagonal and the off-diagonal entries of $\boldsymbol{R}$, respectively. From [26], the following inequalities hold

$$\lambda_{\max}(\boldsymbol{R}_O) \leq d(\boldsymbol{R}_O) \leq d(|\boldsymbol{R}_O|) \leq \max_{1\leq k\leq K}\sum_{i=1}^{K}|[\boldsymbol{R}_O]_{i,k}| < \max_{1\leq k\leq K}[\boldsymbol{R}_D]_{k,k} = \lambda_{\max}(\boldsymbol{R}_D). \tag{2.A-4}$$

The fourth inequality is because $\sum_{i=1,i\neq k}^{K}|[\boldsymbol{R}]_{i,k}| < [\boldsymbol{R}]_{k,k}$, which can be seen from (2.7) and the first two properties in Lemma 2.1. Furthermore, we have [26]

$$\lambda_{\max}(\boldsymbol{R}) \leq \lambda_{\max}(\boldsymbol{R}_D) + \lambda_{\max}(\boldsymbol{R}_O) < 2\lambda_{\max}(\boldsymbol{R}_D) \leq 2(1 + \sum_{k=1}^{K}|\rho f_k|^2), \tag{2.A-5}$$

where the last inequality is from (2.7) and the first two properties in Lemma 2.1.

In [14], it has been shown that $1+\sum_{k=1}^{K}|\rho f_k|^2$ is independent of E, i.e. $1+\sum_{k=1}^{K}|\rho f_k|^2 \doteq E^0$. Thus, we have

$$I(\tilde{\boldsymbol{X}}; \boldsymbol{y}_D|\tilde{\boldsymbol{w}}) \dot{\geq} \log\left(1 + \tilde{\boldsymbol{w}}\tilde{\boldsymbol{X}}\tilde{\boldsymbol{X}}^H\tilde{\boldsymbol{w}}^H\right) \tag{2.A-6}$$

$$\doteq \log\left(1 + c_s E\tilde{\boldsymbol{w}}\tilde{\boldsymbol{w}}^H\right), \tag{2.A-7}$$

where the last step is because $T \geq K$ and $\tilde{\boldsymbol{X}}$ is full rank. In [14], it has been shown that the average outage probability of (2.A-7) decays with E as fast as $1/E^K$. Therefore, the average outage probability of the cooperative networks using the DOSTBCs decays with E as fast as $1/E^K$, i.e. the full diversity order K is achieved.

2.9 Appendix 2-B: Proof of Theorem 2.1

The sufficient part is easy to verify. We only prove the necessary part here, i.e. if $\boldsymbol{R}$ is a diagonal matrix, $\boldsymbol{A}_k$ and $\boldsymbol{B}_k$ are row-monomial. This is done by contradiction. If $\boldsymbol{R}$ is a diagonal matrix, the off-diagonal entries $[\boldsymbol{R}]_{t_1,t_2}$, $1 \leq t_1 \neq t_2 \leq T$, are equal to zero. According to (2.7), we have

$$[\boldsymbol{R}]_{t_1,t_2} = \sum_{k=1}^{K} \left[|\rho\, f_k|^2 \left(\sum_{n=1}^{N} [\boldsymbol{A}_k]^*_{n,t_1} [\boldsymbol{A}_k]_{n,t_2} + \sum_{n=1}^{N} [\boldsymbol{B}_k]^*_{n,t_1} [\boldsymbol{B}_k]_{n,t_2} \right) \right] = 0. \tag{2.B-1}$$

In order to make the equality hold for every possible f_k, the following equality must hold

$$\sum_{n=1}^{N} [\boldsymbol{A}_k]^*_{n,t_1} [\boldsymbol{A}_k]_{n,t_2} + \sum_{n=1}^{N} [\boldsymbol{B}_k]^*_{n,t_1} [\boldsymbol{B}_k]_{n,t_2} \;\; = \;\; 0, \qquad\qquad 1 \leq k \leq K. \tag{2.B-2}$$

Let us assume that the $n^{'}$-th, $1 \leq n^{'} \leq N$, row of $\boldsymbol{A}_k$ contains two non-zero entries: $[\boldsymbol{A}_k]_{n^{'},t_1}$ and $[\boldsymbol{A}_k]_{n^{'},t_2}$, $1 \leq t_1 \neq t_2 \leq T$. Because $\boldsymbol{A}_k$ is column-monomial according to Lemma 2.1, $[\boldsymbol{A}_k]_{n,t_1} = [\boldsymbol{A}_k]_{n,t_2} = 0$, $1 \leq n \neq n^{'} \leq N$, and hence,

$$\sum_{n=1}^{N} [\boldsymbol{A}_k]^*_{n,t_1} [\boldsymbol{A}_k]_{n,t_2} = [\boldsymbol{A}_k]^*_{n^{'},t_1} [\boldsymbol{A}_k]_{n^{'},t_2} \neq 0. \tag{2.B-3}$$

On the other hand, because $\boldsymbol{A}_k$ and $\boldsymbol{B}_k$ cannot have non-zero entries at the same place according to Lemma 2.1, we have $[\boldsymbol{B}_k]_{n^{'},t_1} = [\boldsymbol{B}_k]_{n^{'},t_2} = 0$. Furthermore, because $\boldsymbol{A}_k + \boldsymbol{B}_k$ is column-monomial, $[\boldsymbol{B}_k]_{n,t_1} = [\boldsymbol{B}_k]_{n,t_2} = 0$, $1 \leq n \neq n^{'} \leq N$. Therefore, $[\boldsymbol{B}_k]_{n,t_1} = [\boldsymbol{B}_k]_{n,t_2} = 0$, $1 \leq n \leq N$, and consequently, $\sum_{n=1}^{N} [\boldsymbol{B}_k]^*_{n,t_1} [\boldsymbol{B}_k]_{n,t_2} = 0$. It follows from (2.B-2) and $\sum_{n=1}^{N} [\boldsymbol{B}_k]^*_{n,t_1} [\boldsymbol{B}_k]_{n,t_2} = 0$ that

$$\sum_{n=1}^{N} [\boldsymbol{A}_k]^*_{n,t_1} [\boldsymbol{A}_k]_{n,t_2} = 0. \tag{2.B-4}$$

Because (2.B-3) and (2.B-4) contradict with each other, we can conclude that any row of $\boldsymbol{A}_k$ cannot contain two non-zero entries. Furthermore, in the same way, it can be easily shown that any row of $\boldsymbol{A}_k$ cannot contain more than two non-zero entries, and hence, $\boldsymbol{A}_k$ is row-monomial. Similarly, we can show that $\boldsymbol{B}_k$ is row-monomial, which completes the proof of the necessary part.

2.10 Appendix 2-C: Proof of Lemma 2.3

The proof is by contradiction. We assume that the $t^{'}$-th column of $\boldsymbol{A}_{k_1}$ and $\boldsymbol{A}_{k_2}$, $1 \leq k_1 \neq k_2 \leq K$, contains a non-zero entry $[\boldsymbol{A}_{k_1}]_{n_1,t'}$ and a non-zero entry $[\boldsymbol{A}_{k_2}]_{n_2,t'}$, respectively. By Definition 2.2, $\boldsymbol{A}_{k_1}$ and $\boldsymbol{A}_{k_2}$ are both row-monomial, we have $[\boldsymbol{A}_{k_1}]_{n_1,t} = [\boldsymbol{A}_{k_2}]_{n_2,t} = 0$, $1 \leq t \neq t^{'} \leq T$, and hence,

$$\sum_{t=1}^{T} [\boldsymbol{A}_{k_1}]_{n_1,t} [\boldsymbol{R}^{-1}]_{t,t} [\boldsymbol{A}_{k_2}]^*_{n_2,t} = [\boldsymbol{A}_{k_1}]_{n_1,t'} [\boldsymbol{R}^{-1}]_{t',t'} [\boldsymbol{A}_{k_2}]^*_{n_2,t'} \neq 0. \tag{2.C-1}$$

On the other hand, by the third property in Lemma 2.1 and the fact that $\boldsymbol{R}$ is diagonal, $[\boldsymbol{A}_{k_1} \boldsymbol{R}^{-1} \boldsymbol{A}^H_{k_2}]_{n_1,n_2}$ is given by

$$[\boldsymbol{A}_{k_1} \boldsymbol{R}^{-1} \boldsymbol{A}^H_{k_2}]_{n_1,n_2} = \sum_{t=1}^{T} [\boldsymbol{A}_{k_1}]_{n_1,t} [\boldsymbol{R}^{-1}]_{t,t} [\boldsymbol{A}_{k_2}]^*_{n_2,t} = 0. \tag{2.C-2}$$

Because (2.C-1) and (2.C-2) contradict with each other, we conclude that $\boldsymbol{A}_{k_1}$ and $\boldsymbol{A}_{k_2}$, $1 \leq k_1 \neq k_2 \leq K$, cannot contain non-zero entries on the same column simultaneously. Therefore, $\boldsymbol{A}_{k_1}$ and $\boldsymbol{A}_{k_2}$ are column-disjoint when $k_1 \neq k_2$. Similarly, we can show that $\boldsymbol{B}_{k_1}$ and $\boldsymbol{B}_{k_2}$ are column-disjoint when $k_1 \neq k_2$.

2.11 Appendix 2-D: Proof of Lemma 2.4

If no Type-II column exists in $\boldsymbol{X}$, it is trivial that the number of the Type-II columns in $\boldsymbol{X}$ is even. If there is one Type-II column in $\boldsymbol{X}$, without loss of generality, we assume that the t_1-th column in $\boldsymbol{X}$ is a Type-II column and it contains $h_{k_1} s_{n_1}$ and $h^*_{k_2} s^*_{n_2}$ on the k_1-th and k_2-th row, respectively. Consequently, $[\boldsymbol{X}\boldsymbol{R}^{-1}\boldsymbol{X}^H]_{k_1,k_2}$ will contain the term $h_{k_1} s_{n_1} h_{k_2} s_{n_2} [\boldsymbol{R}^{-1}]_{t_1,t_1}$. On the other hand, because $\boldsymbol{X}$ is a row-monomial DOSTBC, $[\boldsymbol{X}\boldsymbol{R}^{-1}\boldsymbol{X}^H]_{k_1,k_2}$ should be null by the definition. Thus, in order to cancel the term $h_{k_1} s_{n_1} h_{k_2} s_{n_2} [\boldsymbol{R}^{-1}]_{t_1,t_1}$, there must be another Type-II column, for example the t_2-th column, $t_1 \neq t_2$, which contains $-h_{k_1} s_{n_2}$ and

$h_{k_2}^* s_{n_1}^*$ on the k_1-th and k_2-th row, respectively.[5] Therefore, the Type-II columns in $\boldsymbol{X}$ always appear in pairs, and hence, the total number of the Type-II columns in $\boldsymbol{X}$ is even.

For convenience, we will refer to any entry in $\boldsymbol{X}$ that contains s_n or s_n^* as the s_n-entry. If no s_n-entry exists in the Type-II columns of $\boldsymbol{X}$, it is trivial that the total number of s_n-entries in the Type-II columns of $\boldsymbol{X}$ is even. If there is one s_n-entry in a Type-II column of $\boldsymbol{X}$, we assume it contains s_n without loss of generality. From the proof of the first property in Lemma 2.4, we can see that there must be an s_n-entry in another Type-II column and it contains s_n^*. Therefore, in the Type-II columns of $\boldsymbol{X}$, the s_n-entries always appear in pairs, and hence, the total number of the s_n-entries in the Type-II columns of $\boldsymbol{X}$ is even.

2.12 Appendix 2-E: Proof of Theorem 2.2

For convenience, we will refer to any entry in $\boldsymbol{X}$ that contains s_n or s_n^* as the s_n-entry. Let U denote the total number of non-zero entries in $\boldsymbol{X}$; V_n the total number of s_n-entries in $\boldsymbol{X}$; W_k the total number of non-zero entries in the k-th row of $\boldsymbol{X}$. Obviously, $U = \sum_{n=1}^{N} V_n = \sum_{k=1}^{K} W_k$. According to the fourth property in Lemma 2.1, at least one $[\boldsymbol{A}_k]_{n,t}$ or one $[\boldsymbol{B}_k]_{n,t}$ is non-zero, $1 \leq n \leq N$ and $1 \leq k \leq K$. Thus, every row of $\boldsymbol{X}$ has at least one s_n-entry, $1 \leq n \leq N$. On the other hand, by the row-monomial condition of $\boldsymbol{A}_k$ and $\boldsymbol{B}_k$, every row of $\boldsymbol{X}$ has at most two s_n-entries, where one contains s_n and the other contains s_n^*. Therefore, every row of $\boldsymbol{X}$ contains at least N and at most $2N$ non-zero entries, i.e. $N \leq W_k \leq 2N$, $1 \leq k \leq K$. For the same reason, we have $K \leq V_n \leq 2K$, $1 \leq n \leq N$. Consequently, we have $NK \leq U \leq 2NK$.

[5] The t_2-th column will produce a term $-h_{k_1} s_{n_1} h_{k_2} s_{n_2} [\boldsymbol{R}^{-1}]_{t_2,t_2}$. Because the t_1-th and t_2-th columns have non-zero entries only on the k_1-th and k_2-th rows, we have $[\boldsymbol{R}^{-1}]_{t_1,t_1} = [\boldsymbol{R}^{-1}]_{t_2,t_2} = 1/(1+|\rho f_{k_1}|^2 + |\rho f_{k_2}|^2)$ from (2.7). Aa a result, $h_{k_1} s_{n_1} h_{k_2} s_{n_2} [\boldsymbol{R}^{-1}]_{t_1,t_1}$ is cancelled by $-h_{k_1} s_{n_1} h_{k_2} s_{n_2} [\boldsymbol{R}^{-1}]_{t_2,t_2}$, and $[\boldsymbol{X}\boldsymbol{R}^{-1}\boldsymbol{X}^H]_{k_1,k_2}$ becomes null.

Case I: $N = 2l$ and $K = 2m$. When $N = 2l$ and $K = 2m$, $U \geq NK = 4lm$. Because a pair of Type-II columns contains four non-zero entries, at least $\lceil 4lm/4 \rceil$ pairs of Type-II columns are needed to transmit all the non-zero entries. Since T is the total number of columns in $\boldsymbol{X}$, we have the following inequality

$$T \geq 2\left\lceil \frac{4lm}{4} \right\rceil = 2lm, \tag{2.E-1}$$

and hence,

$$\mathscr{R}_R \leq \frac{1}{m}. \tag{2.E-2}$$

Case II: $N = 2l+1$ and $K = 2m$. When $N = 2l+1$ and $K = 2m$, without loss of generality, we assume $W_1, \cdots, W_w$ are even and $W_{1+w}, \cdots, W_{2m}$ are odd, where $1 \leq w \leq 2m$. We first have $U \geq NK = 4lm + 2m$. Furthermore, because W_k is even for $1 \leq k \leq w$, $W_k \geq N+1 = 2l+2$. Consequently, $U \geq 4lm + 2m + w$. On the other hand, because the Type-II columns always appear in pairs, the k-th row of $\boldsymbol{X}$, $w+1 \leq k \leq 2m$, must contain at least one Type-I column; otherwise, W_k will be even, which violates our assumption. Therefore, there are at least $2m-w$ Type-I columns in $\boldsymbol{X}$ and they contain $2m-w$ non-zero entries. Because a pair of Type-II columns contains four non-zero entries, the rest non-zero entries need at least $\lceil (4lm+2m+w-(2m-w))/4 \rceil$ pairs of Type-II columns to transmit. Therefore, we have the following inequality

$$\begin{aligned} T &\geq 2m - w + 2\left\lceil \frac{4lm+2m+w-(2m-w)}{4} \right\rceil && \text{(2.E-3)} \\ &\geq 2m - w + \frac{4lm+2m+w-(2m-w)}{2} && \text{(2.E-4)} \\ &= 2lm + 2m, && \text{(2.E-5)} \end{aligned}$$

and hence,

$$\mathscr{R}_R \leq \frac{2l+1}{2lm+2m}. \tag{2.E-6}$$

Case III: $N = 2l$ and $K = 2m+1$. When $N = 2l$ and $K = 2m+1$, without loss of generality, we assume $V_1, \cdots, V_v$ are even and $V_{v+1}, \cdots, V_{2l}$ are odd, where $1 \leq v \leq 2l$. We first have $U \geq NK = 4lm+2l$. Furthermore, because V_n is even for $1 \leq n \leq v$, $V_n \geq K+1 = 2m+2$. Consequently, $U \geq 4lm+2l+v$. On the other hand, because the total number of s_n-entries in the Type-II columns of $\boldsymbol{X}$ is even, at least one s_n-entry, $v+1 \leq n \leq 2l$, is in a Type-I column; otherwise, V_n will be even, which violates our assumption. Thus, there are at least $2l-v$ Type-I columns in $\boldsymbol{X}$ and they contain $2l-v$ non-zero entries. Because a pair of Type-II columns contains four non-zero entries, the rest non-zero entries need at least $\lceil (4lm+2l+v-(2l-v))/4 \rceil$ pairs of Type-II columns to transmit. Therefore, we have the following inequality

$$\begin{aligned} T &\geq 2l-v+2\left\lceil \frac{4lm+2l+v-(2l-v)}{4} \right\rceil && \text{(2.E-7)} \\ &\geq 2l-v+\frac{4lm+2l+v-(2l-v)}{2} && \text{(2.E-8)} \\ &= 2lm+2l, && \text{(2.E-9)} \end{aligned}$$

and hence,

$$\mathscr{R}_R \leq \frac{1}{m+1}. \quad \text{(2.E-10)}$$

Case IV: $N = 2l+1$ and $K = 2m+1$. When $N = 2l+1$ and $K = 2m+1$, we can assume that $W_1, \cdots, W_w$ are even and $W_{1+w}, \cdots, W_{2m+1}$ are odd, where $1 \leq w \leq 2m+1$. By following the proof of Case II, we have

$$\begin{aligned} T &\geq 2m+1-w+2\left\lceil \frac{4lm+2l+2m+1+w-(2m+1-w)}{4} \right\rceil && \text{(2.E-11)} \\ &\geq 2m+1-w+\frac{4lm+2l+2m+1+w-(2m+1-w)}{2} && \text{(2.E-12)} \\ &= 2lm+2m+l+1. && \text{(2.E-13)} \end{aligned}$$

On the other hand, we can assume $V_1, \cdots, V_v$ are even and $V_{v+1}, \cdots, V_{2l+1}$ are odd, where $1 \leq v \leq 2l+1$. By following the proof of Case III, we have

$$\begin{aligned} T &\geq 2l+1-v+2\left\lceil \frac{4lm+2l+2m+1+v-(2l+1-v)}{4} \right\rceil && \text{(2.E-14)} \\ &\geq 2l+1-v+\frac{4lm+2l+2m+1+v-(2l+1-v)}{2} && \text{(2.E-15)} \\ &= 2lm+2l+m+1. && \text{(2.E-16)} \end{aligned}$$

From (2.E-13) and (2.E-16), it is immediate that

$$T \geq \max(2lm+2m+l+1, 2lm+2l+m+1), \quad \text{(2.E-17)}$$

and

$$\mathscr{R}_R \leq \min\left(\frac{2l+1}{2lm+2m+l+1}, \frac{2l+1}{2lm+2l+m+1}\right). \quad \text{(2.E-18)}$$

Chapter 3

The Impact of Noise Correlation and Channel Phase Information on the Data-Rate of Single-Symbol ML Decodable Distributed STBCs

In Chapter 2, we proposed the row-monomial distributed orthogonal space-time block codes (DOSTBCs) and showed that the row-monomial DOSTBCs achieved approximately twice higher bandwidth efficiency than the repetition-based cooperative strategy. However, we imposed two limitations on the row-monomial DOSTBCs. The first one was that the associated matrices of the codes must be row-monomial. The other was the assumption that the relays did not have any channel state information (CSI) of the channels from the source to the relays, although this CSI could be readily obtained at the relays without any additional pilot signals or any feedback overhead. In this chapter, we first remove the row-monomial limitation; but keep the CSI limitation. In this case, we derive an upper bound of the data-rate of the DOSTBC. Secondly, we abandon the CSI limitation; but keep the row-monomial limitation. Specifically, we propose the row-monomial DOSTBCs with channel

phase information (DOSTBCs-CPI) and derive an upper bound of the data-rate of those codes. The row-monomial DOSTBCs-CPI have higher data-rates than the DOSTBCs and the row-monomial DOSTBCs. Furthermore, we find the actual row-monomial DOSTBCs-CPI which achieve the upper bound of the data-rate.

3.1 Introduction

In a cooperative network, the relays cooperate to help the source transmit the information-bearing symbols to the destination. The relay cooperation improves the performance of the network considerably [33, 34, 49, 50]. The cooperative strategy of the relays is crucial and it decides the performance of a cooperative network. A simple cooperative strategy is the *repetition-based cooperative strategy* which was proposed in [33] and studied in [2, 6, 21, 22, 45]. This cooperative strategy achieves the full diversity order in the number K of relays.[1] Furthermore, the maximum likelihood (ML) decoding at the destination is single-symbol ML decodable.[2] However, the repetition-based cooperative strategy has poor bandwidth efficiency, since its data-rate[3] is just $1/K$. Many works have been devoted to improve the bandwidth efficiency of the cooperative networks, such as the cooperative

[1] We say a cooperative strategy achieves the full diversity order when its average bit error rate (BER) or outage capacity decays with the transmission power in an order of K [35]. Furthermore, unless otherwise indicated, saying one code or one scheme achieves the full diversity order in this chapter means it achieves the full diversity in an arbitrary signal constellation.

[2] A code or a scheme is single-symbol ML decodable if the joint decoding of all the information-bearing symbols can be decoupled into several scalar decoding problems, each of which contains only one information-bearing symbol.

[3] In this chapter, the data-rate of a cooperative strategy or a distributed space-time block code is equal to the ratio of the number of transmitted information-bearing symbols to the number of time slots used by the relays to transmit all these symbols.

beamforming [35, 64] and the relay selection [66, 69, 70]. More attentions have been given to the *distributed space-time block codes* (DSTBCs) [35, 41, 63]. Furthermore, many practical codes have been proposed in [10, 16, 27, 32, 36, 40, 68]. Although all those codes could improve the bandwidth efficiency, they were not single-symbol ML decodable in general, and hence, they had much higher decoding complexities than the repetition-based cooperative strategy.

Very few works have tried to propose the DSTBCs achieving the single-symbol ML decodability and the full diversity order. In [25], Hua *et al.* used the existing orthogonal designs in cooperative networks; but they found that most codes were not single-symbol ML decodable any more. In [43], Rajan *et al.* used the orthogonal designs, generalized coordinate interleaved orthogonal designs, and clifford unitary weight single-symbol decodable codes in cooperative networks. They claimed that those codes achieved the single-symbol ML decodability when the noise covariance matrix at the destination was a scaled identity matrix. Furthermore, the authors proposed a class of DSTBCs based on the clifford unitary weight single-symbol decodable codes. However, those codes were single-symbol ML decodable only when there were four relays and they could not achieve the full diversity order in an arbitrary signal constellation. In [28], Jing *et al.* applied the orthogonal and quasi-orthogonal designs in cooperative networks and they analyzed the diversity order of the codes. The authors of [28] claimed that the codes achieved the single-symbol ML decodability as long as the noises at the destination were uncorrelated. However, we noticed that the rate-$3/4$ code given in [28] was actually not single-symbol ML decodable, although it generated uncorrelated noises at the destination. Actually in this chapter, we will show that, when the noises are uncorrelated, the codes have to satisfy another constraint in order to be single-symbol ML decodable.

Only very recently, the DSTBCs achieving the single-symbol ML decodability have

been studied. In Chapter 2, we considered a cooperative network working in the amplify-and-forward mode, where every relay amplified the received signals from the source and then forwarded them to the destination. We proposed the distributed orthogonal space-time block codes (DOSTBCs), and we showed that the DOSTBCs achieved the single-symbol ML decodability and the full diversity order. Moreover, we systematically studied some special DOSTBCs, namely the row-monomial DOSTBCs, which generated uncorrelated noises at the destination. Specifically, an upper bound of the data-rate of the row-monomial DOSTBC was derived. This upper bound suggested that the row-monomial DOSTBCs had approximately twice higher bandwidth efficiency than the repetition-based cooperative strategy. In Chapter 2, however, we imposed two limitations on the row-monomial DOSTBCs, in order to simplify the analysis. The first one was that the associated matrices of the codes must be row-monomial, which ensured uncorrelated noises at the destination. The other was the assumption that the relays did not have any channel state information (CSI) of the channels from the source to the relays, i.e. the channels of the first-hop. Actually, since we assumed the destination had the CSI of the channels from the source to the relays and the channels from the relays to the destination in Chapter 2, the CSI of the first-hop channels could be easily obtained at the relays without requiring additional pilot signals or any feedback overhead.[4] But, it is still unknown what impact those two limitations have on the data-rate of the codes. This has motivated our work.

In this chapter, we first abandon the row-monomial limitation; but keep the CSI limitation. That is, we consider the DOSTBCs where the noises at the destination are possibly

[4]In order to make the destination have the CSI of the channels from the source to the relays and the channels from the relays to the destination, the source needs to broadcast pilot signals to the relays and the relays need to forward these pilot signals to the destination. If the relays are equipped with channel estimation devices, they can estimate the channels from the source to themselves based on the pilot signals broadcasted by the source. This does not require any additional pilot signals or any feedback overhead.

correlated and the relays do not have any CSI of the first-hop channels. By deriving an upper bound of the data-rate of the DOSTBC, we show that the data-rate cannot be substantially improved from the row-monomial DOSTBCs by removing the row-monomial limitation. Like the row-monomial DOSTBCs, the DOSTBCs may not have good bandwidth efficiency in a cooperative network with many relays, because the upper bound of the data-rate of the DOSTBC decreases with the number K of relays. Secondly, we remove the CSI limitation; but keep the row-monomial limitation. Specifically, the relays know the channel phase information (CPI) of the first-hop channels and use this information in the code construction. Those codes are referred to as the *row-monomial DOSTBCs with CPI* (DOSTBCs-CPI). We derive an upper bound of the data-rate of the row-monomial DOSTBC-CPI and also find the actual codes achieving this upper bound. The upper bound of the data-rate of the row-monomial DOSTBC-CPI is higher than those of the DOSTBCs and the row-monomial DOSTBCs. Thus, the row-monomial DOSTBCs-CPI have better bandwidth efficiency than the DOSTBCs and the row-monomial DOSTBCs. Furthermore, the upper bound of the data-rate of the row-monomial DOSTBC-CPI is independent of the number K of relays, which ensures the codes have good bandwidth efficiency even when there are many relays.

The rest of this chapter is organized as follows. In Section 3.2, we remove the row-monomial limitation; but the relays do not have any CSI. Specifically, we study the DOSTBCs and derive an upper bound of the data-rate of the DOSTBC. In Section 3.3, the relays exploit the CPI to construct the codes; but the row-monomial limitation is maintained. Specifically, we first define the row-monomial DOSTBCs-CPI and then derive an upper bound of the data-rate of the row-monomial DOSTBC-CPI. We present some numerical results in Section 3.4 and conclude this chapter in Section 3.5.

Notations: Bold upper and lower letters denote matrices and row vectors, respectively.

Also, diag$[x_1,\cdots,x_K]$ denotes the $K\times K$ diagonal matrix with $x_1,\cdots,x_K$ on its main diagonal; $\mathbf{0}_{k_1\times k_2}$ the $k_1\times k_2$ all-zero matrix; $\boldsymbol{I}_{T\times T}$ the $T\times T$ identity matrix; det$(\cdot)$ the determinant of a matrix; $[\cdot]_k$ the k-th entry of a vector; $[\cdot]_{k_1,k_2}$ the (k_1,k_2)-th entry of a matrix; $(\cdot)^*$ the complex conjugate; $(\cdot)^H$ the Hermitian; $(\cdot)^T$ the transpose. Let $\boldsymbol{X}=[\boldsymbol{x}_1;\cdots;\boldsymbol{x}_K]$ denote the matrix with $\boldsymbol{x}_k$ as its k-th row, $1\leq k\leq K$. For a real number a, $\lceil a\rceil$ denotes the ceiling function of a.

3.2 Distributed Orthogonal Space-Time Block Codes

In this section, we study the DOSTBCs. Specifically, we abandon the row-monomial limitation, which was adopted in the construction of the row-monomial DOSTBCs in Chapter 2. Thus, the DOSTBCs possibly generate correlated noises at the destination. However, we still keep the CSI limitation, i.e. the relays do not have any CSI. The system model of the DOSTBCs is presented first. Then we derive an upper bound of the data-rate of the DOSTBC.

3.2.1 System Model of the DOSTBCs

Consider a cooperative network with one source, K relays, and one destination. Every terminal has only one antenna and is half-duplex. Denote the channel from the source to the k-th relay by h_k and the channel from the k-th relay to the destination by f_k, where h_k and f_k are spatially uncorrelated complex Gaussian random variables with zero mean and unit variance. We assume that the destination has full CSI, i.e. it knows the instantaneous values of h_k and f_k by using pilot signals. We also assume that there is no direct link between the source and destination. The same assumption has been made in many previous publications [27, 28, 36, 68]

At the beginning, the source transmits N complex-valued information-bearing symbols over N consecutive time slots. If the information-bearing symbols are real-valued, the construction of the single-symbol ML decodable DSTBCs has been solved in [25]. For this special case, Hua *et al.* showed that the rate-one real orthogonal design proposed by [56] could be used in the cooperative networks without any changes. Furthermore, the codes achieved the full diversity order. Therefore, in this chapter, we focus on the complex-valued symbols, which is more general than the work in [25]. Let $\boldsymbol{s} = [s_1, \cdots, s_N]$ denote the information-bearing symbol vector transmitted from the source, where the power of s_n is E_s. Assume the coherence time of h_k is larger than N; then the received signal vector $\boldsymbol{y}_k$ at the k-th relay is $\boldsymbol{y}_k = h_k\boldsymbol{s} + \boldsymbol{n}_k$, where $\boldsymbol{n}_k = [n_{k,1}, \cdots, n_{k,N}]$ is the additive noise at the k-th relay and it is uncorrelated complex Gaussian with zero mean and identity covariance matrix. All the relays are working in the amplify-and-forward mode and the amplifying coefficient ρ is $\sqrt{E_r/(1+E_s)}$ for every relay, where E_r is the transmission power at every relay. We set $\rho = \sqrt{E_r/(1+E_s)}$ as in many previous publications including [27,28,41,43]. This ensures the average transmission power of every relay is E_r in the long term. Based on the received signal vector $\boldsymbol{y}_k$, the k-th relay produces a transmitted signal vector and forwards it to the destination.

In this section, we assume that the k-th relay has no CSI of the first-hop channels. This can be true when the relays do not have any channel estimation devices due to strict power and/or size constraints. Note that, even when the relays cannot estimate the channels, the destination is still able to obtain the full CSI. This is because the destination usually dose not have any power or size limitation, and hence, it can be equipped with sophisticated channel estimation devices. Furthermore, although the relays cannot estimate the channels, they can forward the pilot signals from the source to the destination, and they can transmit their own pilot signals to the destination. Based on those pilot signals, the destination is

able to obtain the full CSI, which has been discussed in [25, 66].

The k-th relay produces the transmitted signal vector $\boldsymbol{x}_k^D$ as follows:

$$\begin{aligned} \boldsymbol{x}_k^D &= \rho(\boldsymbol{y}_k \boldsymbol{A}_k + \boldsymbol{y}_k^* \boldsymbol{B}_k) \\ &= \rho h_k \boldsymbol{s} \boldsymbol{A}_k + \rho h_k^* \boldsymbol{s}^* \boldsymbol{B}_k + \rho \boldsymbol{n}_k \boldsymbol{A}_k + \rho \boldsymbol{n}_k^* \boldsymbol{B}_k. \end{aligned} \tag{3.1}$$

The matrices $\boldsymbol{A}_k$ and $\boldsymbol{B}_k$ are called the associated matrices. They have the dimension of $N \times T$ and their properties will be discussed in detail later. Assume the coherence time of f_k is larger than T. Furthermore, perfect synchronization among the relays is assumed as in [16, 27, 68], and [25, 28, 43]. Although synchronization is a critical issue for the practical implementation of cooperative networks, it is beyond the scope of this chapter. The received signal vector at the destination is given by

$$\begin{aligned} \boldsymbol{y}_D &= \sum_{k=1}^{K} f_k \boldsymbol{x}_k^D + \boldsymbol{n}_d \\ &= \sum_{k=1}^{K} (\rho f_k h_k \boldsymbol{s} \boldsymbol{A}_k + \rho f_k h_k^* \boldsymbol{s}^* \boldsymbol{B}_k) + \sum_{k=1}^{K} (\rho f_k \boldsymbol{n}_k \boldsymbol{A}_k + \rho f_k \boldsymbol{n}_k^* \boldsymbol{B}_k) + \boldsymbol{n}_d, \end{aligned} \tag{3.2}$$

where $\boldsymbol{n}_d = [n_{d,1}, \cdots, n_{d,T}]$ is the additive noise at the destination and it is uncorrelated complex Gaussian with zero mean and identity covariance matrix. Define $\boldsymbol{w}_D$, $\boldsymbol{X}_D$, and $\boldsymbol{n}_D$ as follows:

$$\boldsymbol{w}_D = [\rho f_1, \cdots, \rho f_K] \tag{3.3}$$

$$\boldsymbol{X}_D = [h_1 \boldsymbol{s} \boldsymbol{A}_1 + h_1^* \boldsymbol{s}^* \boldsymbol{B}_1; \cdots; h_K \boldsymbol{s} \boldsymbol{A}_K + h_K^* \boldsymbol{s}^* \boldsymbol{B}_K] \tag{3.4}$$

$$\boldsymbol{n}_D = \sum_{k=1}^{K} (\rho f_k \boldsymbol{n}_k \boldsymbol{A}_k + \rho f_k \boldsymbol{n}_k^* \boldsymbol{B}_k) + \boldsymbol{n}_d; \tag{3.5}$$

then we can rewrite (3.2) in the following way

$$\boldsymbol{y}_D = \boldsymbol{w}_D \boldsymbol{X}_D + \boldsymbol{n}_D. \tag{3.6}$$

Furthermore, from (3.5), it is easy to see that the mean of $\boldsymbol{n}_D$ is zero and the covariance

matrix $\boldsymbol{R}$ of $\boldsymbol{n}_D$ is given by

$$\boldsymbol{R} = \sum_{k=1}^{K} \left(|\rho f_k|^2 \left(\boldsymbol{A}_k^H \boldsymbol{A}_k + \boldsymbol{B}_k^H \boldsymbol{B}_k \right) \right) + \boldsymbol{I}. \tag{3.7}$$

3.2.2 Upper Bound of the Data-Rate of the DOSTBC

The definition of the DOSTBCs was proposed in Chapter 2 and it is as follows:

Definition 3.1: A $K \times T$ code matrix $\boldsymbol{X}_D$ is called a DOSTBC in variables $s_1, \cdots, s_N$ if the following two conditions are satisfied:

D3.1.1) The entries of $\boldsymbol{X}_D$ are 0, $\pm h_k s_n$, $\pm h_k^* s_n^*$, or multiples of these indeterminates by **j**, where $\mathbf{j} = \sqrt{-1}$.

D3.1.2) The matrix $\boldsymbol{X}_D$ satisfies the following equality

$$\boldsymbol{X}_D \boldsymbol{R}^{-1} \boldsymbol{X}_D^H = |s_1|^2 \boldsymbol{D}_1 + \cdots + |s_N|^2 \boldsymbol{D}_N, \tag{3.8}$$

where $\boldsymbol{D}_n = \text{diag}[|h_1|^2 D_{n,1}, \cdots, |h_K|^2 D_{n,K}]$ and $D_{n,1}, \cdots, D_{n,K}$ are non-zero.

Note that Definition 3.1 actually defines a subset of all the single-symbol ML decodable DSTBCs. This is because condition D3.1.1 constrains that the entries of $\boldsymbol{X}_D$ can only be 0, $\pm h_k s_n$, $\pm h_k^* s_n^*$, or multiples of these indeterminates by **j**. The upper bound derived in Theorem 3.2 only applies to the codes in this subset. One can relax condition D3.1.1 and define more general single-symbol ML decodable DSTBCs. For example, one can use the generalized coordinate interleaved orthogonal designs and clifford unitary weight codes in cooperative networks.

In Chapter 2, it has been shown that the DOSTBCs are single-symbol ML decodable and achieve the full diversity order K. However, the data-rate of the DOSTBC has not been

analyzed in Chapter 2. In the following, we derive an upper bound of the data-rate of the DOSTBC. To this end, one may think of redefining $\boldsymbol{w}_D$ and $\boldsymbol{X}_D$ as follows

$$\boldsymbol{w}_D = [\rho f_1|h_1|, \cdots, \rho f_K|h_K|] \tag{3.9}$$

$$\boldsymbol{X}_D = [s\tilde{\boldsymbol{A}}_1 + s^*\tilde{\boldsymbol{B}}_1; \cdots; s\tilde{\boldsymbol{A}}_K + s^*\tilde{\boldsymbol{B}}_K], \tag{3.10}$$

where $\tilde{\boldsymbol{A}}_k = e^{j\theta_k}\boldsymbol{A}_k$ and $\tilde{\boldsymbol{B}}_k = e^{-j\theta_k}\boldsymbol{B}_k$. Then $\boldsymbol{X}_D$ can be seen as the generalized orthogonal designs, and hence, the results in [61] may be directly used. Actually, this method will make the analysis more complicated. Note that the new associated matrices $\tilde{\boldsymbol{A}}_k$ and $\tilde{\boldsymbol{B}}_k$ have a fundamental difference with the associated matrices of the generalized orthogonal design in [61]. That is, $\tilde{\boldsymbol{A}}_k$ and $\tilde{\boldsymbol{B}}_k$ contain θ_k, which is a random variable. Due to this reason, it is very hard to find the properties of $\tilde{\boldsymbol{A}}_k$ and $\tilde{\boldsymbol{B}}_k$ by using the results in [61], and hence, it is very complicated to derive an upper bound by using (3.9) and (3.10). Instead of this approach, in this chapter, we define $\boldsymbol{w}_D$ and $\boldsymbol{X}_D$ as in (3.3) and (3.4), respectively, and derive an upper bound of the data-rate by analyzing the properties of $\boldsymbol{A}_k$ and $\boldsymbol{B}_k$. Some fundamental properties of $\boldsymbol{A}_k$ and $\boldsymbol{B}_k$ are given in the following lemma at first.

Lemma 3.1. *If a DOSTBC $\boldsymbol{X}_D$ in variables $s_1, \cdots, s_N$ exists, its associated matrices $\boldsymbol{A}_k$, $\boldsymbol{B}_k$, and $\boldsymbol{A}_k + \boldsymbol{B}_k$ are column-monomial. Furthermore, the orthogonal condition (3.8) on $\boldsymbol{X}_D$ holds if and only if*

$$\boldsymbol{A}_{k_1}\boldsymbol{R}^{-1}\boldsymbol{A}_{k_2}^H = \boldsymbol{0}, \qquad k_1 \neq k_2 \tag{3.11}$$

$$\boldsymbol{B}_{k_1}\boldsymbol{R}^{-1}\boldsymbol{B}_{k_2}^H = \boldsymbol{0}, \qquad k_1 \neq k_2 \tag{3.12}$$

$$\boldsymbol{A}_{k_1}\boldsymbol{R}^{-1}\boldsymbol{B}_{k_2}^H + \boldsymbol{B}_{k_2}^*\boldsymbol{R}^{-1}\boldsymbol{A}_{k_1}^T = \boldsymbol{0}, \tag{3.13}$$

$$\boldsymbol{B}_{k_1}\boldsymbol{R}^{-1}\boldsymbol{A}_{k_2}^H + \boldsymbol{A}_{k_2}^*\boldsymbol{R}^{-1}\boldsymbol{B}_{k_1}^T = \boldsymbol{0}, \tag{3.14}$$

$$\boldsymbol{A}_k\boldsymbol{R}^{-1}\boldsymbol{A}_k^H + \boldsymbol{B}_k^*\boldsymbol{R}^{-1}\boldsymbol{B}_k^T = \mathrm{diag}[D_{1,k}, \cdots, D_{N,k}]. \tag{3.15}$$

Proof: See Appendix 3-A. ■

Lemma 3.1 gives us some fundamental properties of $\boldsymbol{A}_k$ and $\boldsymbol{B}_k$. However, due to the existence of $\boldsymbol{R}^{-1}$, we cannot obtain an upper bound by using the conditions (3.11)–(3.15) directly. Therefore, we simplify those conditions in the following theorem by eliminating $\boldsymbol{R}^{-1}$.

Theorem 3.1. *If a DOSTBC $\boldsymbol{X}_D$ in variables $s_1, \cdots, s_N$ exists, we have*

$$\boldsymbol{X}_D \boldsymbol{X}_D^H = |s_1|^2 \boldsymbol{E}_1 + \cdots + |s_N|^2 \boldsymbol{E}_N, \tag{3.16}$$

where $\boldsymbol{E}_n = \mathrm{diag}[|h_1|^2 E_{n,1}, \cdots, |h_K|^2 E_{n,K}]$ and $E_{n,1}, \cdots, E_{n,K}$ are strictly positive. Equivalently, the associated matrices $\boldsymbol{A}_k$ and $\boldsymbol{B}_k$ satisfy the following conditions

$$\boldsymbol{A}_{k_1} \boldsymbol{A}_{k_2}^H = \boldsymbol{0}, \qquad k_1 \neq k_2 \tag{3.17}$$

$$\boldsymbol{B}_{k_1} \boldsymbol{B}_{k_2}^H = \boldsymbol{0}, \qquad k_1 \neq k_2 \tag{3.18}$$

$$\boldsymbol{A}_{k_1} \boldsymbol{B}_{k_2}^H + \boldsymbol{B}_{k_2}^* \boldsymbol{A}_{k_1}^T = \boldsymbol{0} \tag{3.19}$$

$$\boldsymbol{B}_{k_1} \boldsymbol{A}_{k_2}^H + \boldsymbol{A}_{k_2}^* \boldsymbol{B}_{k_1}^T = \boldsymbol{0} \tag{3.20}$$

$$\boldsymbol{A}_k \boldsymbol{A}_k^H + \boldsymbol{B}_k^* \boldsymbol{B}_k^T = \mathrm{diag}[E_{1,k}, \cdots, E_{N,k}]. \tag{3.21}$$

Proof: See Appendix 3-B. ■

After comparing Theorem 3.1 and the definition of the generalized orthogonal design in [61], it seems that the DOSTBCs represent subset of the generalized orthogonal design. However, note that there is a fundamental difference between the DOSTBCs and the generalized orthogonal design. That is, the code matrix $\boldsymbol{X}_D$ of a DOSTBC contains the channel coefficients h_k. Actually, this fundamental difference explains why $\tilde{\boldsymbol{A}}_k$ and $\tilde{\boldsymbol{B}}_k$ in (3.10) contain θ_k. Furthermore, this fundamental difference induces the conditions (3.17) and (3.18). Those two conditions help derive an upper bound of the data-rate of the DOSTBC in the following theorem.

Theorem 3.2. *If a DOSTBC $\boldsymbol{X}_D$ in variables $s_1, \cdots, s_N$ exists, its data-rate $\mathscr{R}_D$ satisfies the following inequality:*

$$\mathscr{R}_D = \frac{N}{T} \leq \frac{N}{\lceil \frac{NK}{2} \rceil}. \tag{3.22}$$

Proof: See Appendix 3-C. ■

Theorem 3.2 suggests that the DOSTBCs have approximately twice higher bandwidth efficiency than the repetition-based cooperative strategy. It is worthy of mentioning that the DOSTBCs have the same decoding complexity and diversity order as the repetition-based cooperative strategy. For comparison, we restate the upper bound of the data-rate $\mathscr{R}_R$ of the row-monomial DOSTBC here

$$\mathscr{R}_R = \frac{N}{T} \leq \begin{cases} \frac{1}{m}, & \text{when} \quad N = 2l, K = 2m \\ \frac{2l+1}{2lm+2m}, & \text{when} \quad N = 2l+1, K = 2m \\ \frac{1}{m+1}, & \text{when} \quad N = 2l, K = 2m+1 \\ \min\left(\frac{2l+1}{2lm+2m+l+1}, \frac{2l+1}{2lm+2l+m+1}\right) & \text{when} \quad N = 2l+1, K = 2m+1 \end{cases}. \tag{3.23}$$

When N and K are even, the upper bounds of (3.22) and (3.23) both equal to $2/K$. Thus, for this case, the data-rate cannot be improved from the row-monomial DOSTBCs by removing the row-monomial limitation. Furthermore, we can construct the DOSTBCs achieving the upper bound $2/K$ by using the systematic construction method proposed in Chapter 2. When K is even and N is odd, the upper bound (3.22) is equal to $2/K$ as well. Thus, the highest data-rate the codes can achieve is $2/K$ and the delay of such codes is $NK/2$. On the other hand, if we reduce the value of N by 1, the upper bound becomes $(N-1)/\lceil (N-1)K/2 \rceil$, which is equal to $2/K$. The highest data-rate of the codes is still $2/K$, but the delay of the codes is reduced to $(N-1)K/2$, which is smaller than $NK/2$. Furthermore, after reducing N by 1, the value of $N-1$ is even and we can construct the actual codes achieving the upper bound $2/K$ by using the systematic construction method proposed in Chapter 2. Therefore, when K is even and N is odd, we should always reduce N by 1

first and then we can construct the actual DOSTBCs achieving the upper bound (3.22). However, when K is odd, we cannot find any DOSTBCs achieving the upper bound (3.22).

Like the row-monomial DOSTBCs, the DOSTBCs may have poor bandwidth efficiency, when there are many relays. This is because the upper bound (3.22) decreases with the number K of relays. This problem can be solved very well when the relays can exploit the CPI to construct the codes, which will be shown in the next section.

3.3 Row-Monomial Distributed Orthogonal Space-Time Block Codes with Channel Phase Information

In this section, we investigate the row-monomial DOSTBCs-CPI. Specifically, we remove the CSI limitation and assume the relays use the CPI to construct the codes. But, we still keep the row-monomial limitation, in order to facilitate the analysis. The system model of the row-monomial DOSTBCs-CPI is described first. Then we derive an upper bound of the data-rate of the row-monomial DOSTBC-CPI and construct the actual codes achieving this upper bound.

3.3.1 System Model of the Row-Monomial DOSTBCs-CPI

The system model of the row-monomial DOSTBCs-CPI is similar to that of the DOSTBCs, which was given in Subsection 3.2.1. The information-bearing symbol vector is given by $\boldsymbol{s} = [s_1, \cdots, s_N]$ and the received signal vector at the k-th relay is $\boldsymbol{y}_k = h_k \boldsymbol{s} + \boldsymbol{n}_k$. We still choose the amplify coefficient as $\rho = \sqrt{E_r/(1+E_s)}$. In this section, however, we assume that there is no strict power or size constraint on the relays and the relays can obtain partial CSI of the first-hop channels by the equipped channel estimation devices. Specifically, we assume the k-th relay has the CPI of the first-hop channels, i.e. it knows the phase θ_k of

the channel coefficient h_k. Note that this assumption does not imply more pilot signals compared to the assumption that relays have no CSI of the first-hop channels. Actually, in order to make the destination have full CSI, the relays always need to forward the pilot signals from the source to the relays. Furthermore, the relays always need to transmit their own pilot signals to the destination. Therefore, the same number of pilot signals is needed in all circumstances. Furthermore, the assumption that the relays have the CPI of the first-hop channels does not imply any feedback overhead, because the relays do not need to have any CSI of the channels from themselves to the destination.

Based on the CPI, the k-th relay first obtains $\boldsymbol{y}_k^C$ by $\boldsymbol{y}_k^C = e^{-j\theta_k}\boldsymbol{y}_k$ and then builds the transmitted signal vector $\boldsymbol{x}_k^C$ as

$$\begin{aligned} \boldsymbol{x}_k^C &= \rho(\boldsymbol{y}_k^C\boldsymbol{A}_k + \boldsymbol{y}_k^{C*}\boldsymbol{B}_k) \\ &= \rho|h_k|\boldsymbol{s}\boldsymbol{A}_k + \rho|h_k|\boldsymbol{s}^*\boldsymbol{B}_k + \rho e^{-j\theta_k}\boldsymbol{n}_k\boldsymbol{A}_k + \rho e^{j\theta_k}\boldsymbol{n}_k^*\boldsymbol{B}_k. \end{aligned} \tag{3.24}$$

Consequently, the received signal vector at the destination is given by

$$\boldsymbol{y}_C = \boldsymbol{w}_C\boldsymbol{X}_C + \boldsymbol{n}_C, \tag{3.25}$$

where

$$\boldsymbol{w}_C = [\rho f_1|h_1|, \cdots, \rho f_K|h_K|] \tag{3.26}$$

$$\boldsymbol{X}_C = [\boldsymbol{s}\boldsymbol{A}_1 + \boldsymbol{s}^*\boldsymbol{B}_1; \cdots; \boldsymbol{s}\boldsymbol{A}_K + \boldsymbol{s}^*\boldsymbol{B}_K] \tag{3.27}$$

$$\boldsymbol{n}_C = \sum_{k=1}^{K}(\rho f_k e^{-j\theta_k}\boldsymbol{n}_k\boldsymbol{A}_k + \rho f_k e^{j\theta_k}\boldsymbol{n}_k^*\boldsymbol{B}_k) + \boldsymbol{n}_d. \tag{3.28}$$

From (3.28), it is easy to see that the mean of $\boldsymbol{n}_C$ is zero and the covariance matrix $\boldsymbol{R}$ of $\boldsymbol{n}_C$ is still given by (3.7).

3.3.2 Upper Bound of the Data-Rate of the Row-Monomial DOSTBC-CPI

We define the row-monomial DOSTBCs-CPI in the following way.

Definition 3.2: A $K \times T$ code matrix $\boldsymbol{X}_C$ is called a row-monomial DOSTBC-CPI in variables $s_1, \cdots, s_N$ if the following three conditions are satisfied:

D3.2.1) The entries of $\boldsymbol{X}_C$ are 0, $\pm s_n$, $\pm s_n^*$, or multiples of these indeterminates by **j**.

D3.2.2) The matrix $\boldsymbol{X}_C$ satisfies the following equality

$$\boldsymbol{X}_C \boldsymbol{R}^{-1} \boldsymbol{X}_C^H = |s_1|^2 \boldsymbol{F}_1 + \cdots + |s_N|^2 \boldsymbol{F}_N, \tag{3.29}$$

where $\boldsymbol{F}_n = \text{diag}[F_{n,1}, \cdots, F_{n,K}]$ and $F_{n,1}, \cdots, F_{n,K}$ are non-zero.

D3.2.3) The associated matrices $\boldsymbol{A}_k$ and $\boldsymbol{B}_k$, $1 \leq k \leq K$, are all row-monomial.

It should be noted that Definition 3.2 actually defines a subset of all the single-symbol ML decodable DSTBCs and the upper bound derived in Theorem 3.5 only applies to the codes in this subset. One can define more general single-symbol ML decodable DSTBCs by following the approach in [31]. For example, in [43,54], the authors proposed more general single-symbol ML decodable DSTBCs based on the generalized coordinate interleaved orthogonal designs.[5]

[5] In [54], Sreedhar *et al.* found a rate-one code and it had a higher data-rate than the row-monomial DOSTBCs-CPI. However, this code was only for $K = 4$. For other values of K, the authors did not find any codes that had higher data-rates than the row-monomial DOSTBCs-CPI. Actually, the authors of [54] did not attempt to derive the upper bound of the data-rate of the single-symbol ML decodable DSTBCs. Furthermore, the rate-one code in [54] could achieve the full diversity order only in a specially designed constellation.

Condition D3.2.2 in Definition 3.2 ensures that the row-monomial DOSTBCs-CPI are single-symbol ML decodable. The following Lemma shows that the row-monomial DOSTBCs-CPI achieve the full diversity order.

Lemma 3.2. *Assume $T \geq K$, $E_r = c_r E$, and $E_s = c_s E$, where c_r and c_s are positive constants. The row-monomial DOSTBCs-CPI can achieve the full diversity order K.*

Proof: See Appendix 3-D. ■

Furthermore, we can show that a row-monomial DOSTBC-CPI $\boldsymbol{X}_C$ satisfies the following equality

$$\boldsymbol{X}_C \boldsymbol{X}_C^H = |s_1|^2 \boldsymbol{G}_1 + \cdots + |s_N|^2 \boldsymbol{G}_N, \tag{3.30}$$

where $\boldsymbol{G}_n = \text{diag}[G_{n,1}, \cdots, G_{n,K}]$ and $G_{n,1}, \cdots, G_{n,K}$ are strictly positive. The proof is based on evaluating $[\boldsymbol{R}]_{t_1,t_2}$ and it follows exactly the same way as the proofs of Lemma 3.1 and Theorem 3.1. Note that the code matrix $\boldsymbol{X}_C$ of a row-monomial DOSTBC-CPI does not contain any channel coefficients. By comparing (3.30) and the definition of the generalized orthogonal design, we notice that a row-monomial DOSTBC-CPI must be a generalized orthogonal design. All the analyses of the generalized orthogonal design in [61] are valid for the row-monomial DOSTBCs-CPI. In particular, when $K = 2$, the data-rate of the row-monomial DOSTBC-CPI can be as large as one using the Alamouti code proposed in [1]; when $K > 2$, the data-rate of the row-monomial DOSTBC-CPI is upper-bounded by $4/5$, which is the upper bound of the data-rate of the generalized orthogonal design [61].

Actually, the row-monomial DOSTBCs-CPI have some unique properties which the generalized orthogonal design does not have. Those unique properties help find a tighter upper bound of the data-rate of the row-monomial DOSTBC-CPI. To this end, we first have the following theorem.

Theorem 3.3. *Assume $\boldsymbol{X}_C$ is a DSTBC in variables $s_1, \cdots, s_N$, i.e. every row of $\boldsymbol{X}_C$ contains the information-bearing symbols $s_1, \cdots, s_N$. Moreover, assume that the noise covariance matrix $\boldsymbol{R}$ of $\boldsymbol{X}_C$ is diagonal. Let W denote the number of distinct main diagonal entries in $\boldsymbol{R}^{-1}$. After proper column permutations, we can partition $\boldsymbol{R}^{-1}$ into $\boldsymbol{R}^{-1} = \text{diag}[\boldsymbol{R}_1, \boldsymbol{R}_2, \cdots, \boldsymbol{R}_W]$ such that the main diagonal entries of $\boldsymbol{R}_w$ are all equal to R_w and $R_i \neq R_j$ for $i \neq j$. By the same column permutations, we can partition $\boldsymbol{X}_C$ into W sub-matrices and let $\boldsymbol{X}_{Cw}$ denote the non-zero rows in the w-th sub-matrix.*[6] *Assume that $\boldsymbol{X}_{Cw}$ contains N_w different information-bearing symbols and they are $s_1^w, \cdots, s_{N_w}^w$.*[7] *Then $\boldsymbol{X}_C$ is a row-monomial DOSTBC-CPI if and only if every sub-matrix $\boldsymbol{X}_{Cw}$ is a row-monomial DOSTBC-CPI in variables $s_1^w, \cdots, s_{N_w}^w$.*

Proof: See Appendix 3-E. ■

Theorem 3.3 means that, when a DSTBC $\boldsymbol{X}_C$ generates uncorrelated noises at the destination, the code is single-symbol ML decodable as long as it can be partitioned into several single-symbol ML decodable codes. We can use this theorem to show that the rate-$3/4$ code in [28] is not single-symbol ML decodable. The rate-$3/4$ code generates uncorrelated noises at the destination; but the main diagonal entries of $\boldsymbol{R}$ are all different. If we partition the rate-$3/4$ code in the way presented in Theorem 3.3, we will see that every sub-matrix $\boldsymbol{X}_{Cw}$ is actually a column vector. Thus, $\boldsymbol{X}_{Cw}$ cannot be a row-monomial DOSTBC-CPI, and hence, it is not single-symbol ML decodable. By Theorem 3.3, the rate-$3/4$ code cannot be a row-monomial DOSTBC-CPI either and it is not single-symbol ML decodable.

[6] As an example, if $\boldsymbol{X}_C = \begin{bmatrix} s_1 & -s_2 & 0 & 0 \\ s_2^* & s_1^* & 0 & 0 \\ 0 & 0 & s_1 & s_2 \end{bmatrix}$, we have $W = 2$, $\boldsymbol{R}_1 = \text{diag}[1 + |\rho f_1|^2 + |\rho f_2|^2, 1 + |\rho f_1|^2 + |\rho f_2|^2]$, $\boldsymbol{R}_2 = \text{diag}[1 + |\rho f_3|^2, 1 + |\rho f_3|^2]$, $\boldsymbol{X}_{C1} = \begin{bmatrix} s_1 & -s_2 \\ s_2^* & s_1^* \end{bmatrix}$, and $\boldsymbol{X}_{C2} = [s_1 \;\; s_2]$.

[7] Note that $s_1^w, \cdots, s_{N_w}^w$ are all from the set $\boldsymbol{s} = [s_1, \cdots, s_N]$.

Theorem 3.3 is crucial to derive an upper bound of the data-rate of the row-monomial DOSTBC-CPI. This is because it enables us to analyze the data-rate of every individual sub-matrix $\boldsymbol{X}_{Cw}$ instead of $\boldsymbol{X}_C$ itself. When $\boldsymbol{X}_{Cw}$ has one or two rows, its data-rate can be as large as one by using the Alamouti code. When $\boldsymbol{X}_{Cw}$ has more than two rows, the following theorem shows that the data-rate of $\boldsymbol{X}_{Cw}$ is exactly $1/2$.

Theorem 3.4. *Assume $\boldsymbol{X}_C$ is a row-monomial DOSTBC-CPI and its noise covariance matrix is $\boldsymbol{R}$. Let W denote the number of distinct main diagonal entries in $\boldsymbol{R}^{-1}$. After proper column permutations, we can partition $\boldsymbol{R}^{-1}$ into $\boldsymbol{R}^{-1} = \mathrm{diag}[\boldsymbol{R}_1, \boldsymbol{R}_2, \cdots, \boldsymbol{R}_W]$ such that the main diagonal entries of $\boldsymbol{R}_w$ are all equal to R_w and $R_i \neq R_j$ for $i \neq j$. By the same column permutations, we can partition $\boldsymbol{X}_C$ into W sub-matrices and let $\boldsymbol{X}_{Cw}$ denote the non-zero rows in the w-th sub-matrix. Assume the dimension of $\boldsymbol{X}_{Cw}$ is $K_w \times T_w$. Then the data-rate of $\boldsymbol{X}_{Cw}$ is exactly $1/2$ when $K_w > 2$.*

Proof: See Appendix 3-F. ■

Based on Theorems 3.3 and 3.4, we derive an upper bound of the data-rate of the row-monomial DOSTBC-CPI in the following theorem.

Theorem 3.5. *When $K > 2$, the data-rate $\mathscr{R}_C$ of the row-monomial DOSTBC-CPI satisfies the following inequality*

$$\mathscr{R}_C = \frac{N}{T} \leq \frac{1}{2}. \tag{3.31}$$

Proof: See Appendix 3-G. ■

We notice that the data-rate of the row-monomial DOSTBC-CPI is independent of the number K of relays. Thus, the row-monomial DOSTBCs-CPI have good bandwidth efficiency even in a cooperative network with many relays. Furthermore, compared to the row-monomial DOSTBCs and the DOSTBCs, the row-monomial DOSTBCs-CPI improve the bandwidth efficiency considerably, especially when the cooperative network has a large

number of relays. This improvement is mainly because the relays exploit the CPI to construct the codes. As we have seen, because the code matrix $\boldsymbol{X}_D$ of a DOSTBC contains the channel coefficient h_k, the conditions (3.11) and (3.12) are induced. From (3.11) and (3.12), we obtain (3.17) and (3.18), and those two conditions severely constrain the data-rate of the DOSTBC. On the other hand, by exploiting the CPI, the code matrix $\boldsymbol{X}_C$ of a row-monomial DOSTBC-CPI does not have any channel coefficients. As a result, when $k_1 \neq k_2$, it follows from (3.29) that $[\boldsymbol{X}_C \boldsymbol{R}^{-1} \boldsymbol{X}_C^H]_{k_1,k_2}$ is given by

$$\begin{aligned}[\boldsymbol{X}_C \boldsymbol{R}^{-1} \boldsymbol{X}_C^H]_{k_1,k_2} &= \boldsymbol{s}(\boldsymbol{A}_{k_1} \boldsymbol{R}^{-1} \boldsymbol{A}_{k_2}^H + \boldsymbol{B}_{k_2}^* \boldsymbol{R}^{-1} \boldsymbol{B}_{k_1}^T)\boldsymbol{s}^H \\ &\quad + \boldsymbol{s}\boldsymbol{A}_{k_1} \boldsymbol{R}^{-1} \boldsymbol{B}_{k_2}^H \boldsymbol{s}^T + \boldsymbol{s}^* \boldsymbol{B}_{k_1} \boldsymbol{R}^{-1} \boldsymbol{A}_{k_2}^H \boldsymbol{s}^H \\ &= 0. \end{aligned} \tag{3.32}$$

By Lemma 1 of [38], we have the summation $\boldsymbol{A}_{k_1} \boldsymbol{R}^{-1} \boldsymbol{A}_{k_2}^H + \boldsymbol{B}_{k_2}^* \boldsymbol{R}^{-1} \boldsymbol{B}_{k_1}^T = 0$ instead of (3.11) and (3.12). Thus, the conditions (3.11), (3.12), (3.17), and (3.18) do not apply to the row-monomial DOSTBCs-CPI and the data-rate is greatly improved. Furthermore, recall that exploiting the CPI at the relays does not increase the pilot signals or require any feedback overhead. Compared to the DOSTBCs, the only extra cost of the row-monomial DOSTBCs-CPI is that the relays should be equipped with some channel estimation devices to estimate θ_k.

Interestingly, the row-monomial DOSTBCs-CPI achieving the upper bound $1/2$ are easy to construct and they are given in the following theorem.

Theorem 3.6. *The rate-halving codes developed in [56] can be used as the row-monomial DOSTBCs-CPI achieving the upper bound* $1/2$ *of the data-rate.*

Proof: See Appendix 3-H.[8] ■

[8] In [54], the authors also proved that the rate-halving codes achieved the single-symbol ML decodability when they were used in cooperative networks. However, the authors of [54] did not show that the upper

As an example, when $N = 4$ and $K = 4$, the row-monomial DOSTBC-CPI achieving the upper bound $1/2$ is given as follows:

$$\boldsymbol{X}_C = \begin{bmatrix} s_1 & -s_2 & -s_3 & -s_4 & s_1^* & -s_2^* & -s_3^* & -s_4^* \\ s_2 & s_1 & s_4 & -s_3 & s_2^* & s_1^* & s_4^* & -s_3^* \\ s_3 & -s_4 & s_1 & s_2 & s_3^* & -s_4^* & s_1^* & s_2^* \\ s_4 & s_3 & -s_2 & s_1 & s_4^* & s_3^* & -s_2^* & s_1^* \end{bmatrix}. \tag{3.33}$$

As future work, the row-monomial DOSTBCs-CPI may be extended in the following two ways. First, it will be very interesting to consider a more general case, where the noises at the destination are possibly correlated. Intuitively, such codes should have even higher data-rate than the row-monomial DOSTBCs-CPI. But, we conjecture that the improvement of the data-rate is just marginal. This is because, by comparing the DOSTBCs and the row-monomial DOSTBCs, we notice that removing the row-monomial limitation just slightly improves the data-rate. Secondly, we can assume that the relays have the full CSI, including not only the channel phase θ_k but also the channel magnitude $|h_k|$, of the first-hop channels and use this information in the code construction. We notice that the use of the channel magnitude $|h_k|$ only affects the structure of the noise covariance matrix $\boldsymbol{R}$; but it cannot change the structure of the code matrix $\boldsymbol{X}_C$. Therefore, we conjecture that the data-rate cannot be improved by assuming the relays have the full CSI of the first-hop channels.

3.4 Numerical Results

In this section, we present some numerical results to demonstrate the performance of the DOSTBCs and the row-monomial DOSTBCs-CPI. In our simulation, we define the average signal to noise ratio (SNR) per bit as the ratio of E_r to the logarithm of the size of

bound of the data-rate was $1/2$.

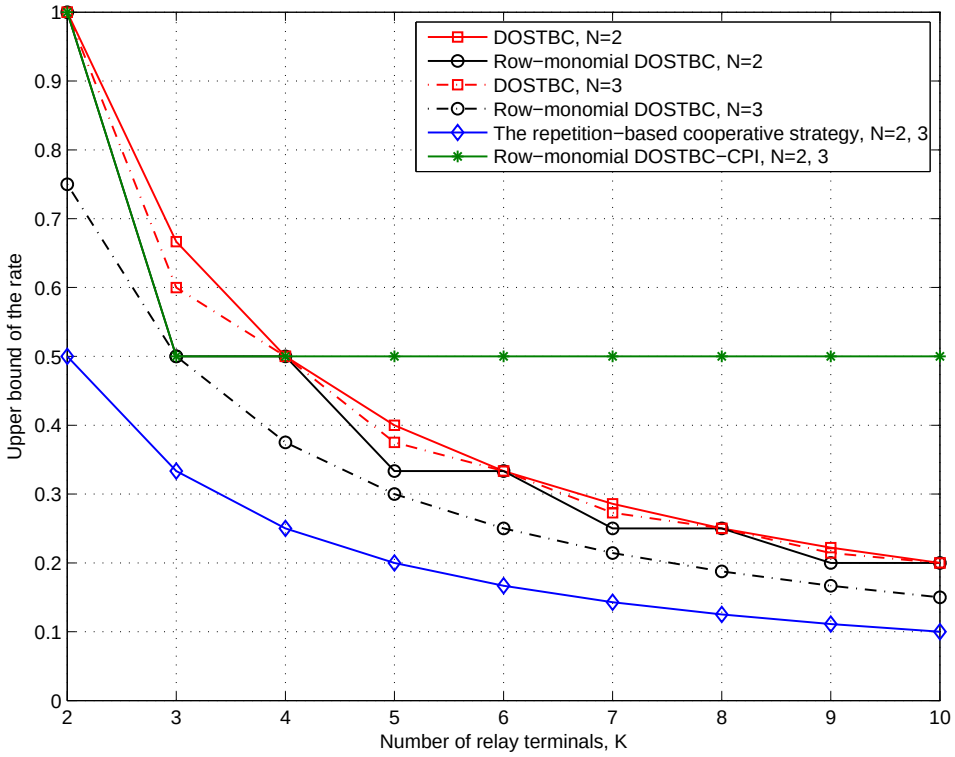

Figure 3.1. Comparison of the upper bounds of the data-rates of the DOSTBC, row-monomial DOSTBC, row-monomial DOSTBC-CPI, and repetition-based cooperative strategy, $N = 2, 3$.

the modulation scheme. We adopt the power allocation proposed in [27], i.e. $E_s = KE_r$. Moreover, We assume that wireless channels are uncorrelated Rayleigh fading channels.

In Fig. 3.1, we compare the upper bounds of the data-rates of the row-monomial DOSTBC, DOSTBC, row-monomial DOSTBC-CPI, and the repetition-based cooperative strategy. The row-monomial DOSTBCs, DOSTBCs, and row-monomial DOSTBCs-CPI all achieve better data-rates than the repetition-based cooperative strategy. Note that those DSTBCs have the same diversity order and decoding complexity as the repetition-based cooperative strategy. Among those DSTBCs, the row-monomial DOSTBC-CPI is the most attractive, because its data-rate does not decrease with K.

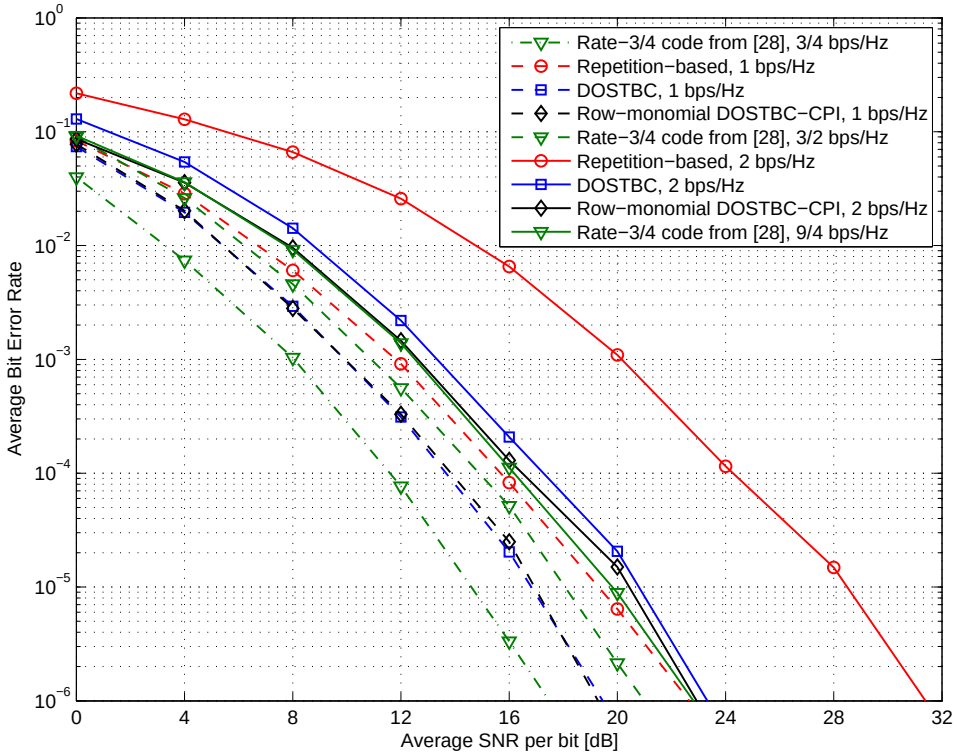

Figure 3.2. Comparison of the rate-$3/4$ code from [28], the DOSTBCs, the row-monomial DOSTBCs-CPI, and the repetition-based cooperative strategy, $N = 4$, $K = 4$.

In Fig. 3.2, we let $N = 4$ and $K = 4$. For this case, we see that the average BER performance of the DOSTBCs and the row-monomial DOSTBCs-CPI is much better than that of the repetition-based cooperative strategy, especially when the bandwidth efficiency is 2 bps/Hz. The DOSTBCs and the row-monomial DOSTBCs-CPI have almost the same performance. This is because, when $N = 4$ and $K = 4$, the DOSTBCs and the row-monomial DOSTBCs-CPI have the same data-rate $1/2$, and hence, they use the same modulation schemes. Fig. 3.2 also demonstrates that the performance of the DOSTBCs and the row-monomial DOSTBCs-CPI is slightly worse than that of the rate-$3/4$ code proposed in [28]. But, note that the rate-$3/4$ code is not single-symbol ML decodable, and hence, its decoding

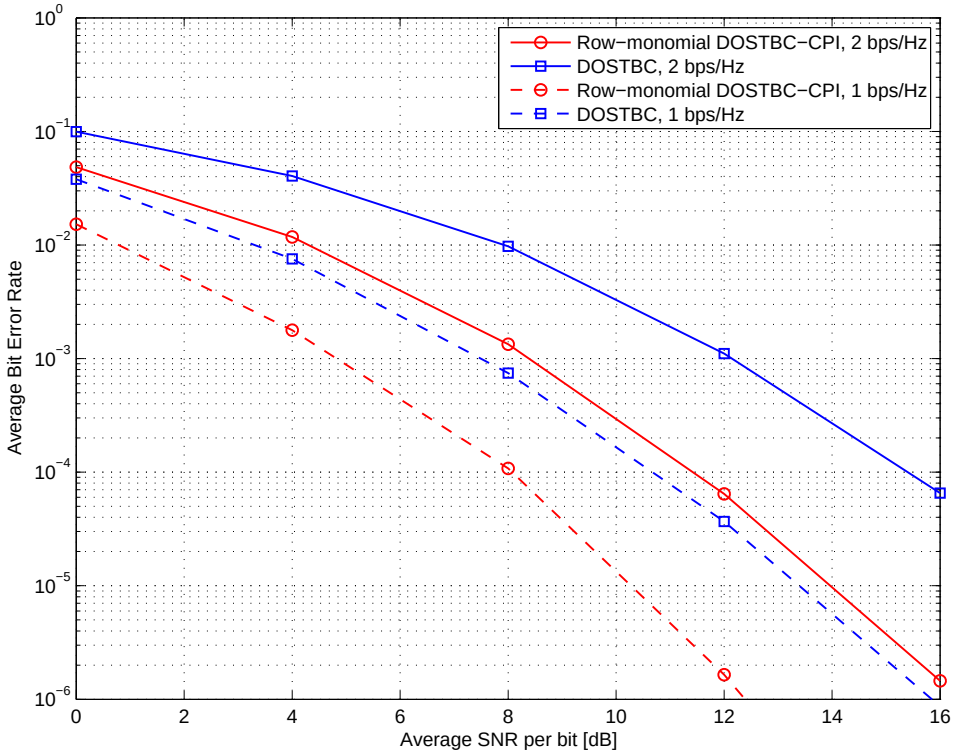

Figure 3.3. Comparison of the DOSTBCs and the row-monomial DOSTBCs-CPI, $N = 8$, $K = 6$.

complexity is much higher than that of the DOSTBCs and the row-monomial DOSTBCs-CPI.

In Fig. 3.3, we set $N = 8$ and $K = 6$. Because the row-monomial DOSTBCs-CPI use more CSI than the DOSTBCs, the row-monomial DOSTBCs-CPI have a better performance for this case. Specifically, the data-rate of the row-monomial DOSTBC-CPI is $1/2$ for this case. Thus, the row-monomial DOSTBCs-CPI use QPSK and 16-QAM to achieve the bandwidth efficiency 1 bps/Hz and 2 bps/Hz, respectively. On the other hand, the data-rate of the DOSTBC becomes $1/3$ for this case. Thus, the DOSTBCs use 8-PSK and 64-QAM to achieve the bandwidth efficiency 1 bps/Hz and 2 bps/Hz, respectively. Because the row-monomial DOSTBCs-CPI use modulation schemes with smaller sizes, they

have a better performance than the DOSTBCs.

3.5 Conclusion

In the first part of this chapter, we consider the DOSTBCs, where the noises at the destination are possibly correlated and the relays have no CSI of the first-hop channels. An upper bound of the data-rate of the DOSTBC is derived. When N and K are even, the DOSTBCs and the row-monomial DOSTBCs have the same data-rate. Thus, we can construct the DOSTBCs achieving the upper bound by using the systematic construction method proposed in Chapter 2. When K is even and N is odd, we should always reduce the value of N by 1 first. This does not affect the data-rate of the codes, but reduces the delay of the codes. Then we can construct the DOSTBCs achieving the upper bound by using the systematic construction method proposed in Chapter 2. When K is odd, however, we have not found any DOSTBCs achieving the upper bound. Like the row-monomial DOSTBCs, the DOSTBCs may not have good bandwidth efficiency in a cooperative network with many relays, because the upper-bound of the data-rate of the DOSTBC decreases with the number K of the relays. In the second part of this chapter, we propose the row-monomial DOSTBCs-CPI, where the noises at the destination are always uncorrelated and the relays exploit the CPI of the first-hop channels to construct the codes. We derive an upper bound of the data-rate of those codes and find the actual codes achieving this upper bound. The upper bound of the data-rate of the row-monomial DOSTBC-CPI suggests that the row-monomial DOSTBCs-CPI have better bandwidth efficiency than the DOSTBCs and the row-monomial DOSTBCs. Moreover, the upper bound of the data-rate of the row-monomial DOSTBC-CPI is independent of the number K of the relays, and hence, the codes have good bandwidth efficiency even in a cooperative network with many relays.

3.6 Appendix 3-A: Proof of Lemma 3.1

We first prove that $\boldsymbol{A}_k$ is column-monomial by contradiction. We assume that the t-th column of $\boldsymbol{A}_k$ has two non-zero entries: $[\boldsymbol{A}_k]_{n_1,t}$ and $[\boldsymbol{A}_k]_{n_2,t}$, $n_1 \neq n_2$. Then $[\boldsymbol{X}_D]_{k,t}$ will be a linear combination of $h_k s_{n_1}$ and $h_k s_{n_2}$, which violates the definition of the DOSTBCs in Definition 3.1. Therefore, any column of $\boldsymbol{A}_k$ cannot contain two non-zero entries. In the same way, it can be easily shown that any column of $\boldsymbol{A}_k$ cannot contain more than two non-zero entries, and hence, $\boldsymbol{A}_k$ is column-monomial. Similarly, we can show that $\boldsymbol{B}_k$ and $\boldsymbol{A}_k + \boldsymbol{B}_k$ are column-monomial.

It is not hard to show (3.11)–(3.15) by following the proof of Lemma 1 in Chapter 2 and the proof of Proposition 1 in [61]. For example, we show the proof of (3.11) and (3.12) in the following, because they are very important to derive the upper bound of the data-rate of the DOSTBC. When $k_1 \neq k_2$, it follows from (3.8) that $[\boldsymbol{X}_D \boldsymbol{R}^{-1} \boldsymbol{X}_D^H]_{k_1,k_2}$ is given by

$$\begin{aligned}
[\boldsymbol{X}_D \boldsymbol{R}^{-1} \boldsymbol{X}_D^H]_{k_1,k_2} &= h_{k_1} h_{k_2}^* \boldsymbol{s} \boldsymbol{A}_{k_1} \boldsymbol{R}^{-1} \boldsymbol{A}_{k_2}^H \boldsymbol{s}^H + h_{k_1}^* h_{k_2}^* \boldsymbol{s}^* \boldsymbol{B}_{k_1} \boldsymbol{R}^{-1} \boldsymbol{A}_{k_2}^H \boldsymbol{s}^H \\
&\quad + h_{k_1} h_{k_2} \boldsymbol{s} \boldsymbol{A}_{k_1} \boldsymbol{R}^{-1} \boldsymbol{B}_{k_2}^H \boldsymbol{s}^T + h_{k_1}^* h_{k_2} \boldsymbol{s}^* \boldsymbol{B}_{k_1} \boldsymbol{R}^{-1} \boldsymbol{B}_{k_2}^H \boldsymbol{s}^T \\
&= 0. \qquad \text{(3.A-1)}
\end{aligned}$$

Note that h_{k_1} and h_{k_2} can be any complex numbers. Thus, in order to make (3.A-1) hold for every possible value of h_{k_1} and h_{k_2}, the following equalities must hold

$$\boldsymbol{s} \boldsymbol{A}_{k_1} \boldsymbol{R}^{-1} \boldsymbol{A}_{k_2}^H \boldsymbol{s}^H = 0 \qquad \text{(3.A-2)}$$

$$\boldsymbol{s}^* \boldsymbol{B}_{k_1} \boldsymbol{R}^{-1} \boldsymbol{B}_{k_2}^T \boldsymbol{s}^H = 0. \qquad \text{(3.A-3)}$$

By using Lemma 1 of [38], we obtain (3.11) and (3.12).

3.7 Appendix 3-B: Proof of Theorem 3.1

By following the proof of Lemma 3.1, it can be easily shown that (3.16) is equivalent to the conditions (3.17)–(3.21). On the other hand, if a DOSTBC $\boldsymbol{X}_D$ exists, (3.8) holds by Definition 3.1, and hence, (3.11)–(3.15) hold by Lemma 3.1. Therefore, in order to prove Theorem 3.1, we only need to show that, if (3.11)–(3.15) hold, (3.17)–(3.21) hold and $E_{n,k}$ is strictly positive.

We start our proof by evaluating $[\boldsymbol{R}]_{t_1,t_2}$ and $[\boldsymbol{R}^{-1}]_{t_1,t_2}$. According to (3.7), when $t_1 \neq t_2$, $[\boldsymbol{R}]_{t_1,t_2}$ can be either null or a sum of several terms containing $|\rho f_k|^2$; when $t_1 = t_2 = t$, $[\boldsymbol{R}]_{t,t}$ is a sum of a constant 1, which is from the identity matrix, and several terms containing $|\rho f_k|^2$. Therefore, we can rewrite $[\boldsymbol{R}]_{t,t}$ as $[\boldsymbol{R}]_{t,t} = \bar{R}_{t,t} + 1$, where $\bar{R}_{t,t}$ accounts for all the terms containing $|\rho f_k|^2$. $[\boldsymbol{R}^{-1}]_{t_1,t_2}$ is given by $[\boldsymbol{R}^{-1}]_{t_1,t_2} = C_{t_2,t_1}/\det(\boldsymbol{R})$, where C_{t_2,t_1} is the matrix cofactor of $[\boldsymbol{R}]_{t_2,t_1}$. When $t_1 = t_2 = t$, by the definition of matrix cofactor, $C_{t,t}$ contains a constant 1 generated by the product $\prod_{i=1,i\neq t}^{T}[\boldsymbol{R}]_{i,i} = \prod_{i=1,i\neq t}^{T}(\bar{R}_{i,i}+1)$. This product generates only one constant, and hence, the constant 1 is the only constant term in $C_{t,t}$. Thus, $C_{t,t}$ can be rewritten as $C_{t,t} = \bar{C}_{t,t} + 1$ and there is no constant term in $\bar{C}_{t,t}$. Consequently, $[\boldsymbol{R}^{-1}]_{t,t}$ can be rewritten as $[\boldsymbol{R}^{-1}]_{t,t} = \bar{C}_{t,t}/\det(\boldsymbol{R}) + 1/\det(\boldsymbol{R})$. When $t_1 \neq t_2$, C_{t_2,t_1} does not contain any constant term, and hence, $[\boldsymbol{R}^{-1}]_{t_1,t_2}$ does not contain the term $1/\det(\boldsymbol{R})$.[9] Therefore, we can extract the term $1/\det(\boldsymbol{R})$ from every main diagonal entry of $\boldsymbol{R}^{-1}$ and rewrite $\boldsymbol{R}^{-1}$ in the following way

$$\boldsymbol{R}^{-1} \;=\; \frac{1}{\det(\boldsymbol{R})}\bar{\boldsymbol{C}} + \frac{1}{\det(\boldsymbol{R})}\boldsymbol{I}_{T\times T}. \tag{3.B-1}$$

Then we show that (3.17) holds if (3.11) holds. If (3.11) holds, we have

$$\boldsymbol{A}_{k_1}\boldsymbol{R}^{-1}\boldsymbol{A}_{k_2}^{H} = \frac{1}{\det(\boldsymbol{R})}\boldsymbol{A}_{k_1}\bar{\boldsymbol{C}}\boldsymbol{A}_{k_2}^{H} + \frac{1}{\det(\boldsymbol{R})}\boldsymbol{A}_{k_1}\boldsymbol{A}_{k_2}^{H} = \boldsymbol{0}_{N\times N}. \tag{3.B-2}$$

[9] C_{t_2,t_1} may be zero; but it does not change the conclusion that $[\boldsymbol{R}^{-1}]_{t_1,t_2}$ does not contain the term $1/\det(\boldsymbol{R})$.

Note that $\boldsymbol{R}^{-1}$ and $\bar{\boldsymbol{C}}$ are random matrices. In order to make (3.B-2) hold for every possible $\boldsymbol{R}^{-1}$ and $\bar{\boldsymbol{C}}$, both terms in (3.B-2) must be equal to zero. Therefore, (3.17) holds. Similarly, we can show that (3.18)–(3.20) hold if (3.12)–(3.14) hold. Now, we show that (3.21) holds if (3.15) holds. If (3.15) holds, we have

$$\begin{aligned}\boldsymbol{A}_k\boldsymbol{R}^{-1}\boldsymbol{A}_k^H+\boldsymbol{B}_k^*\boldsymbol{R}^{-1}\boldsymbol{B}_k^T &= \frac{1}{\det(\boldsymbol{R})}\left(\boldsymbol{A}_k\bar{\boldsymbol{C}}\boldsymbol{A}_k^H+\boldsymbol{B}_k^*\bar{\boldsymbol{C}}\boldsymbol{B}_k^T\right)+\frac{1}{\det(\boldsymbol{R})}\left(\boldsymbol{A}_k\boldsymbol{A}_k^H+\boldsymbol{B}_k^*\boldsymbol{B}_k^T\right)\\ &= \mathrm{diag}[D_{1,k},\cdots,D_{N,k}]. \qquad (3.\text{B-}3)\end{aligned}$$

For the same reason as in (3.B-2), the off-diagonal entries of $\boldsymbol{A}_k\boldsymbol{A}_k^H+\boldsymbol{B}_k^*\boldsymbol{B}_k^T$ must be zero, and hence, (3.21) holds.

Lastly, we show that $E_{n,k}$ is strictly positive if (3.15) holds. From (3.15) and (3.21), we have

$$D_{n,k} = \sum_{t=1}^{T}\sum_{i=1}^{T}[\boldsymbol{R}^{-1}]_{i,t}([\boldsymbol{A}_k]_{n,i}[\boldsymbol{A}_k]_{n,t}^*+[\boldsymbol{B}_k]_{n,i}^*[\boldsymbol{B}_k]_{n,t}) \qquad (3.\text{B-}4)$$

$$E_{n,k} = \sum_{t=1}^{T}(|[\boldsymbol{A}_k]_{n,t}|^2+|[\boldsymbol{B}_k]_{n,t}|^2). \qquad (3.\text{B-}5)$$

Since $D_{n,k}$ is non-zero, at least one $[\boldsymbol{A}_k]_{n,t}$ or one $[\boldsymbol{B}_k]_{n,t}$ is non-zero. Therefore, $E_{n,k}=\sum_{t=1}^{T}(|[\boldsymbol{A}_k]_{n,t}|^2+|[\boldsymbol{B}_k]_{n,t}|^2)$ is strictly positive, which completes the proof of Theorem 3.1.

3.8 Appendix 3-C: Proof of Theorem 3.2

Let $\underline{\boldsymbol{A}}=[\boldsymbol{A}_1,\cdots,\boldsymbol{A}_K]^T$ and $\underline{\boldsymbol{B}}=[\boldsymbol{B}_1,\cdots,\boldsymbol{B}_K]^T$; then the dimension of $\underline{\boldsymbol{A}}$ and $\underline{\boldsymbol{B}}$ is $NK\times T$. From (3.17), every row of $\boldsymbol{A}_{k_1}$ is orthogonal with every row of $\boldsymbol{A}_{k_2}$ when $k_1\neq k_2$.[10] Furthermore, because $\boldsymbol{A}_k$ is column-monomial by Lemma 3.1, every row of $\boldsymbol{A}_k$ is orthogonal with every other row of $\boldsymbol{A}_k$. Therefore, any two different rows in $\underline{\boldsymbol{A}}$ are orthogonal with each other, and hence, $\mathrm{rank}(\underline{\boldsymbol{A}})=\sum_{k=1}^{K}\mathrm{rank}(\boldsymbol{A}_k)$. Similarly, any two different rows in $\underline{\boldsymbol{B}}$ are orthogonal with each other, and hence, $\mathrm{rank}(\underline{\boldsymbol{B}})=\sum_{k=1}^{K}\mathrm{rank}(\boldsymbol{B}_k)$.

[10] A row vector $\boldsymbol{x}$ is said to be orthogonal with another row vector $\boldsymbol{y}$ if $\boldsymbol{x}\boldsymbol{y}^H$ is equal to zero.

On the other hand, from (3.21), we have

$$\text{rank}(\boldsymbol{A}_k) + \text{rank}(\boldsymbol{B}_k) \geq \text{rank}(\text{diag}[E_{1,k}, \cdots, E_{N,k}]) = N, \tag{3.C-1}$$

where the inequality is from the rank inequality 3) in [61], and hence,

$$\sum_{k=1}^{K} \text{rank}(\boldsymbol{A}_k) + \sum_{k=1}^{K} \text{rank}(\boldsymbol{B}_k) \geq NK. \tag{3.C-2}$$

Because $\text{rank}(\underline{\boldsymbol{A}})$ and $\text{rank}(\underline{\boldsymbol{B}})$ are integers, we have

$$\text{rank}(\underline{\boldsymbol{A}}) = \sum_{k=1}^{K} \text{rank}(\boldsymbol{A}_k) \geq \left\lceil \frac{NK}{2} \right\rceil \tag{3.C-3}$$

or

$$\text{rank}(\underline{\boldsymbol{B}}) = \sum_{k=1}^{K} \text{rank}(\boldsymbol{B}_k) \geq \left\lceil \frac{NK}{2} \right\rceil. \tag{3.C-4}$$

If (3.C-3) is true, $T \geq \text{rank}(\underline{\boldsymbol{A}}) \geq \lceil (NK)/2 \rceil$ and (3.22) holds. If (3.C-4) is true, the same conclusion can be made.

3.9 Appendix 3-D: Proof of Lemma 3.2

As in [71], we use $\doteq$ and $\dot{\geq}$ to denote the asymptotic exponential equality and inequality, respectively.

When $\boldsymbol{w}_C$ is given, it follows from (3.25) that the mutual information between $\boldsymbol{y}_C$ and $\boldsymbol{X}_C$ is given by

$$\begin{aligned} I(\boldsymbol{X}_C; \boldsymbol{y}_C | \boldsymbol{w}_C) &= \log(1 + \boldsymbol{w}_C \boldsymbol{X}_C \boldsymbol{R}^{-1} \boldsymbol{X}_C^H \boldsymbol{w}_C^H) \\ &\geq \log\left(1 + \frac{1}{\lambda_{\max}(\boldsymbol{R})} \boldsymbol{w}_C \boldsymbol{X}_C \boldsymbol{X}_C^H \boldsymbol{w}_C^H\right), \end{aligned} \tag{3.D-1}$$

where $\lambda_{\max}(\boldsymbol{R})$ is the largest eigenvalue of $\boldsymbol{R}$. The inequality in because R is always a diagonal matrix when the code is a row-monomial DOSTBC-CPI. Because $\boldsymbol{X}_C$ is a row-monomial DOSTBC-CPI, $\boldsymbol{R}$ is a diagonal matrix and $\lambda_{\max}(\boldsymbol{R})$ is equal to the largest main

diagonal entry of $\boldsymbol{R}$. The main diagonal entries of $\boldsymbol{R}$ can be obtained from (3.7)

$$[\boldsymbol{R}]_{t,t} = \sum_{k=1}^{K} |\rho f_k|^2 \left(\sum_{n=1}^{N} |[\boldsymbol{A}_k]_{n,t}|^2 + |[\boldsymbol{B}_k]_{n,t}|^2 \right) + 1 \tag{3.D-2}$$

By Lemma 3.1, the associated matrices $\boldsymbol{A}_k$, $\boldsymbol{B}_k$, and $\boldsymbol{A}_k + \boldsymbol{B}_k$ are column-monomial. Therefore, we have

$$[\boldsymbol{R}]_{t,t} \leq \sum_{k=1}^{K} |\rho f_k|^2 + 1, \tag{3.D-3}$$

and

$$\lambda_{\max}(\boldsymbol{R}) = \max_{t=1,\cdots,T} [\boldsymbol{R}]_{t,t} \leq \sum_{k=1}^{K} |\rho f_k|^2 + 1. \tag{3.D-4}$$

In [14], it has been shown that $\sum_{k=1}^{K} |\rho f_k|^2 + 1$ is independent of E, i.e. $\sum_{k=1}^{K} |\rho f_k|^2 + 1 \doteq E^0$. Thus, we have

$$I(\boldsymbol{X}_C; \boldsymbol{y}_C | \boldsymbol{w}_C) \quad \dot{\geq} \quad \log\left(1 + \boldsymbol{w}_C \boldsymbol{X}_C \boldsymbol{X}_C^H \boldsymbol{w}_C^H\right) \tag{3.D-5}$$

$$\doteq \quad \log\left(1 + c_s E \boldsymbol{w}_C \boldsymbol{w}_C^H\right). \tag{3.D-6}$$

The last step is because of the assumption $T \geq K$ and the fact that $\boldsymbol{X}_C$ is full rank by (3.29) and (3.30). In [14], it has been shown that the average outage probability of (3.D-6) decays with E as fast as $1/E^K$. Therefore, the average outage probability of the cooperative networks using the row-monomial DOSTBCs-CPI decays with E as fast as $1/E^K$, i.e. the full diversity order K is achieved.

3.10 Appendix 3-E: Proof of Theorem 3.3

The sufficient part is easy to verify. Thus, we focus on the necessary part, i.e. if $\boldsymbol{X}_C$ is a row-monomial DOSTBC-CPI, all the sub-matrices $\boldsymbol{X}_{Cw}$ are also row-monomial DOSTBCs-CPI. Assume that the dimension of $\boldsymbol{R}_w$ is $T_w \times T_w$.

Firstly, we show that $\boldsymbol{X}_{Cw} \boldsymbol{R}_w \boldsymbol{X}_{Cw}^H$ is a diagonal matrix. Because $\boldsymbol{X}_{C1}, \cdots, \boldsymbol{X}_{CW}$ contain all the non-zero entries in $\boldsymbol{X}_C$, it follows from (3.29) that, when $k_1 \neq k_2$, $[\boldsymbol{X}_C \boldsymbol{R}^{-1} \boldsymbol{X}_C^H]_{k_1,k_2}$ is

given by

$$[\boldsymbol{X}_C\boldsymbol{R}^{-1}\boldsymbol{X}_C^H]_{k_1,k_2} = \sum_{w=1}^{W}\sum_{t=1}^{T_w}[\boldsymbol{X}_{Cw}]_{k_1,t}[\boldsymbol{X}_{Cw}]^*_{k_2,t}R_w = 0. \tag{3.E-1}$$

If all the terms in this summation are zero, it is trivial to show that $\sum_{t=1}^{T_w}[\boldsymbol{X}_{Cw}]_{k_1,t}[\boldsymbol{X}_{Cw}]^*_{k_2,t}R_w = 0$ for $1 \le w \le W$, which means $\boldsymbol{X}_{Cw}\boldsymbol{R}_w\boldsymbol{X}_{Cw}^H$ is a diagonal matrix.

If there is one term $[\boldsymbol{X}_{Cw_1}]_{k_1,t_1}[\boldsymbol{X}_{Cw_1}]^*_{k_2,t_1}R_{w_1} \neq 0$, some other terms must cancel this term in order to make (3.E-1) hold. Actually, the non-zero term $[\boldsymbol{X}_{Cw_1}]_{k_1,t_1}[\boldsymbol{X}_{Cw_1}]^*_{k_2,t_1}R_{w_1}$ must be cancelled by exactly one other term. This can be shown by contradiction. We assume that $[\boldsymbol{X}_{Cw_1}]_{k_1,t_1}[\boldsymbol{X}_{Cw_1}]^*_{k_2,t_1}R_{w_1}$ is cancelled by two other terms together, i.e.

$$[\boldsymbol{X}_{Cw_1}]_{k_1,t_1}[\boldsymbol{X}_{Cw_1}]^*_{k_2,t_1}R_{w_1} + [\boldsymbol{X}_{Cw_2}]_{k_1,t_2}[\boldsymbol{X}_{Cw_2}]^*_{k_2,t_2}R_{w_2} + [\boldsymbol{X}_{Cw_3}]_{k_1,t_3}[\boldsymbol{X}_{Cw_3}]^*_{k_2,t_3}R_{w_3} = 0. \tag{3.E-2}$$

In order to make this equality hold, one of the following three equalities must hold: 1) $[\boldsymbol{X}_{Cw_2}]_{k_1,t_2} = \pm[\boldsymbol{X}_{Cw_1}]_{k_1,t_1}$; 2) $[\boldsymbol{X}_{Cw_3}]_{k_1,t_3} = \pm[\boldsymbol{X}_{Cw_1}]_{k_1,t_1}$; 3) $\pm[\boldsymbol{X}_{Cw_2}]_{k_1,t_2} = \pm[\boldsymbol{X}_{Cw_3}]_{k_1,t_3} = [\boldsymbol{X}_{Cw_1}]^*_{k_2,t_1}$. However, those three equalities all contradict with our assumption that the covariance matrix $\boldsymbol{R}$ is diagonal. For example, we assume $[\boldsymbol{X}_{Cw_1}]_{k_1,t_1} = s_n^{w_1}$, $1 \le n \le N_{w_1}$, and the equality $[\boldsymbol{X}_{Cw_2}]_{k_1,t_2} = \pm[\boldsymbol{X}_{Cw_1}]_{k_1,t_1}$ holds. Thus, $[\boldsymbol{X}_{Cw_2}]_{k_1,t_2} = \pm s_n^{w_1}$ and $s_n^{w_1}$ is transmitted in the k_1-th row of $\boldsymbol{X}_C$ for at least twice. This makes the noise covariance matrix $\boldsymbol{R}$ non-diagonal, which contradicts with our assumption. If we assume $[\boldsymbol{X}_{Cw_1}]_{k_1,t_1}[\boldsymbol{X}_{Cw_1}]^*_{k_2,t_1}R_{w_1}$ is cancelled by more than two other terms, the same contradiction can be seen similarly. Thus, $[\boldsymbol{X}_{Cw_1}]_{k_1,t_1}[\boldsymbol{X}_{Cw_1}]^*_{k_2,t_1}R_{w_1}$ is cancelled by exactly one other term in the summation (3.E-1) and we have

$$[\boldsymbol{X}_{Cw_1}]_{k_1,t_1}[\boldsymbol{X}_{Cw_1}]^*_{k_2,t_1}R_{w_1} + [\boldsymbol{X}_{Cw_2}]_{k_1,t_2}[\boldsymbol{X}_{Cw_2}]^*_{k_2,t_2}R_{w_2} = 0. \tag{3.E-3}$$

Furthermore, because $R_i \neq R_j$ when $i \neq j$, (3.E-3) also implies that $R_{w_1} = R_{w_2}$ and $w_1 = w_2$. This means that, if one term in the summation (3.E-1) is non-zero, it must be cancelled by exactly one other term, which is from the same sub-matrix $\boldsymbol{X}_{Cw}$. Therefore, we have

$\sum_{t=1}^{T_w}[\boldsymbol{X}_{Cw}]_{k_1,t}[\boldsymbol{X}_{Cw}]^*_{k_2,t}R_w = 0$, when $k_1 \neq k_2$, and $\boldsymbol{X}_{Cw}\boldsymbol{R}_w\boldsymbol{X}^H_{Cw}$ is a diagonal matrix.

Secondly, we show that the information-bearing symbols $s^w_1,\cdots,s^w_{N_w}$ are contained in every row of $\boldsymbol{X}_{Cw}$. Because every main diagonal entry of $\boldsymbol{R}_w$ is the same and $\boldsymbol{X}_{Cw}$ only contains non-zero rows, it follows from (3.7) that $\boldsymbol{X}_{Cw}$ actually does not contain any zero entries. Then we assume that $[\boldsymbol{X}_{Cw}]_{k_1,t_1} = s^w_n$, $1 \leq n \leq N_w$. Because every entry in $\boldsymbol{X}_{Cw}$ is non-zero, we can find another non-zero entry $[\boldsymbol{X}_{Cw}]_{k_2,t_1}$, $k_1 \neq k_2$, from the t_1-th column of $\boldsymbol{X}_{Cw}$. Thus, $[\boldsymbol{X}_{Cw}\boldsymbol{R}_w\boldsymbol{X}^H_{Cw}]_{k_1,k_2}$ must contain the term $[\boldsymbol{X}_{Cw}]_{k_1,t_1}[\boldsymbol{X}_{Cw}]^*_{k_2,t_1}R_w$. Because $[\boldsymbol{X}_{Cw}\boldsymbol{R}_w\boldsymbol{X}^H_{Cw}]_{k_1,k_2} = 0$, $[\boldsymbol{X}_{Cw}]_{k_1,t_1}[\boldsymbol{X}_{Cw}]^*_{k_2,t_1}R_w$ must be cancelled by another term and we assume it is $[\boldsymbol{X}_{Cw}]_{k_1,t_2}[\boldsymbol{X}_{Cw}]^*_{k_2,t_2}R_w$, $t_1 \neq t_2$. In order to make $[\boldsymbol{X}_{Cw}]_{k_1,t_1}[\boldsymbol{X}_{Cw}]^*_{k_2,t_1}R_w + [\boldsymbol{X}_{Cw}]_{k_1,t_2}[\boldsymbol{X}_{Cw}]^*_{k_2,t_2}R_w = 0$, we must have $[\boldsymbol{X}_{Cw}]_{k_1,t_2} = \pm[\boldsymbol{X}_{Cw}]_{k_1,t_1}$ or $[\boldsymbol{X}_{Cw}]^*_{k_2,t_2} = \pm[\boldsymbol{X}_{Cw}]_{k_1,t_1}$. Due to the row-monomial condition, $[\boldsymbol{X}_{Cw}]_{k_1,t_2}$ cannot be $\pm[\boldsymbol{X}_{Cw}]_{k_1,t_1}$, and hence, we have $[\boldsymbol{X}_{Cw}]_{k_2,t_2} = \pm[\boldsymbol{X}_{Cw}]^*_{k_1,t_1} = \pm s^{w*}_n$. This means that the k_2-th row contains the information-bearing symbol s^w_n as well. Taking a similar approach, we can show that the information-bearing symbols $s^w_1,\cdots,s^w_{N_w}$ are contained in every row of $\boldsymbol{X}_{Cw}$.

Because $\boldsymbol{X}_{Cw}\boldsymbol{R}_w\boldsymbol{X}^H_{Cw}$ is a diagonal matrix and every row of $\boldsymbol{X}_{Cw}$ contains all the information-bearing symbols $s^w_1,\cdots,s^w_{N_w}$, $\boldsymbol{X}_{Cw}\boldsymbol{R}_w\boldsymbol{X}^H_{Cw}$ can be written as

$$\boldsymbol{X}_{Cw}\boldsymbol{R}_w\boldsymbol{X}^H_{Cw} = |s^w_1|^2\boldsymbol{M}_1 + \cdots + |s^w_{N_w}|^2\boldsymbol{M}_{N_w}, \tag{3.E-4}$$

where $\boldsymbol{M}_n$ are diagonal and all the main diagonal entries are non-zero. Note that, if the relays only transmit $\boldsymbol{X}_{Cw}$ to the destination, $\boldsymbol{R}_w$ is actually the inverse of the noise covariance matrix at the destination. This is because $\boldsymbol{X}_{Cw}$ and $\boldsymbol{R}_w$ are obtained after the same column permutations. Therefore, (3.E-4) is equivalent to (3.29). Furthermore, since $\boldsymbol{X}_{Cw}$ is a sub-matrix of $\boldsymbol{X}_C$, it automatically satisfies condition D3.1.1 and the row-monomial condition. Thus, we conclude that $\boldsymbol{X}_{Cw}$ satisfies Definition 3.2 and it is a row-monomial DOSTBC-CPI.

3.11 Appendix 3-F: Proof of Theorem 3.4

From Theorem 3.3, every sub-matrix $\boldsymbol{X}_{Cw}$ is a row-monomial DOSTBC-CPI in variables $s_1^w, \cdots, s_{N_w}^w$. Furthermore, by (3.30), every sub-matrix $\boldsymbol{X}_{Cw}$ is also a generalized orthogonal design. For convenience, we refer to any entry containing $s_{n_w}^w$ as the $s_{n_w}^w$-entry. Similarly, any entry containing $s_{n_w}^{w*}$ is referred to as the $s_{n_w}^{w*}$-entry.

By the row-monomial condition, any row in $\boldsymbol{X}_{Cw}$ cannot contain more than one $s_{n_w}^w$-entry or $s_{n_w}^{w*}$-entry. Therefore, the data-rate of $\boldsymbol{X}_{Cw}$ is lower-bounded by $1/2$, which is achieved when every row contains exactly one $s_{n_w}^w$-entry and one $s_{n_w}^{w*}$-entry for $1 \leq n_w \leq N_w$.

Then we show that the data-rate cannot be strictly larger than $1/2$ by contradiction. Without loss of generality, we assume the first row of $\boldsymbol{X}_{Cw}$ is $[s_1^w, \cdots, s_{N_w}^w, s_1^{w*}, \cdots, s_{N_w^{'}}^{w*}]$, where $N_w^{'} < N_w$. Hence, the data-rate of $\boldsymbol{X}_{Cw}$ is $N_w/(N_w + N_w^{'})$ and it is strictly larger than $1/2$. Furthermore, because every entry in $\boldsymbol{X}_{Cw}$ is non-zero, every row in $\boldsymbol{X}_{Cw}$ contains exactly $N_w + N_w^{'}$ non-zero entries. Because $s_{N_w^{'}+1}^{w*}, \cdots, s_{N_w}^{w*}$ are not transmitted by the first row, the second row cannot have any $s_{n_w}^w$-entries, $N_w^{'} + 1 \leq n_w \leq N_w$. This can be shown by contradiction. For example, if the second row has $s_{N_w^{'}+1}^w$ on the first column, the inner product of the first and second rows must have the term $s_1^w s_{N_w^{'}+1}^{w*}$. Because $\boldsymbol{X}_{Cw}$ is a generalized orthogonal design, the inner product of any two rows must be zero. In order to cancel the term $s_1^w s_{N_w^{'}+1}^{w*}$, the first row must have an $s_{N_w^{'}+1}^{w*}$-entry, which contradicts our assumption. Thus, the second row cannot contain any $s_{n_w}^w$-entries, $N_w^{'} + 1 \leq n_w \leq N_w$. On the other hand, because the second row must contain exactly $N_w + N_w^{'}$ non-zero entries, it must have the $s_{n_w}^w$-entries for $1 \leq n_w \leq N_w^{'}$ and the $s_{n_w}^{w*}$-entries for $1 \leq n_w \leq N_w$.

Since $K_w > 2$, we can do further investigation on the third row of $\boldsymbol{X}_{Cw}$. The third row is decided by the first and the second row jointly. Because the first row does not have $s_{N_w^{'}+1}^{w*}, \cdots, s_{N_w}^{w*}$, the third rows cannot have any $s_{n_w}^w$-entries, $N_w^{'} + 1 \leq n_w \leq N_w$. Furthermore, because the second row does not have any $s_{n_w}^w$-entries, $N_w^{'} + 1 \leq n_w \leq N_w$, the third row

cannot have any $s_{n_w}^{w*}$-entries, $N_w^{'}+1 \leq n_w \leq N_w$. Hence, the third row can only have the $s_{n_w}^{w}$-entries and the $s_{n_w}^{w*}$-entries for $1 \leq n_w \leq N_w^{'}$. There are at most $2N_w^{'}$ non-zero entries in the third row and it contradicts with the fact that every row in $\boldsymbol{X}_{Cw}$ contains exactly $N_w+N_w^{'}$ non-zero entries. This means that the data-rate of $\boldsymbol{X}_{Cw}$ cannot be strictly larger than $1/2$. Because it has been shown that the data-rate of $\boldsymbol{X}_{Cw}$ is lower-bounded by $1/2$, we conclude that the data-rate of $\boldsymbol{X}_{Cw}$ is exactly $1/2$ when $K_w > 2$.

3.12 Appendix 3-G: Proof of Theorem 3.5

Like in Theorems 3.3 and 3.4, we still partition $\boldsymbol{X}_C$ into $\boldsymbol{X}_{C1},\cdots,\boldsymbol{X}_{CW}$, and we assume the dimension of $\boldsymbol{X}_{Cw}$ is $K_w \times T_w$. Because $\boldsymbol{X}_{Cw}$ does not contain any zero entries, the total number of non-zero entries in $\boldsymbol{X}_{Cw}$ is $K_w T_w$. For convenience, we refer to any entry containing s_n as the s_n-entry. Similarly, any entry containing s_n^* is referred to as the s_n^*-entry.

We first consider the case that $K=3$. Because $K=3$, there is only one sub-matrix in $\boldsymbol{X}_{C1},\cdots,\boldsymbol{X}_{CW}$ that contains three rows. Without loss of generality, we can assume that $\boldsymbol{X}_{C1}$ is such sub-matrix, i.e. $K_1=3$. Then we partition $\boldsymbol{X}_C$ into $\boldsymbol{X}_C=[\boldsymbol{X}_{C1},\boldsymbol{X}_C^{'}]$. Note that every column in $\boldsymbol{X}_C^{'}$ can contain at most two non-zero entries; otherwise, this column should be included in $\boldsymbol{X}_{C1}$. By Theorem 3.4, $\boldsymbol{X}_{C1}$ is a row-monomial DOSTBC-CPI and its data-rate is exactly $1/2$. Furthermore, we assume $\boldsymbol{X}_{C1}$ is in variables $s_1,\cdots,s_{N_1}$, $1 \leq N_1 \leq N$. By the proof of Theorem 3.4, every row of $\boldsymbol{X}_{C1}$ contains exactly one s_n-entry and one s_n^*-entry, $1 \leq n \leq N_1$. Therefore, there is no s_n-entry or s_n^*-entry in $\boldsymbol{X}_C^{'}$; otherwise, there will be more than one s_n-entries or s_n^*-entries in a row of $\boldsymbol{X}_C$, which will make the noise covariance matrix $\boldsymbol{R}$ non-diagonal. Thus, the matrix $\boldsymbol{X}_C^{'}$ is actually a row-monomial DOSTBC-CPI in variables $s_{N_1+1},\cdots,s_N$. Furthermore, because every column in $\boldsymbol{X}_C^{'}$ has at most two non-zero entries, it is easy to show that its data-rate cannot be larger than $1/2$ by following the

proof of Theorem 2 in Chapter 2.[11] Because the data-rate of $\boldsymbol{X}_{C1}$ is exactly $1/2$ and the data-rate of $\boldsymbol{X}_C^{'}$ is less than $1/2$, the data-rate of $\boldsymbol{X}_C = [\boldsymbol{X}_{C1}, \boldsymbol{X}_C^{'}]$ must be upper-bounded by $1/2$ when $K = 3$.

Secondly, we consider the case that $K > 3$. We assume the sub-matrices $\boldsymbol{X}_{C1}, \cdots, \boldsymbol{X}_{CW'}$ contain one or two rows and the sub-matrices $\boldsymbol{X}_{C(W'+1)}, \cdots, \boldsymbol{X}_{CW}$ contain three or more rows, i.e. $K_w \leq 2$ for $1 \leq w \leq W^{'}$ and $K_w \geq 3$ for $W^{'} + 1 \leq w \leq W$. Thus, the data-rate of $\boldsymbol{X}_{Cw}$ is exactly $1/2$ for $W^{'} + 1 \leq w \leq W$. This means, if an information-bearing symbol s_n appears in a row of $\boldsymbol{X}_{Cw}$,$W^{'} \leq w \leq W$, it appears exactly twice. On the other hand, (3.30) implies that every row of $\boldsymbol{X}_C$ must have the information-bearing symbol s_n for at least once, $1 \leq n \leq N$. Therefore, the following inequality holds

$$\sum_{w=1}^{W^{'}} K_w T_w + \sum_{w=W^{'}+1}^{W} \frac{K_w T_w}{2} \quad \geq \quad NK. \tag{3.G-1}$$

On the other hand, there are totally T_w columns in $\boldsymbol{X}_{Cw}$. Thus, the total number T of columns in $\boldsymbol{X}_C$ is given by

$$T \quad = \quad \sum_{w=1}^{W} T_w. \tag{3.G-2}$$

By (3.G-1) and (3.G-2), it is easy to obtain $2N \leq T$ under the assumption that $K > 3$ and $K_w \leq 2$ for $1 \leq w \leq W^{'}$, and hence, the data-rate of $\boldsymbol{X}_C$ is upper-bounded by $1/2$ when $K > 3$.

[11] Note that $\boldsymbol{X}_C^{'}$ is a row-monomial DOSTBC-CPI in $N - N_1$ different variables. Furthermore, it only has three rows and every column in $\boldsymbol{X}_C^{'}$ has at most two non-zero entries. Therefore, when $N - N_1$ is even, we can follow Case III in the proof of Theorem 2 in Chapter 2 and show that the data-rate of $\boldsymbol{X}_C^{'}$ cannot be larger than $1/2$. When $N - N_1$ is odd, the same conclusion can be made by following Case IV in the proof of Theorem 2 in Chapter 2.

3.13 Appendix 3-H: Proof of Theorem 3.6

For convenience, we refer to any entry containing s_n as the s_n-entry. Similarly, any entry containing s_n^* is referred to as the s_n^*-entry.

It is well-known that a rate-halving code is given by $\boldsymbol{X}_C = [\boldsymbol{X}_O, \boldsymbol{X}_O^*]$, where $\boldsymbol{X}_O$ is a rate-one real orthogonal design [56]. By the properties of rate-one real orthogonal design, the entries of $\boldsymbol{X}_O$ can only be $\pm s_n$ and the entries of $\boldsymbol{X}_O^*$ can only be $\pm s_n^*$. Therefore, the entries of $\boldsymbol{X}_C$ can only be $\pm s_n$ and $\pm s_n^*$. That is, the rate-halving codes satisfy condition D3.2.1 in Definition 3.2.

Then we show that $\boldsymbol{A}_k$ and $\boldsymbol{B}_k$ are row-monomial. Due to the fact that the data-rate of $\boldsymbol{X}_O$ is one, there is exactly one s_n-entry in every row of $\boldsymbol{X}_O$. Because $\boldsymbol{X}_O^*$ contains s_n^*-entries only, there is exactly one s_n-entry in every row of $\boldsymbol{X}_C$. It follows from (3.27) that $\boldsymbol{A}_k$ is row-monomial; otherwise, there will be more than one s_n-entries in the k-th row of $\boldsymbol{X}_C$. Similarly, $\boldsymbol{B}_k$ is row-monomial.

Lastly, we show that rate-halving codes satisfy condition D3.2.2 in Definition 3.2. Because there are no zero entries in $\boldsymbol{X}_O$, no zero entries exist in $\boldsymbol{X}_C$. Thus, it follows from (3.27) that there is at least one non-zero entry in every column of $\boldsymbol{A}_k + \boldsymbol{B}_k$; otherwise, there will be a zero entry in the k-th row of $\boldsymbol{X}_C$. On the other hand, because $\boldsymbol{X}_O$ does not have any linear combinations of s_n, $\boldsymbol{X}_C$ does not have any linear combinations of s_n. As a result, there is at most one non-zero entry in every column of $\boldsymbol{A}_k + \boldsymbol{B}_k$ by (3.27). Therefore, there is exactly one non-zero entry in every column of $\boldsymbol{A}_k + \boldsymbol{B}_k$. It follows from (3.7) that all the main diagonal entries of $\boldsymbol{R}$ equal to $\sum_{k=1}^{K} |\rho f_k|^2 + 1$. Furthermore, because we have shown that $\boldsymbol{A}_k$ and $\boldsymbol{B}_k$ are row-monomial, $\boldsymbol{R}$ is a diagonal matrix based on Theorem 2.1 in Chapter 2. Then we can rewrite (3.29) as follows:

$$\boldsymbol{X}_C \boldsymbol{R}^{-1} \boldsymbol{X}_C^H = \frac{1}{\sum_{k=1}^{K} |\rho f_k|^2 + 1} [\boldsymbol{X}_O, \boldsymbol{X}_O^*] \begin{bmatrix} \boldsymbol{X}_O^H \\ \boldsymbol{X}_O^T \end{bmatrix} \tag{3.H-1}$$

$$= \frac{2}{\sum_{k=1}^{K} |\rho f_k|^2 + 1} \left(|s_1|^2 + \cdots + |s_N|^2 \right) \boldsymbol{I}_{K \times K}, \qquad \text{(3.H-2)}$$

where the last equality is because the rate-halving codes are single-symbol ML decodable in co-located MIMO systems [56]. Therefore, rate-halving codes satisfy condition D3.2.2.

Chapter 4

Approximate BER Expressions of Distributed Alamouti's Code in Dissimilar Cooperative Networks with Blind Relays

This chapter focuses on error performance analysis of distributed Alamouti's code. Recently, many works have been devoted to the performance analysis of this code. In order to simplify the analysis, however, they either assumed the channels in the cooperative network had the same variances or only considered asymptotic error performance at high signal-to-noise ratio (SNR). In this chapter, we study a general dissimilar cooperative network, where the channels have different variances. Two closed-form and accurate approximate bit error rate (BER) expressions are proposed in order to evaluate the error performance of the distributed Alamouti's code. We also investigate how the values of channel variances affect the accuracies of the proposed approximate BER expressions. Analytical and numerical results demonstrate that our closed-form approximate BER expressions are very close to the exact BER over the whole SNR range. Furthermore, we show that the distributed Alamouti's code achieves the full diversity order in dissimilar cooperative networks.

4.1 Introduction

In a cooperative network, several single-antenna relays help the source transmit signals to the destination by forming a distributed multiple-antenna system [33, 49, 50]. Specifically, in an amplify-and-forward (AF) cooperative network, each relay multiplies the received signal with an amplifying coefficient and then forwards it to the destination. In order to coordinate the transmissions from the relays, a *repetition-based cooperative strategy* was proposed in [33] and it achieved the full diversity order in AF cooperative networks. Furthermore, the error performance of this cooperative strategy was studied in [2, 22, 23, 45]. However, the repetition-based cooperative strategy has very poor bandwidth efficiency, because it allows only one relay to forward signals at each time slot. In order to improve the bandwidth efficiency, *distributed space-time block codes* (DSTBCs) were proposed and extensively studied in Chapter 2 and [25, 35, 41].

Many works have been devoted to the error performance and diversity order analysis of DSTBCs in AF cooperative networks. Jing *et al.* considered a cooperative network with *blind relays*, i.e. the relays did not have any channel state information (CSI) and set the amplifying coefficients as constants. Furthermore, it was assumed that *all* the channels in the cooperative network had the same variance. Under this assumption, the authors used linear dispersion codes in the cooperative network and they showed that the codes could achieve the full diversity order. In a cooperative network with blind relays, Anghel *et al.* [3] considered *distributed Alamouti's code* which was single-symbol decodable and achieved the full rate one; but they only found an asymptotic BER expression of this code. Furthermore, in [5], the authors also considered an Alamouti's-coded cooperative network with blind relays and they presented a BER expression of the code at high SNR range. At low and moderate SNR range, however, the BER expressions in [3, 5] were not accurate.

Very recently, Ju *et al.* found the exact BER expression of the distributed Alamouti's

code [29] in an AF cooperative network with blind relays. However, the authors of [29] assumed that the first-hop channels, i.e. the channels from the source to the relays, had the same variance and the second-hop channels, i.e. the channels from the relays to the destination, also had the same variance. In practice, it is more important to consider a *dissimilar* cooperative network, where all the channels possibly have different variances. Unfortunately, it is very hard to extend the results in [29] to a dissimilar cooperative network. To the best of our knowledge, the error performance of the distributed Alamouti's code has not been analyzed in dissimilar cooperative networks with blind relays. This has motivated our work.

In this chapter, we study the BER of the distributed Alamouti's code in a dissimilar AF cooperative network with blind relays. We propose two closed-form approximate expressions of the exact BER of the distributed Alamouti's code. The first approximate BER is very close to the exact BER except when the variances of the second-hop channels are very small. On the other hand, the second approximate BER expression is very accurate except when the variances of the second-hop channels are very large. Therefore, irrespective of the values of the channel variances, we can always use one of the two proposed closed-form approximate BER expressions and accurately evaluate the BER of the distributed Alamouti's code. Furthermore, based on the approximate BER expressions, we show that the distributed Alamouti's code achieves the full diversity order two in a dissimilar AF cooperative network with two blind relays.

The rest of this chapter is organized as follows. Section 4.2 describes the cooperative network studied in this chapter. In Section 4.3, two closed-form approximate BER expressions are derived for the distributed Alamouti's code in a dissimilar cooperative network with blind relays. Then we analyze the diversity order of the code. Section 4.4 presents some numerical results and Section 4.5 concludes this chapter.

Notations: We use $A =: B$ to denote B, by definition, equals A. For a random variable X, $\mathbb{E}[X]$ and $\mathrm{Var}[X]$ denote its mean and variance, respectively. $X \sim \mathscr{CN}(0, \Omega_X)$ means X is a circularly symmetric complex Gaussian random variable with zero mean and variance Ω_X. For two random variables X and Y, $\mathscr{C}(X,Y)$ and $\mathrm{Cov}(X,Y)$ denote their correlation coefficient and covariance, respectively.

4.2 System Model

We consider an AF cooperative network with one source, two relays, and one destination. Every terminal has only one antenna and is half-duplex. Let h_k and f_k denote the channel from the source to the k-th relay and the channel from the k-th relay to the destination, respectively. The channel coefficient h_k is modelled as $h_k = \bar{h}_k \sqrt{d_{s,k}^{-\beta_{s,k}}}$, where $\bar{h}_k \sim \mathscr{CN}(0,1)$, $\beta_{s,k}$ is the path loss exponent for this channel, and $d_{s,k}$ is the normalized distance from the source to the k-th relay. The value of $d_{s,k}$ is decided by $d_{s,k} = \bar{d}_{s,k}/D$, where $\bar{d}_{s,k}$ is the actual distance from the source to the k-th relay and D is the reference distance determined from measurements.[1] Similarly, we model the channel coefficient f_k as $f_k = \bar{f}_k \sqrt{d_{k,d}^{-\beta_{k,d}}}$, where $d_{k,d}$ is the normalized distance from the k-th relay to the destination, $\beta_{k,d}$ is the path loss exponent for this channel, and $\bar{f}_k \sim \mathscr{CN}(0,1)$. The value of $d_{k,d}$ is decided by $d_{k,d} = \bar{d}_{k,d}/D$, where $\bar{d}_{k,d}$ is the actual distance from the k-th relay to the destination. Thus, the variances Ω_{h_k} and Ω_{f_k} of h_k and f_k equal to $\Omega_{h_k} = d_{s,k}^{-\beta_{s,k}}$ and $\Omega_{f_k} = d_{k,d}^{-\beta_{k,d}}$, respectively.

At the first and second time slots, the source transmits two information-bearing symbols x_1 and x_2 to the relays, respectively. The transmission power at the source is E_s. The received signal $y_{k,t}$ of the k-th relay at the t-th time slot is given by $y_{k,t} = \sqrt{E_s} h_k x_t + n_{k,t}$,

[1] This chapter does not consider the measurement of the reference distances. This topic has been extensively studied in [44] for a variety of radio propagation environments.

where $n_{k,t}$ is the additive white Gaussian noise and $n_{k,t} \sim \mathscr{CN}(0, \sigma_n^2)$. In this chapter, we assume all the relays are blind relays as in [3, 23, 27, 29], i.e. the relays have no CSI at all. Therefore, the amplifying coefficient ρ_k at the k-th relay is given by

$$\rho_k = \sqrt{\frac{E_{rk}}{E_s \Omega_{h_k} + \sigma_n^2}}, \qquad k = 1, 2, \tag{4.1}$$

where E_{rk} is the transmission power from the k-th relay. This amplifying coefficient ρ_k ensures that the average power of the transmitted signal from the k-th relay is E_{rk} in the long term.

At the third and fourth time slots, the two relays use the distributed Alamouti's code to transmit the signals to the destination. Specifically, at the third time slot, the first relay transmits $\rho_1 y_{1,1}$ and the second relay transmits $-\rho_2 y_{2,2}^*$ to the destination. Thus, the received signal at the destination is $y_1 = \rho_1 f_1 y_{1,1} - \rho_2 f_2 y_{2,2}^* + n_1$, where n_1 is the additive white Gaussian noise and $n_1 \sim \mathscr{CN}(0, \sigma_n^2)$. At the fourth time slot, the first relay transmits $\rho_1 y_{1,2}$ and the second relay transmits $\rho_2 y_{2,1}^*$ to the destination. Consequently, the received signal at the destination is $y_2 = \rho_1 f_1 y_{1,2} + \rho_2 f_2 y_{2,1}^* + n_2$, where n_2 is the additive white Gaussian noise and $n_2 \sim \mathscr{CN}(0, \sigma_n^2)$. Due to the orthogonal structure of the distributed Alamouti's code, it is easy to obtain the maximum likelihood (ML) estimate $\hat{x}_1$ of x_1 [29] and it is given by $\hat{x}_1 = \rho_1 f_1^* h_1^* y_1 + \rho_2 f_2 h_2^* y_2^*$. Thus, the instantaneous SNR γ of $\hat{x}_1$ is given by

$$\gamma = \frac{E_s(\rho_1^2 |f_1 h_1|^2 + \rho_2^2 |f_2 h_2|^2)}{\sigma_n^2(\rho_1^2 |f_1|^2 + \rho_2^2 |f_2|^2 + 1)}. \tag{4.2}$$

Similarly, we can obtain the ML estimate $\hat{x}_2$ of x_2 and its instantaneous SNR is equal to γ as well. Furthermore, if M-quadrature amplitude modulation (QAM) is used as the modulation scheme and Gray mapping is used, the conditional BER $P_b(\gamma)$, conditioned on

instantaneous channel coefficients, of $\hat{x}_1$ or $\hat{x}_2$ is given by [8][2]

$$P_b(\gamma) = \frac{1}{\log_2 M} \sum_{j=1}^{\log_2 \sqrt{M}} P_{b,j}(\gamma) \tag{4.3}$$

and $P_{b,j}(\gamma)$ is given by

$$P_{b,j}(\gamma) = \frac{2}{\sqrt{M}} \sum_{i=0}^{\left(1-2^{-j}\right)\sqrt{M}-1} \left\{ (-1)^{\lfloor 2^{j-1} i/M \rfloor} \left(2^{j-1} - \left\lfloor \frac{2^{j-1} i}{\sqrt{M}} + \frac{1}{2} \right\rfloor \right) \times Q\left[(2i+1) \sqrt{\frac{3\gamma}{M-1}} \right] \right\}, \tag{4.4}$$

where $\lfloor \cdot \rfloor$ denotes the floor function and $Q(\cdot)$ denotes the Q-function defined in [52].. The exact average BER P_b of $\hat{x}_1$ or $\hat{x}_2$ can be obtained by averaging $P_b(\gamma)$ over γ, i.e. $P_b = \mathbb{E}[P_b(\gamma)]$.

4.3 BER and Diversity Order Analysis of the Distributed Alamouti's Code

In this section, we consider a dissimilar cooperative network where the variances Ω_{h_k} and Ω_{f_k} of the channels are possibly different. We derive two approximate BER expressions of the distributed Alamouti's code and show that the code achieves the full diversity order two.

In order to derive the exact BER P_b of $\hat{x}_1$ or $\hat{x}_2$, one needs the moment generating function (MGF) of γ; but it is very hard to obtain. Due to this reason, we try to find approximate BER expressions instead.

[2] If other modulation schemes are used, the conditional BER can be obtained by using [8] as well. Moreover, conditional SER can be obtained by using [42] and [52].

4.3.1 First approximate BER expression

We rewrite the instantaneous SNR γ in (4.2) as

$$\begin{aligned}\gamma &= \frac{E_s}{\sigma_n^2}\left(\frac{\min(|h_1|^2,|h_2|^2)(\rho_1^2|f_1|^2+\rho_2^2|f_2|^2)}{\rho_1^2|f_1|^2+\rho_2^2|f_2|^2+1}\right. \\ &\qquad \left.+\frac{(\max(|h_1|^2,|h_2|^2)-\min(|h_1|^2,|h_2|^2))\rho_p|f_p|^2}{\rho_1^2|f_1|^2+\rho_2^2|f_2|^2+1}\right) \qquad (4.5)\\ &=: \frac{E_s}{\sigma_n^2}\left(\gamma_1^{\text{app1}}+\gamma_2^{\text{app1}}\right), \qquad (4.6)\end{aligned}$$

where $p = \arg\max_{k=1,2}|h_k|^2$. In order to derive an approximate BER expression, it is desirable to find the MGFs of γ_1^{app1} and γ_2^{app1}. To this end, we develop the following lemma.

Lemma 4.1. *Assume X_1, X_2, Y_1, and Y_2 are exponential random variables with means a_1, a_2, b_1, and b_2, respectively. The MGF $\mathscr{M}_1(s;a_1,a_2,b_1,b_2)$ of the function $\min(X_1,X_2)(Y_1+Y_2)/(Y_1+Y_2+1)$ is given as follows:*

$$\mathscr{M}_1(s;a_1,a_2,b_1,b_2) = H\left(s,\frac{a_1a_2}{a_1+a_2},b_1,b_2\right), \qquad (4.7)$$

where the function $H(w,x,y,z)$ is given by

$$\begin{aligned}H(w,x,y,z) &= \frac{1}{(1-wx)^2(y-z)}\left[(1-wx)(y-z)-wxe^{\frac{1}{y(1-wx)}}\text{Ei}\left(\frac{1}{y(1-wx)}\right)\right. \\ &\qquad \left.+wxe^{\frac{1}{z(1-wx)}}\text{Ei}\left(\frac{1}{z(1-wx)}\right)\right], \qquad (4.8)\end{aligned}$$

and $\text{Ei}(\cdot)$ is the exponential integral function [19]. Let $p = \arg\max_{k=1,2}X_k$ and then the MGF $\mathscr{M}_2(s;a_1,a_2,b_1,b_2)$ of the function $(\max(X_1,X_2)-\min(X_1,X_2))Y_p/(Y_1+Y_2+1)$ is given by

$$\begin{aligned}&\mathscr{M}_2(s;a_1,a_2,b_1,b_2)\\ &= \frac{a_1}{(a_1+a_2)^2}\left[a_1+a_1^2sM\left(\frac{b_2}{b_1},-a_1s,\frac{1}{b_1}\right)+a_2+a_2^2sM\left(\frac{b_2}{b_1},-a_2s,\frac{1}{b_1}\right)\right]\end{aligned}$$

$$+\frac{a_2}{(a_1+a_2)^2}\left[a_1+a_1^2 sM\left(\frac{b_1}{b_2},-a_1 s,\frac{1}{b_2}\right)+a_2+a_2^2 sM\left(\frac{b_1}{b_2},-a_2 s,\frac{1}{b_2}\right)\right], \quad (4.9)$$

where the function $M(x,y,z)$ is given by

$$\begin{aligned} M(x,y,z) &= \frac{1}{(x-y-1)^2(y+1)}\Big[(y+1)(y+1-x)+e^{\frac{z}{x}}\mathrm{Ei}\left(\frac{z}{x}\right)x(y+1) \\ &\quad +e^{\frac{z}{1+y}}\mathrm{Ei}\left(\frac{z}{1+y}\right)(xz-(x+z)(y+1))\Big]. \quad (4.10)\end{aligned}$$

Proof: See Appendix 4-A. ■

The MGFs $\mathscr{M}_{\gamma_1^{\mathrm{app1}}}(s)$ and $\mathscr{M}_{\gamma_2^{\mathrm{app1}}}(s)$ of γ_1^{app1} and γ_2^{app1} in (4.6) can be easily obtained by using (4.7) and (4.9), respectively, and they are given by

$$\mathscr{M}_{\gamma_1^{\mathrm{app1}}}(s) = \mathscr{M}_1\left(s\frac{E_s}{\sigma_n^2};\Omega_{h_1},\Omega_{h_2},\rho_1^2\Omega_{f_1},\rho_2^2\Omega_{f_2}\right), \quad (4.11)$$

$$\mathscr{M}_{\gamma_2^{\mathrm{app1}}}(s) = \mathscr{M}_2\left(s\frac{E_s}{\sigma_n^2};\Omega_{h_1},\Omega_{h_2},\rho_1^2\Omega_{f_1},\rho_2^2\Omega_{f_2}\right). \quad (4.12)$$

Although γ_1^{app1} and γ_2^{app1} are dependent with each other, we ignore such dependency in this chapter and approximate the MGF $\mathscr{M}_\gamma(s)$ of γ in the following way

$$\mathscr{M}_\gamma(s) \approx \mathscr{M}^{\mathrm{app1}}(s) = \mathscr{M}_{\gamma_1^{\mathrm{app1}}}(s)\mathscr{M}_{\gamma_2^{\mathrm{app1}}}(s). \quad (4.13)$$

Based on (4.13), an approximate BER expression is derived in the following theorem. We will discuss how the approximation in (4.13), i.e. ignoring the dependency between γ_1^{app1} and γ_2^{app1}, affects the accuracy of the proposed approximate BER expression in detail later.

Theorem 4.1. *When M-QAM is used as the modulation scheme, the exact BER P_b can be approximated by*

$$P_b \approx P_b^{\mathrm{app1}} = \frac{1}{\log_2 M}\sum_{j=1}^{\log_2\sqrt{M}} P_{b,j}^{\mathrm{app1}}, \quad (4.14)$$

where $P_{b,j}^{\mathrm{app1}}$ is given by

$$P_{b,j}^{\mathrm{app1}} = \frac{2}{\sqrt{M}}\sum_{i=0}^{\left(1-2^{-j}\right)\sqrt{M}-1}\left\{(-1)^{\lfloor 2^{j-1}i/M\rfloor}\left(2^{j-1}-\left\lfloor\frac{2^{j-1}i}{\sqrt{M}}+\frac{1}{2}\right\rfloor\right)\right.$$

$$\times \left[\frac{1}{12} \mathscr{M}^{\text{app1}} \left(-\frac{3(2i+1)^2}{2(M-1)} \right) + \frac{1}{4} \mathscr{M}^{\text{app1}} \left(-\frac{2(2i+1)^2}{M-1} \right) \right] \Bigg\}. \quad (4.15)$$

Proof: It is well-known that Q-function can be very accurately approximated by [7]

$$Q(x) \approx \frac{1}{12} e^{-\frac{1}{2}x^2} + \frac{1}{4} e^{-\frac{2}{3}x^2}. \quad (4.16)$$

By using (4.16), all the Q-functions in (4.4) can be replaced by exponential functions. Then, by using $\mathscr{M}^{\text{app1}}(s)$ in (4.13), we can easily obtain (4.14) and (4.15). ■

Note that our proposed approximate BER P_b^{app1} in (4.14) is given in closed-form. Furthermore, numeric results demonstrate that P_b^{app1} is very close to P_b except when the variances Ω_{f_1} and Ω_{f_2} are both very small. In order to show the reason, we rewrite the instantaneous SNR γ of (4.2) as follows:

$$\gamma = \frac{E_s}{\sigma_n^2} \left(\gamma_{1(a)}^{\text{app1}} \gamma_{1(b)}^{\text{app1}} + \gamma_{2(a)}^{\text{app1}} \gamma_{2(b)}^{\text{app1}} \right), \quad (4.17)$$

where

$$\begin{aligned}
\gamma_{1(a)}^{\text{app1}} &= \min(|h_1|^2, |h_2|^2), && (4.18)\\
\gamma_{1(b)}^{\text{app1}} &= \frac{\rho_1^2 |f_1|^2 + \rho_2^2 |f_2|^2}{\rho_1^2 |f_1|^2 + \rho_2^2 |f_2|^2 + 1}, && (4.19)\\
\gamma_{2(a)}^{\text{app1}} &= \max(|h_1|^2, |h_2|^2) - \min(|h_1|^2, |h_2|^2), && (4.20)\\
\gamma_{2(b)}^{\text{app1}} &= \frac{\rho_p^2 |f_p|^2}{\rho_1^2 |f_1|^2 + \rho_2^2 |f_2|^2 + 1}, && (4.21)
\end{aligned}$$

and $p = \arg\max_{k=1,2} |h_k|^2$. When we derive P_b^{app1}, the dependency between γ_1^{app1} and γ_2^{app1} in (4.6) is neglected. Thus, P_b^{app1} may not be accurate when such dependency is strong. In order to investigate the dependency between γ_1^{app1} and γ_2^{app1}, we first notice that $\gamma_{1(a)}^{\text{app1}}$ is independent of both $\gamma_{1(b)}^{\text{app1}}$ and $\gamma_{2(b)}^{\text{app1}}$. Moreover, $\gamma_{2(a)}^{\text{app1}}$ is independent of both $\gamma_{1(b)}^{\text{app1}}$ and $\gamma_{2(b)}^{\text{app1}}$ as well. Secondly, the dependency between $\gamma_{1(a)}^{\text{app1}}$ and $\gamma_{2(a)}^{\text{app1}}$ is actually very weak, because their correlation coefficient $\mathscr{C}(\gamma_{1(a)}^{\text{app1}}, \gamma_{2(a)}^{\text{app1}})$ is equal to zero as shown in the following lemma.

Lemma 4.2. *The correlation coefficient* $\mathscr{C}(\gamma_{1(a)}^{\text{app1}}, \gamma_{2(a)}^{\text{app1}})$ *of* $\gamma_{1(a)}^{\text{app1}}$ *and* $\gamma_{2(a)}^{\text{app1}}$ *is zero.*

Proof: See Appendix 4-B. ■

As a result, the dependency between γ_1^{app1} and γ_2^{app1} is mainly decided by that between $\gamma_{1(b)}^{\text{app1}}$ and $\gamma_{2(b)}^{\text{app1}}$. We use the correlation coefficient $\mathscr{C}(\gamma_{1(b)}^{\text{app1}}, \gamma_{2(b)}^{\text{app1}})$ to evaluate the dependency between $\gamma_{1(b)}^{\text{app1}}$ and $\gamma_{2(b)}^{\text{app1}}$. The exact closed-form expression of $\mathscr{C}(\gamma_{1(b)}^{\text{app1}}, \gamma_{2(b)}^{\text{app1}})$ is very hard to obtain. However, the following lemma shows that $\mathscr{C}(\gamma_{1(b)}^{\text{app1}}, \gamma_{2(b)}^{\text{app1}})$ is actually very close to zero except when the variances Ω_{f_1} and Ω_{f_2} are both very small.

Lemma 4.3. *When* Ω_{f_1} *and* Ω_{f_2} *are both very small, the correlation coefficient* $\mathscr{C}(\gamma_{1(b)}^{\text{app1}}, \gamma_{2(b)}^{\text{app1}})$ *of* $\gamma_{1(b)}^{\text{app1}}$ *and* $\gamma_{2(b)}^{\text{app1}}$ *can be approximated by*

$$\mathscr{C}(\gamma_{1(b)}^{\text{app1}}, \gamma_{2(b)}^{\text{app1}}) \approx \frac{\Omega_{h_1}}{\Omega_{h_1}+\Omega_{h_2}} \sqrt{\frac{\rho_1^4\Omega_{f_1}^2}{\rho_1^4\Omega_{f_1}^2+\rho_2^4\Omega_{f_2}^2}} + \frac{\Omega_{h_2}}{\Omega_{h_1}+\Omega_{h_2}} \sqrt{\frac{\rho_2^4\Omega_{f_2}^2}{\rho_1^4\Omega_{f_1}^2+\rho_2^4\Omega_{f_2}^2}} \tag{4.22}$$

For all other cases, $\mathscr{C}(\gamma_{1(b)}^{\text{app1}}, \gamma_{2(b)}^{\text{app1}})$ *can be approximated by zero.*

Proof: See Appendix 4-C. ■

By Lemmas 4.2 and 4.3, we see that the dependency between γ_1^{app1} and γ_2^{app1} is strong only when Ω_{f_1} and Ω_{f_2} are both very small. This can be seen from Fig. 4.4 as well. As a result, for this special case, P_b^{app1} cannot approximate P_b very accurately. For all other cases, P_b^{app1} can always provide an accurate approximation of P_b.

4.3.2 Second approximate BER expression

In order to find an accurate approximation of P_b for the case that Ω_{f_1} and Ω_{f_2} are both very small, a second approximate BER expression is derived in the following. We separate the instantaneous SNR γ in (4.2) into two terms in a different way as follows:

$$\gamma = \frac{E_s}{\sigma_n^2}\left(\frac{\rho_1^2|f_1h_1|^2}{\rho_1^2|f_1|^2+\rho_2^2|f_2|^2+1} + \frac{\rho_2^2|f_2h_2|^2}{\rho_1^2|f_1|^2+\rho_2^2|f_2|^2+1}\right) \tag{4.23}$$

$$=: \quad \frac{E_s}{\sigma_n^2}\left(\gamma_1^{\text{app2}}+\gamma_2^{\text{app2}}\right). \tag{4.24}$$

In order to find an approximate BER expression, it is desirable to obtain the MGFs of γ_1^{app2} and γ_2^{app2}. Thus, we show the following lemma.

Lemma 4.4. *Assume X, Y_1, and Y_2 are exponential random variables with means a, b_1, and b_2, respectively. The MGF $\mathscr{M}_3(s;a,b_1,b_2)$ of the function $XY_1/(Y_1+Y_2+1)$ is given as follows:*

$$\mathscr{M}_3(s;a,b_1,b_2) = 1+asM\left(\frac{b_2}{b_1},-as,\frac{1}{b_1}\right), \tag{4.25}$$

where the function $M(x,y,z)$ is given by (4.10).

Proof: See Appendix 4-D. ■

Based on Lemma 4.4, one can easily find the MGFs $\mathscr{M}_{\gamma_1^{\text{app2}}}(s)$ and $\mathscr{M}_{\gamma_2^{\text{app2}}}(s)$ of γ_1^{app2} and γ_2^{app2} in (4.24). They are given as follows:

$$\mathscr{M}_{\gamma_1^{\text{app2}}}(s) = \mathscr{M}_3\left(s\frac{E_s}{\sigma_n^2};\Omega_{h_1},\rho_1^2\Omega_{f_1},\rho_2^2\Omega_{f_2}\right), \tag{4.26}$$

$$\mathscr{M}_{\gamma_2^{\text{app2}}}(s) = \mathscr{M}_3\left(s\frac{E_s}{\sigma_n^2};\Omega_{h_2},\rho_2^2\Omega_{f_2},\rho_1^2\Omega_{f_1}\right). \tag{4.27}$$

In this chapter, we ignore the dependency between γ_1^{app2} and γ_2^{app2} and find an approximation of the MGF $\mathscr{M}_\gamma(s)$ of γ as follows:

$$\mathscr{M}_\gamma(s) \approx \mathscr{M}^{\text{app2}}(s) = \mathscr{M}_{\gamma_1^{\text{app2}}}(s)\mathscr{M}_{\gamma_2^{\text{app2}}}(s). \tag{4.28}$$

The approximate MGF $\mathscr{M}^{\text{app2}}(s)$ enables us to find an approximate BER expression as in the following theorem. Certainly, the dependency between γ_1^{app2} and γ_2^{app2} affects the accuracy of the proposed approximate BER expression and this will be discussed in detail later.

Theorem 4.2. *When M-QAM is used as the modulation scheme, the exact BER P_b can be approximated by*

$$P_b \approx P_b^{\text{app2}} = \frac{1}{\log_2 M} \sum_{j=1}^{\log_2 \sqrt{M}} P_{b,j}^{\text{app2}}, \tag{4.29}$$

where $P_{b,j}^{\text{app2}}$ is given by

$$P_{b,j}^{\text{app2}} = \frac{2}{\sqrt{M}} \sum_{i=0}^{\left(1-2^{-j}\right)\sqrt{M}-1} \left\{ (-1)^{\lfloor 2^{j-1} i/M \rfloor} \left(2^{j-1} - \left\lfloor \frac{2^{j-1} i}{\sqrt{M}} + \frac{1}{2} \right\rfloor \right) \times \left[\frac{1}{12} \mathscr{M}^{\text{app2}} \left(-\frac{3(2i+1)^2}{2(M-1)} \right) + \frac{1}{4} \mathscr{M}^{\text{app2}} \left(-\frac{2(2i+1)^2}{M-1} \right) \right] \right\}. \tag{4.30}$$

Proof: The proof is essentially the same as that of Theorem 4.1 except that we use $\mathscr{M}^{\text{app2}}(s)$ instead of $\mathscr{M}^{\text{app1}}(s)$ in order to obtain a new approximate BER expression. ■

As our first approximate BER expression, the second approximate BER P_b^{app2} in (4.29) is also given in closed form. Moreover, numerical results demonstrate that P_b^{app2} is an accurate approximation of P_b except when Ω_{f_1} and Ω_{f_2} are both very large, which can be explained as follows. We rewrite the instantaneous SNR γ of (4.2) in the following way

$$\gamma = \frac{E_s}{\sigma_n^2} \left(\gamma_{1(a)}^{\text{app2}} |h_1|^2 + \gamma_{2(a)}^{\text{app2}} |h_2|^2 \right), \tag{4.31}$$

where

$$\gamma_{1(a)}^{\text{app2}} = \frac{\rho_1^2 |f_1|^2}{\rho_1^2 |f_1|^2 + \rho_2^2 |f_2|^2 + 1}, \tag{4.32}$$

$$\gamma_{2(a)}^{\text{app2}} = \frac{\rho_2^2 |f_2|^2}{\rho_1^2 |f_1|^2 + \rho_2^2 |f_2|^2 + 1}. \tag{4.33}$$

Since P_b^{app2} is obtained by ignoring the dependency between γ_1^{app2} and γ_2^{app2}, it may have poor accuracy when such dependency is strong. In fact, the dependency between γ_1^{app2} and γ_2^{app2} is purely decided by that between $\gamma_{1(a)}^{\text{app2}}$ and $\gamma_{2(a)}^{\text{app2}}$, because $|h_1|^2$ and $|h_2|^2$ are independent. The dependency between $\gamma_{1(a)}^{\text{app2}}$ and $\gamma_{2(a)}^{\text{app2}}$ can be evaluated by their correlation coefficient $\mathscr{C}(\gamma_{1(a)}^{\text{app2}}, \gamma_{2(a)}^{\text{app2}})$. Although it is very hard to find the exact expression of

$\mathscr{C}(\gamma_{1(a)}^{\text{app2}}, \gamma_{2(a)}^{\text{app2}})$ in closed-form, the following lemma shows that $\mathscr{C}(\gamma_{1(a)}^{\text{app2}}, \gamma_{2(a)}^{\text{app2}})$ is actually very small except when Ω_{f_1} and Ω_{f_2} are both very large.

Lemma 4.5. *When Ω_{f_1} and Ω_{f_2} are both very large, the correlation coefficient $\mathscr{C}(\gamma_{1(a)}^{\text{app2}}, \gamma_{2(a)}^{\text{app2}})$ of $\gamma_{1(a)}^{\text{app2}}$ and $\gamma_{2(a)}^{\text{app2}}$ can be approximated by -1. For the other cases, $\mathscr{C}(\gamma_{1(a)}^{\text{app2}}, \gamma_{2(a)}^{\text{app2}})$ can be approximated by zero.*

Proof: When Ω_{f_1} and Ω_{f_2} are both very large, the values of $\rho_1^2|f_1|^2$ and $\rho_2^2|f_2|^2$ are much larger than one with a very high probability, and hence, $\gamma_{k(a)}^{\text{app2}} \approx \rho_k^2|f_k|^2/(\rho_1^2|f_1|^2 + \rho_2^2|f_2|^2)$, $k = 1, 2$. Therefore, $\gamma_{1(a)}^{\text{app2}} \approx 1 - \gamma_{2(a)}^{\text{app2}}$ which implies $\mathscr{C}(\gamma_{1(a)}^{\text{app2}}, \gamma_{2(a)}^{\text{app2}}) \approx -1$.

When Ω_{f_1} is large and Ω_{f_2} is small, the denominator of $\gamma_{1(a)}^{\text{app2}}$ is dominantly decided by $\rho_1^2|f_1|^2$, and hence, $\gamma_{1(a)}^{\text{app2}} \approx 1$, which is a constant. Therefore, $\mathscr{C}(\gamma_{1(a)}^{\text{app2}}, \gamma_{2(a)}^{\text{app2}})$ can be approximated by zero for this case. Similarly, when Ω_{f_1} is small and Ω_{f_2} is large, and when both Ω_{f_1} and Ω_{f_2} are small, it can be shown that $\mathscr{C}(\gamma_{1(a)}^{\text{app2}}, \gamma_{2(a)}^{\text{app2}})$ is very close to zero.

■

Lemma 4.5 implies that the dependency between γ_1^{app2} and γ_2^{app2} is strong only when Ω_{f_1} and Ω_{f_2} are both very large. This can be seen in Fig. 4.4 as well. Consequently, P_b^{app2} is not very accurate for this special case. For the other cases, however, P_b^{app2} is always an accurate approximation of P_b. Recall that the first approximate BER P_b^{app1} is very close to P_b except when Ω_{f_1} and Ω_{f_2} are both very small. Therefore, depending on the values of Ω_{f_1} and Ω_{f_2}, one can always use either P_b^{app1} or P_b^{app2} in order to accurately approximate P_b. Specifically, when Ω_{f_1} and Ω_{f_2} are both very small, one should choose P_b^{app2}; while, when Ω_{f_1} and Ω_{f_2} are both very large, one should use P_b^{app1}. For the other cases, both P_b^{app1} and P_b^{app2} can be used, because both of them are very close to P_b. The accuracy of P_b^{app1} and P_b^{app2} will be confirmed by our simulation results in Section 4.4.

4.3.3 Diversity order of the distributed Alamouti's code in dissimilar cooperative networks

The approximate BER expressions P_b^{app1} and P_b^{app2} also enable us to find the diversity order of the distributed Alamouti's code in a dissimilar cooperative network with blind relays. In the following lemma, by using P_b^{app1}, we show that the code achieves the full diversity order.

Lemma 4.6. *In a cooperative network with two blind relays, the exact BER P_b of the distributed Alamouti's code behaves like $(\ln(E)/E)^2$ when the transmission power E is sufficiently large. That is, the distributed Alamouti's code achieves the full diversity order two.*

Proof: For simplicity, we assume $E_s = E_{r1} = E_{r2} = E$ and $\sigma_n^2 = 1$. Note that this assumption does not change the diversity order. When E goes to infinity, we have

$$\lim_{E\to\infty} \mathscr{M}^{\text{app1}}\left(-\frac{3(2i+1)^2}{2(M-1)}\right) = C\left(\frac{\ln(E)}{E}\right)^2 + \mathscr{O}\left(\frac{1}{E^3}\right), \tag{4.34}$$

where C is a constant. Therefore, when E is large, $\mathscr{M}^{\text{app1}}\left(-3(2i+1)^2/(2(M-1))\right)$ behaves like $(\ln(E)/E)^2$. The same conclusion also applies to $\mathscr{M}^{\text{app1}}(-2(2i+1)^2/(M-1))$. Thus, when E is large, the approximate BER P_b^{app1} behaves like $(\ln(E)/E)^2$. Since P_b^{app1} accurately approximates P_b, P_b behaves like $(\ln(E)/E)^2$ as well when E is large. Therefore, the distributed Alamouti's code achieves the full diversity order two.[3] ■

In [27], Jing *et al.* has shown that the pairwise error probability of the distributed linear dispersion codes behaves like $(\ln(E)/E)^K$ in a cooperative network with K relays. Since distributed Alamouti's code is a special distributed linear dispersion code, it is not surprising that its error performance behaves like $(\ln(E)/E)^2$. Moreover, when E is sufficiently

[3] We can show that the distributed Alamouti's code achieves the full diversity order by using P_b^{app2} as well. The proof is similar to that of Lemma 4.6.

large, $\ln(E)$ is much smaller than E, and hence, $(\ln(E)/E)^2 \approx 1/E^2$. Therefore, we believe that the distributed Alamouti's code can achieve the full diversity order two at high SNR range. Note that the result in [27] was based on the assumption that the variances of *all* the channels were *identical*. Our work is more general than [27] in the sense that we consider a dissimilar cooperative network where the variances of the channels are possibly different.

4.4 Numerical Results

In this section, we compare the proposed approximate BER expressions with the exact BER obtained by simulation. We use M-QAM as the modulation scheme. The source and the two relays have the same transmission powers, i.e. $E_s = E_{r1} = E_{r2} = E$. Thus, the average SNR per bit is equal to $E/(\sigma_n^2 \log_2 M)$. We assume that the source, the relays, and the destination are located in a straight line. Furthermore, we let the reference distance equal to the distance from the source to the destination, and hence, $d_{s,k} = 1 - d_{k,d}$, $k = 1, 2$. We set the path loss exponents as $\beta_{s,k} = \beta_{k,d} = 4$, $k = 1, 2$, in order to model the wireless channels in an urban area. As a result, the channel variances Ω_{h_k} and Ω_{f_k} are purely decided by the locations of the relays, i.e. $\Omega_{h_k} = d_{s,k}^{-4}$ and $\Omega_{f_k} = d_{k,d}^{-4}$.

In Fig. 4.1, we compare the first approximate BER expression P_b^{app1} with the exact BER P_b. In order to test the accuracy of P_b^{app1}, we consider three channel settings by placing the two relays at three different locations. Fig. 4.1 shows that P_b^{app1} is very accurate in all channel settings. Furthermore, unlike the BER expressions in [3, 5], which is accurate only at high SNR range, P_b^{app1} is accurate over the whole SNR range. In Fig. 4.2, the second approximate BER expression P_b^{app2} is compared with P_b under three different channel settings. We see that P_b^{app2} also provides an accurate approximation of P_b over the whole SNR range.

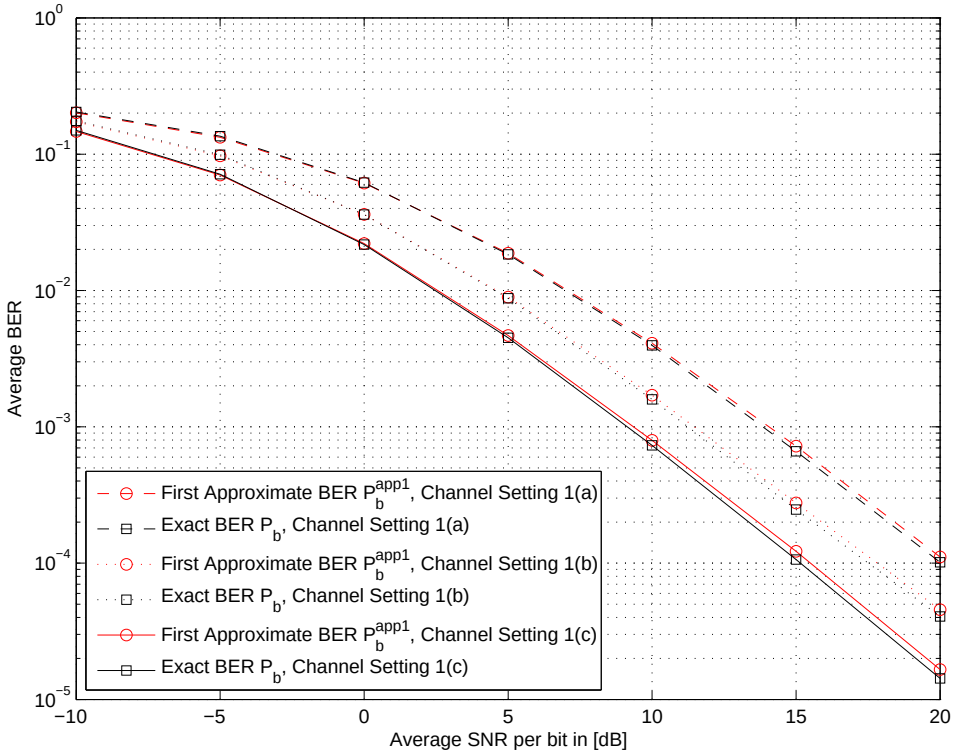

Figure 4.1. Comparison of the exact BER P_b and the first approximate BER P_b^{app1}, 8-QAM. Channel Setting 1(a): $d_{s,1} = 0.7$, $d_{s,2} = 0.8$; Channel Setting 1(b): $d_{s,1} = 0.6$, $d_{s,2} = 0.7$; Channel Setting 1(c): $d_{s,1} = 0.5$, $d_{s,2} = 0.6$.

In Fig. 4.3, we show how the channel variances affect the accuracies of P_b^{app1} and P_b^{app2}. We fix the distance between the two relays and move the two relays between the source and the destination in order to change the values of Ω_{h_k} and Ω_{f_k}. It can be seen that P_b^{app1} is very accurate when the two relays are close to the destination; while it loses accuracy when the relays move toward the source. This can be explained by Lemma 4.3 and can be seen from Fig. 4.4. When the relays get closer to the source, the value of $d_{k,d}$ becomes larger, and hence, the value of Ω_{f_k} becomes smaller. As a result, the dependency between $\gamma_{1(b)}^{\text{app1}}$ and $\gamma_{2(b)}^{\text{app1}}$ gets strong, which makes P_b^{app1} lose its accuracy.

On the other hand, the second approximate BER P_b^{app2} is very accurate when the relays

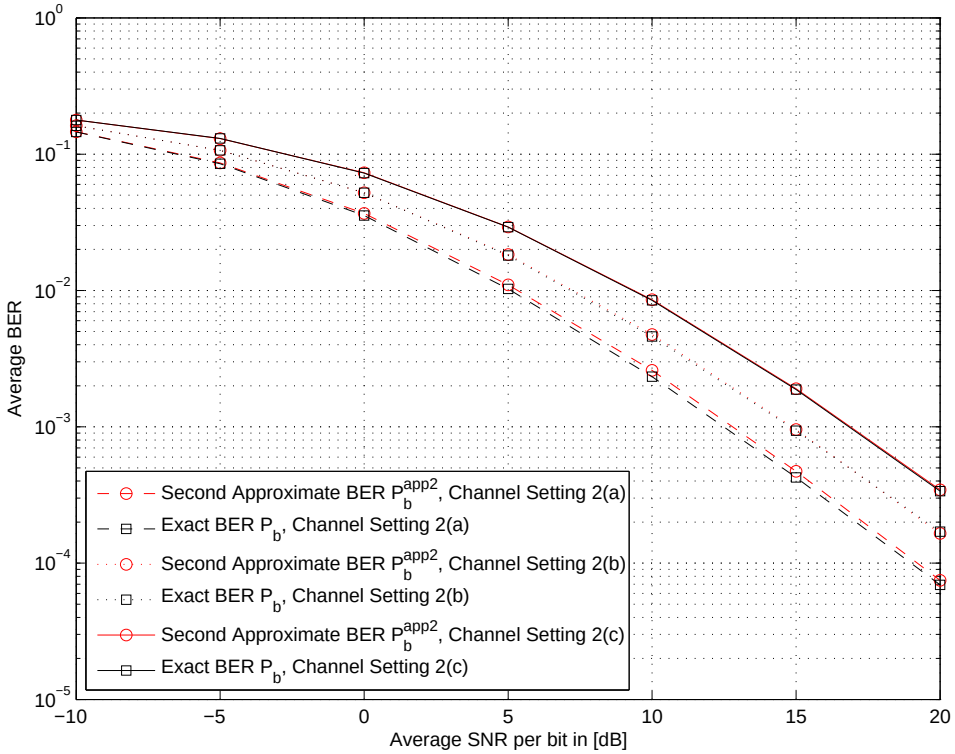

Figure 4.2. Comparison of the exact BER P_b and the second approximate BER P_b^{app2}, 16-QAM. Channel Setting 2(a): $d_{s,1} = 0.3$, $d_{s,2} = 0.4$; Channel Setting 2(b): $d_{s,1} = 0.2$, $d_{s,2} = 0.3$; Channel Setting 2(c): $d_{s,1} = 0.1$, $d_{s,2} = 0.2$.

are close to the source; while it becomes less accurate when the relays move toward the destination. This is because, when the relays are closer to the destination, the value of $d_{k,d}$ gets smaller and the value of Ω_{f_k} gets larger. By Lemma 4.5 and Fig. 4.4., the dependency between $\gamma_{1(a)}^{\text{app2}}$ and $\gamma_{2(a)}^{\text{app2}}$ grows stronger, and hence, P_b^{app2} becomes less accurate. Therefore, Fig. 4.3 demonstrates that, when the relays are close to the destination, we should use P_b^{app1} to approximate the error performance of the distributed Alamouti's code and, when the relays are close to the source, P_b^{app2} should be used.

From Fig. 4.3, it seems that, when the relays are located in the center between the source and the destination, neither P_b^{app1} or P_b^{app2} can approximate P_b well enough. For example, in

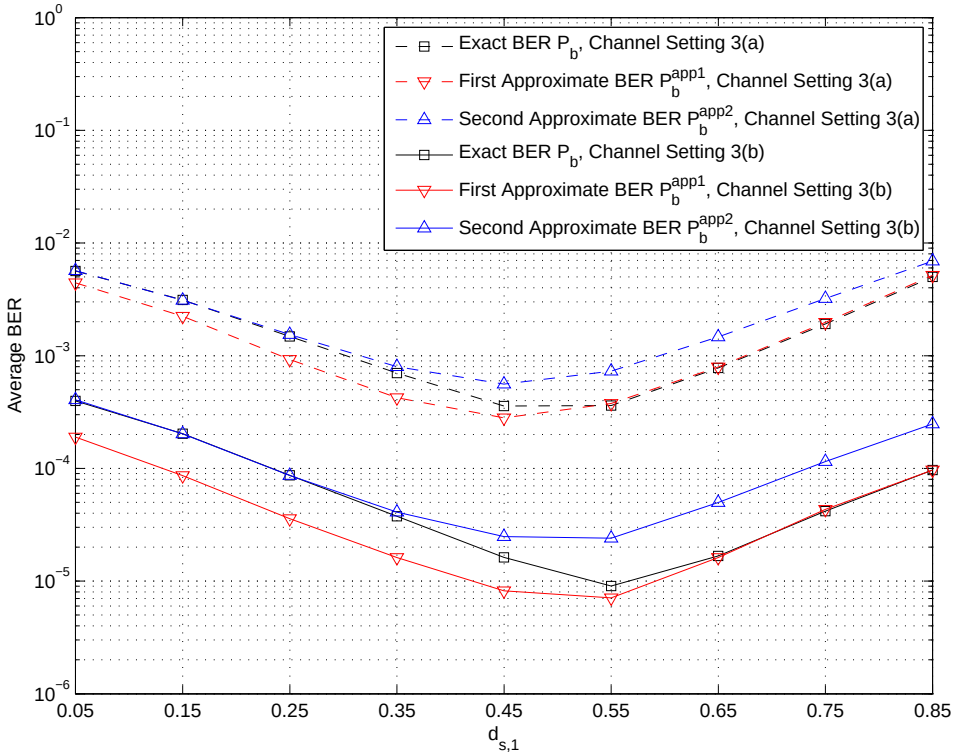

Figure 4.3. Comparison of the exact BER P_b, the first approximate BER P_b^{app1}, and the second approximate BER P_b^{app2}. Channel Setting 3(a): $E/(\sigma_n^2 \log_2 M) = 10$ dB, $d_{s,2} - d_{s,1} = 0.05$, 4-QAM; Channel Setting 3(b): $E/(\sigma_n^2 \log_2 M) = 20$ dB, $d_{s,2} = d_{s,1}$, 8-QAM.

Fig. 4.3, it seems that both P_b^{app1} and P_b^{app2} are not close to P_b when $d_{s,1} = 0.4$, $d_{s,2} = 0.45$, and the average SNR per bit is 10 dB. In order to clarify this point, we provide Figs. 4.5 and 4.6. By those two figures, we see that P_b^{app1} and P_b^{app2} still approximate P_b with a good accuracy at low and medium SNR range when the two relays are placed in the center between the source and the destination. For example, Fig. 4.5 demonstrates that, when $d_{s,1} = 0.4$ and $d_{s,1} = 0.45$, the difference between P_b^{app2} and P_b is about 0.6 dB when the average SNR per bit is at 10 dB. Although the difference between the exact BER and our approximate BER expressions slightly increases with the average SNR per bit, the largest difference is approximately 1 dB at practical average SNR and BER range. Therefore, our

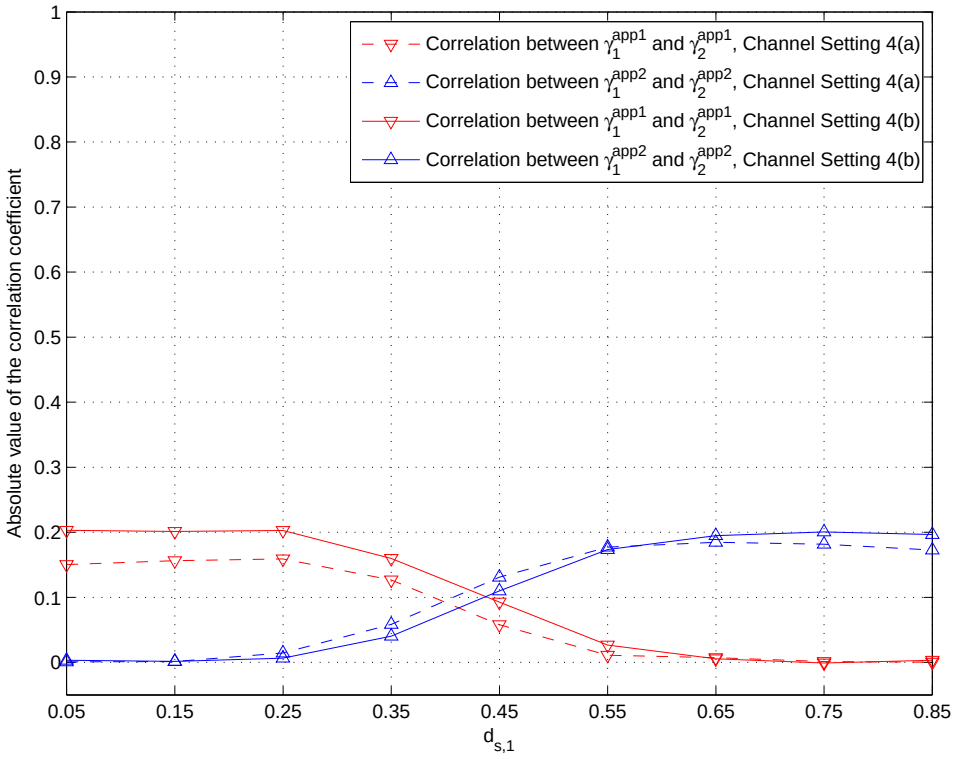

Figure 4.4. Absolute value of the correlation coefficient between $\gamma_1^{app1}(\gamma_1^{app2})$ and $\gamma_2^{app1}(\gamma_2^{app2})$. Channel Setting 4(a): $E/(\sigma_n^2 \log_2 M) = 10$ dB, $d_{s,2} - d_{s,1} = 0.05$; Channel Setting 4(b): $E/(\sigma_n^2 \log_2 M) = 20$ dB, $d_{s,2} = d_{s,1}$.

approximate BER expressions still approximate the exact BER with an acceptable accuracy even when the relays are located in the center between the source and the destination.

4.5 Conclusion

The error performance of the distributed Alamouti's code is studied in this chapter. We consider a general dissimilar cooperative network, where the channel variances may have different values. Two closed-form approximate BER expressions are derived in order to evaluate the error performance of the distributed Alamouti's code. The first approximate

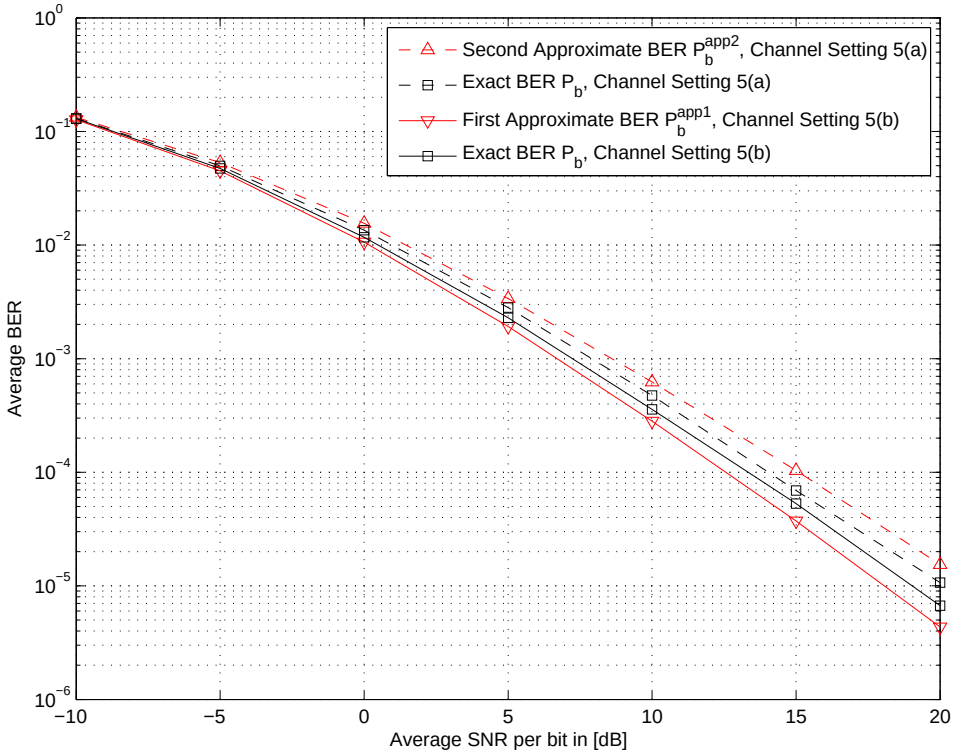

Figure 4.5. Comparison of the exact BER P_b, the first approximate BER P_b^{app1}, and the second approximate BER P_b^{app2}, 4-QAM. Channel Setting 5(a): $d_{s,1} = 0.4$, $d_{s,2} = 0.45$; Channel Setting 5(b): $d_{s,1} = 0.45$, $d_{s,2} = 0.5$.

BER expression is very close to the exact BER except when the variances of the second-hop channels are very small. On the other hand, the second approximate BER expression is very accurate except when the variances of the second-hop channels are very large. Therefore, irrespective of the values of the channel variances, we can always choose one of the two proposed approximate BER expressions and accurately evaluate the error performance of the distributed Alamouti's code. Based on the approximate BER expressions, we also show that the distributed Alamouti's code achieve the full diversity order two in a dissimilar cooperative network with two blind relays.

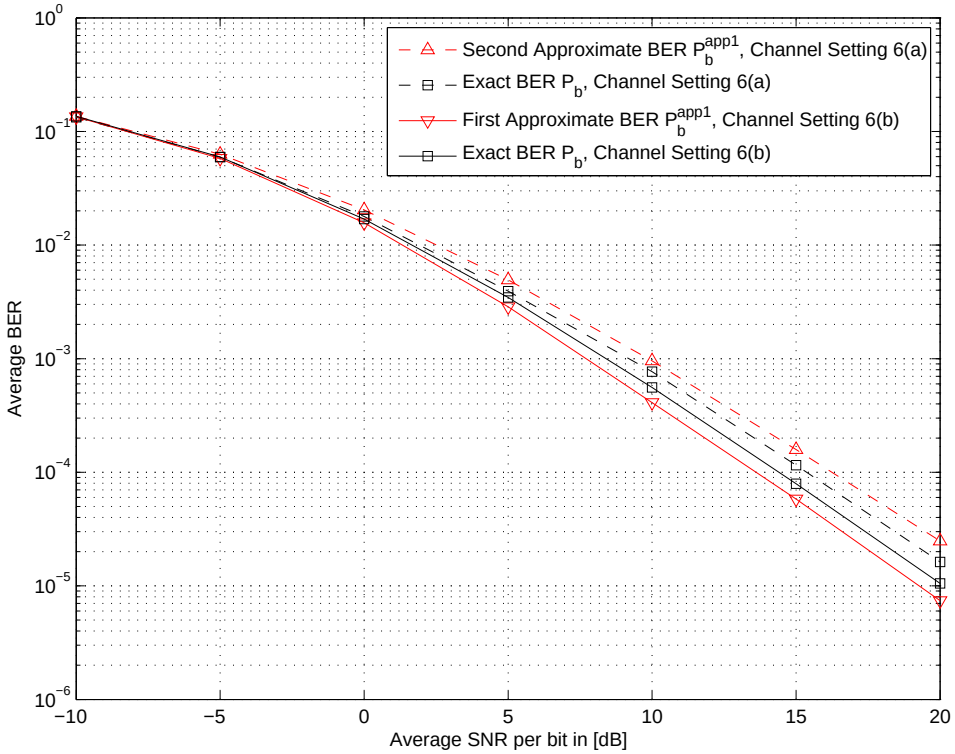

Figure 4.6. Comparison of the exact BER P_b, the first approximate BER P_b^{app1}, and the second approximate BER P_b^{app2}, 8-QAM. Channel Setting 6(a): $d_{s,1} = 0.45$, $d_{s,2} = 0.45$; Channel Setting 6(b): $d_{s,1} = 0.5$, $d_{s,2} = 0.5$.

4.6 Appendix 4-A: Proof of Lemma 4.1

We first show the derivation of $\mathscr{M}_1(s;a_1,a_2,b_1,b_2)$. Let $Z_1 = \min(X_1,X_2)$ and $T_1 = (Y_1 + Y_2)/(Y_1+Y_2+1)$. It is not hard to find the probability density functions (PDFs) $f_{Z_1}(z)$ and $f_{T_1}(t)$ of Z_1 and T_1

$$f_{Z_1}(z) = \left(\frac{1}{a_1}+\frac{1}{a_2}\right) e^{-\left(\frac{1}{a_1}+\frac{1}{a_2}\right)z}, \tag{4.A-1}$$

$$f_{T_1}(t) = \frac{e^{\frac{t}{b_2(t-1)}} - e^{\frac{t}{b_1(t-1)}}}{(t-1)^2(b_2-b_1)}, \qquad 0 \le t \le 1. \tag{4.A-2}$$

Furthermore, the following integration can be derived by [19, pp. 338, 3.353.5] and [19, pp. 337, 3.352.4]

$$\int_0^1 \frac{e^{\frac{t}{z(t-1)}} - e^{\frac{t}{y(t-1)}}}{(z-y)(t-1)^2(1-wxt)}dt \overset{\frac{t}{1-t}=u}{=} \int_0^\infty \frac{e^{-\frac{u}{z}} - e^{-\frac{u}{y}}}{zy}\frac{u+1}{(1-wx)u+1}du \quad (4.A\text{-}3)$$

$$= \int_0^\infty \frac{e^{-\frac{u}{z}} - e^{-\frac{u}{y}}}{zy}\frac{u}{(1-wx)u+1}du + \int_0^\infty \frac{e^{-\frac{u}{z}} - e^{-\frac{u}{y}}}{zy}\frac{1}{(1-wx)u+1}du \quad (4.A\text{-}4)$$

$$= H(w,x,y,z). \quad (4.A\text{-}5)$$

Based on (4.A-5), $\mathscr{M}_1(s;a_1,a_2,b_1,b_2)$ can be obtained as follows:

$$\mathscr{M}_1(s;a_1,a_2,b_1,b_2) = \int_0^1\int_0^\infty e^{szt} f_{Z_1}(z) f_{T_1}(t)dzdt \quad (4.A\text{-}6)$$

$$= \int_0^1 \frac{f_{T_1}(t)}{1-st\frac{a_1a_2}{a_1+a_2}}dt \quad (4.A\text{-}7)$$

$$= H\left(s, \frac{a_1a_2}{a_1+a_2}, b_1, b_2\right). \quad (4.A\text{-}8)$$

Secondly, we show the derivation of $\mathscr{M}_2(s;a_1,a_2,b_1,b_2)$. Let $Z_2 = \max(X_1,X_2) - \min(X_1,X_2)$ and $T_2 = Y_p/(Y_1+Y_2+1)$. The PDF $f_{Z_2}(z)$ of Z_2 can be derived from [58]

$$f_{Z_2}(z) = \frac{e^{-\frac{z}{a_1}}}{a_1+a_2} + \frac{e^{-\frac{z}{a_2}}}{a_1+a_2}. \quad (4.A\text{-}9)$$

We assume $p=2$, and hence, $T_2 = Y_2/(Y_1+Y_2+1)$. It is not hard to find the conditional cumulative distribution function (CDF) $F_{T_2|p=2}(t)$ of T_2

$$F_{T_2|p=2}(t) = \begin{cases} 1 - \frac{e^{-\frac{t}{b_2(1-t)}}}{\frac{b_1t}{b_2(1-t)}+1}, & 0 \le t \le 1 \\ 1, & t \ge 1 \end{cases}. \quad (4.A\text{-}10)$$

Furthermore, we find the following integration

$$\int_0^1 \frac{e^{-z\frac{t}{(1-t)}}}{\frac{xt}{(1-t)}+1}\frac{1}{(1-yt)^2}dt \overset{\frac{t}{1-t}=w}{=} \int_0^\infty \frac{e^{-zw}}{(xw+1)((1+y)w+1)^2}dw \quad (4.A\text{-}11)$$

$$= \int_0^\infty e^{-zw}\left(\frac{x^2}{(xw+1)(x-y-1)^2} - \frac{y+1}{(x-y-1)((1+y)w+1)^2} - \frac{(y+1)x}{((y+1)w+1)(x-y-1)^2}\right)dw \quad (4.A\text{-}12)$$

$$= M(x,y,z), \quad (4.A\text{-}13)$$

where the last step is done by using [19, pp. 337, 3.352.4 and 3.353.3].

Let $f_{T_2|p=2}(t)$ denote the conditional PDF of T_2, then the conditional MGF $\mathscr{M}_2(s;a_1,a_2,b_1,b_2|p=2)$ is given by

$$\mathscr{M}_2(s;a_1,a_2,b_1,b_2|p=2)$$

$$= \int_0^1\int_0^\infty e^{szt} f_{Z_2}(z) f_{T_2|p=2}(t)dzdt \quad (4.A\text{-}14)$$

$$= \frac{1}{a_1+a_2}\left(\int_0^1 \frac{a_1}{1-a_1st}dF_{T_2|p=2}(t) + \int_0^1 \frac{a_2}{1-a_2st}dF_{T_2|p=2}(t)\right) \quad (4.A\text{-}15)$$

$$= \frac{1}{a_1+a_2}\left[a_1 + a_1^2 sM\left(\frac{b_1}{b_2}, -a_1 s, \frac{1}{b_2}\right) + a_2 + a_2^2 sM\left(\frac{b_1}{b_2}, -a_2 s, \frac{1}{b_2}\right)\right] \quad (4.A\text{-}16)$$

where the last equality by using integration by parts and (4.A-13). Similarly, when $p=1$, the conditional MGF $\mathscr{M}_2(s;\, a_1,a_2,b_1,b_2|p=1)$ is given by

$$\mathscr{M}_2(s;a_1,a_2,b_1,b_2|p=1)$$

$$= \frac{1}{a_1+a_2}\left[a_1 + a_1^2 sM\left(\frac{b_2}{b_1}, -a_1 s, \frac{1}{b_1}\right) + a_2 + a_2^2 sM\left(\frac{b_2}{b_1}, -a_2 s, \frac{1}{b_1}\right)\right] \quad (4.A\text{-}17)$$

Based on (4.A-16) and (4.A-17), $\mathscr{M}_2(s;a_1,a_2,b_1,b_2)$ can be obtained by law of total probability

$$\mathscr{M}_2(s;a_1,a_2,b_1,b_2) = \Pr(p=1)\mathscr{M}_2(s;a_1,a_2,b_1,b_2|p=1) + \Pr(p=2)\mathscr{M}_2(s;a_1,a_2,b_1,b_2|p=2), \quad (4.A\text{-}18)$$

and hence, it is given by (4.9).

4.7 Appendix 4-B: Proof of Lemma 4.2

Let Y_1 and Y_2 denote $\min(|h_1|^2, |h_2|^2)$ and $\max(|h_1|^2, |h_2|^2)$, respectively. Thus, $\gamma_{1(a)}^{\text{app1}} = Y_1$ and $\gamma_{2(a)}^{\text{app1}} = Y_2 - Y_1$. Furthermore, by order statistics, it is not hard to show that $\mathbb{E}[Y_1 Y_2] = \Omega_{h_1}\Omega_{h_2}$, $\mathbb{E}[Y_1] = \Omega_{h_1}\Omega_{h_2}/(\Omega_{h_1} + \Omega_{h_2})$, $\mathbb{E}[Y_2] = (\Omega_{h_1}^2 + \Omega_{h_1}\Omega_{h_2} + \Omega_{h_2}^2)/(\Omega_{h_1} + \Omega_{h_2})$, and $\mathbb{E}[Y_1^2] = 2\Omega_{h_1}^2\Omega_{h_2}^2/(\Omega_{h_1} + \Omega_{h_2})^2$. By definition, $\mathscr{C}(\gamma_{1(a)}^{\text{app1}}, \gamma_{2(a)}^{\text{app1}})$ is given by

$$\begin{aligned} \mathscr{C}(\gamma_{1(a)}^{\text{app1}}, \gamma_{2(a)}^{\text{app1}}) &= \mathscr{C}(Y_1, Y_2 - Y_1) && \text{(4.B-1)} \\ &= \frac{\text{Cov}(Y_1, Y_2 - Y_1)}{\sqrt{\text{Var}[Y_1]\text{Var}[Y_2 - Y_1]}}. && \text{(4.B-2)} \end{aligned}$$

The covariance $\text{Cov}(Y_1, Y_2 - Y_1)$ can be obtained as follows:

$$\begin{aligned} \text{Cov}(Y_1, Y_2 - Y_1) &= \mathbb{E}[Y_1(Y_2 - Y_1)] - \mathbb{E}[Y_1]\mathbb{E}[Y_2 - Y_1] && \text{(4.B-3)} \\ &= \mathbb{E}[Y_1 Y_2] - \mathbb{E}\left[Y_1^2\right] - \mathbb{E}[Y_1]\mathbb{E}[Y_2] + \mathbb{E}^2[Y_1] && \text{(4.B-4)} \\ &= 0. && \text{(4.B-5)} \end{aligned}$$

Therefore, $\mathscr{C}(\gamma_{1(a)}^{\text{app1}}, \gamma_{2(a)}^{\text{app1}})$ is zero.

4.8 Appendix 4-C: Proof of Lemma 4.3

Let $Z_1 = \rho_1^2 |f_1|^2$ and $Z_2 = \rho_2^2 |f_2|^2$. Thus, $\gamma_{1(b)}^{\text{app1}} = (Z_1 + Z_2)/(Z_1 + Z_2 + 1)$ and $\gamma_{2(b)}^{\text{app1}} = Z_p/(Z_1 + Z_2 + 1)$ where $p = \arg\max_{k=1,2} |h_k|^2$. When Ω_{f_1} and Ω_{f_2} are both very small, the values of Z_1 and Z_2 are much smaller than one with a very high probability, and hence, $\gamma_{1(b)}^{\text{app1}} \approx Z_1 + Z_2$ and $\gamma_{2(b)}^{\text{app1}} \approx Z_p$. Thus, for this case, $\mathscr{C}(\gamma_{1(b)}^{\text{app1}}, \gamma_{2(b)}^{\text{app1}})$ can approximated by

$$\begin{aligned} \mathscr{C}(\gamma_{1(b)}^{\text{app1}}, \gamma_{2(b)}^{\text{app1}}) &\approx \mathscr{C}(Z_1 + Z_2, Z_p) && \text{(4.C-1)} \\ &= \frac{\Omega_{h_1}}{\Omega_{h_1} + \Omega_{h_2}}\mathscr{C}(Z_1 + Z_2, Z_1) + \frac{\Omega_{h_2}}{\Omega_{h_1} + \Omega_{h_2}}\mathscr{C}(Z_1 + Z_2, Z_2). && \text{(4.C-2)} \end{aligned}$$

Because Z_1 and Z_2 are exponential random variables, it is not hard to show that

$$\mathscr{C}(Z_1+Z_2,Z_1) = \sqrt{\frac{\rho_1^4\Omega_{f_1}^2}{\rho_1^4\Omega_{f_1}^2+\rho_2^4\Omega_{f_2}^2}} \tag{4.C-3}$$

$$\mathscr{C}(Z_1+Z_2,Z_2) = \sqrt{\frac{\rho_2^4\Omega_{f_2}^2}{\rho_1^4\Omega_{f_1}^2+\rho_2^4\Omega_{f_2}^2}}. \tag{4.C-4}$$

Therefore, $\mathscr{C}(\gamma_{1(b)}^{\text{app1}},\gamma_{2(b)}^{\text{app1}})$ is approximated by (4.22) when Ω_{f_1} and Ω_{f_2} are both very small.

When Ω_{f_1} is large and Ω_{f_2} is small, the value of Z_1 is much larger than one with a very high probability, and hence, the denominator Z_1+Z_2+1 of $\gamma_{1(b)}^{\text{app1}}$ is very close to Z_1+Z_2. Thus, $\gamma_{1(b)}^{\text{app1}}$ can be approximated by one, which is a constant. This implies that $\mathscr{C}(\gamma_{1(b)}^{\text{app1}},\gamma_{2(b)}^{\text{app1}})$ is very close to zero. Similarly, when Ω_{f_1} is small and Ω_{f_2} is large, and when both Ω_{f_1} and Ω_{f_2} are large, $\mathscr{C}(\gamma_{1(b)}^{\text{app1}},\gamma_{2(b)}^{\text{app1}})$ is very close to zero as well.

4.9 Appendix 4-D: Proof of Lemma 4.4

Let $T=Y_1/(Y_1+Y_2+1)$ and the CDF $F_T(t)$ of T can be obtained by (4.A-10). Let $f_T(t)$ denote the PDF of T, then $\mathscr{M}_3(s;a,b_1,b_2)$ is given by

$$\mathscr{M}_3(s;a,b_1,b_2) = \int_0^1\int_0^\infty e^{sxt}\frac{1}{a}e^{-\frac{x}{a}}f_T(t)dxdt \tag{4.D-1}$$

$$= \int_0^1 \frac{1}{1-ast}dF_T(t) \tag{4.D-2}$$

$$= \frac{F_T(t)}{1-ast}\,|_{t=0}^1 - \int_0^1 F_T(t)d\frac{1}{1-ast} \tag{4.D-3}$$

$$= 1+asM\left(\frac{b_2}{b_1},-as,\frac{1}{b_1}\right), \tag{4.D-4}$$

where the last step is done by using (4.A-13).

Chapter 5

BER and Diversity Order Analysis of Distributed Alamouti's Code in Dissimilar Cooperative Networks with CSI-Assisted Relays

This chapter focuses on the average bit error rate (BER) and diversity order analysis of the distributed Alamouti's code in dissimilar cooperative networks with channel state information (CSI)-assisted relays. We first assume that the relays adopt the amplifying coefficient proposed in [33]. Lower and upper bound of the average BER of the distributed Alamouti's code are derived. Those two bounds can tightly bound the exact average BER. We then show that the distributed Alamouti's code only achieves diversity order one when the relays use the amplifying coefficient proposed in [33]. Furthermore, in a general cooperative network with more than two relays, we show that the distributed space-time block codes proposed in [27] only achieve diversity order one as well when the amplifying coefficient proposed in [33] is used at the relays. To resolve this problem, we propose a new threshold-based amplifying coefficient for the distributed Alamouti's code based on the work in [23]. This new amplifying coefficient makes the code achieve the full diversity

order two. Moreover, based on three different criteria, three optimum and one suboptimum schemes are developed in order to choose the value of the threshold used in the new amplifying coefficient.

5.1 Introduction

In a cooperative network, several single-antenna relay terminals help the source transmit signals to the destination by forming a distributed multiple-antenna system [23, 27, 33, 64, 66]. Specifically, in an amplify-and-forward (AF) cooperative network, each relay multiplies the received signal with an amplifying coefficient and then forwards it to the destination. In order to coordinate the transmissions from the relays, *distributed space-time block codes* (DSTBCs) have been proposed and extensively studied in Chapter 2 and [27, 35]. Many works have analyzed the error performance and diversity order of the DSTBCs in AF cooperative networks. For example, Jing *et al.* showed that the DSTBCs could achieve the full diversity order in the number of relays [27]. In [29], Ju *et al.* found the exact average BER expression of the distributed Alamouti's code; but the expression was not given in closed-form. In Chapter 4, we derived two closed-form approximate average BER expressions of the distributed Alamouti's code.

However, the authors of [27, 29, 67] all assumed that the relays in the cooperative network did not have any channel side information (CSI) of the first-hop channels, i.e. the channels from the source to the relays. Those relays were called the *blind relays*. As a result, the amplifying coefficients of the relays were fixed numbers and the amplifiers at the relays might go into saturation when the instantaneous gains of the first-hop channels were large [3]. In practical systems, it is preferable to implement the *CSI-assisted relays* which know the instantaneous channel gains of the first-hop channels. In fact, this CSI

can be easily obtained at the relays without any feedback overhead. Laneman *et al.* have proposed an amplifying coefficient for the CSI-assisted relays [33] and it can successfully avoid saturations of the amplifiers [3]. Due to this reason, this amplifying coefficient has been used in many previous publications [2, 45, 48]. It is practically very important to analyze the distributed Alamouti's code in cooperative networks with CSI-assisted relays. Unfortunately, it is very hard extend the results in [27, 29, 67] to such networks. To the best of our knowledge, the error performance and the diversity order of the distributed Alamouti's code have never been studied in cooperative networks with CSI-assisted relays. This has motivated our work.

In this chapter, we first consider a *dissimilar* cooperative network, where all the channels possibly have different variances, and we assume that the CSI-assisted relays in the network adopt the amplifying coefficient proposed in [33]. We derive lower and upper bounds of the average BER of the distributed Alamouti's code. Irrespective of the values of the channel variances, the proposed bounds can tightly bound the average BER. Very surprisingly, we find that, when the relays use the amplifying coefficient proposed in [33], the distributed Alamouti's code only achieves diversity order one. Furthermore, in general cooperative networks with more than two relays, we show that the DSTBCs proposed in [27] can only achieve diversity order one as well when the relays use the amplifying coefficient proposed in [33]. To address this problem, we then propose a new threshold-based amplifying coefficient for the distributed Alamouti's code based on the work in [23]. This new amplifying coefficient makes the code achieve the full diversity order two. Moreover, it also avoids saturations of the amplifiers at the relays. Based on three different criteria, we develop three optimum and one suboptimum schemes in order to choose the value of the threshold used in the new amplifying coefficient.

The rest of this chapter is organized as follows. Section 5.2 describes the cooperative

network studied in this chapter. In Section 5.3, it is assumed that the relays adopt the amplifying coefficient proposed in [33]. We derive lower and upper bounds of the average BER of the distributed Alamouti's code in a dissimilar cooperative network. Furthermore, we show that the diversity order of the DSTBCs, including the distributed Alamouti's code, is just one when the relays use the amplifying coefficient proposed in [33]. In Section 5.4, a new threshold-based amplifying coefficient is proposed. This new amplifying coefficient makes the distributed Alamouti's code achieve the full diversity order two. Moreover, we develop three optimum and one suboptimum schemes in order to choose the value of the threshold used by the new amplifying coefficient. Section 5.5 presents some numerical results and Section 5.6 concludes this chapter.

Notations: We use $A := B$ to denote A, by definition, equals B and use $A =: B$ to denote B, by definition, equals A. For a random variable X, $\mathbb{E}[X]$ denotes its expectation. $X \sim \mathscr{CN}(0, \Omega_X)$ means X is a circularly symmetric complex Gaussian random variable with zero mean and variance Ω_X. Let $\lfloor \cdot \rfloor$, $Q(\cdot)$, ${}_2F_1(1,2;3;\cdot)$, and $\mathrm{Ei}(\cdot)$ denote the floor function, Q-function, hypergeometric function, and exponential integral function [19], respectively.

5.2 System Model

We consider an AF cooperative network with one source, two CSI-assisted relays, and one destination. Every terminal has only one antenna and is half-duplex. Let h_k and f_k denote the channel from the source to the k-th relay and the channel from the k-th relay to the destination, respectively. The channel coefficient h_k is modelled as $h_k = \bar{h}_k \sqrt{d_{s,k}^{-\beta_{s,k}}}$, where $\bar{h}_k \sim \mathscr{CN}(0,1)$, $\beta_{s,k}$ is the path loss exponent for this channel, and $d_{s,k}$ is the normalized distance from the source to the k-th relay. The value of $d_{s,k}$ is decided by $d_{s,k} = \bar{d}_{s,k}/D$, where $\bar{d}_{s,k}$ is the actual distance from the source to the k-th relay and D is the reference

distance determined from measurements.[1] Similarly, we model the channel coefficient f_k as $f_k = \bar{f_k}\sqrt{d_{k,d}^{-\beta_{k,d}}}$, where $d_{k,d}$ is the normalized distance from the k-th relay to the destination, $\beta_{k,d}$ is the path loss exponent for this channel, and $\bar{f_k} \sim \mathscr{CN}(0,1)$. The value of $d_{k,d}$ is decided by $d_{k,d} = \bar{d}_{k,d}/D$, where $\bar{d}_{k,d}$ is the actual distance from the k-th relay to the destination. Thus, the variances Ω_{h_k} and Ω_{f_k} of h_k and f_k equal to $\Omega_{h_k} = d_{s,k}^{-\beta_{s,k}}$ and $\Omega_{f_k} = d_{k,d}^{-\beta_{k,d}}$, respectively.

At the first and second time slots, the source transmits two information-bearing symbols x_1 and x_2 to the relays, respectively. The transmission power at the source is E_s. The received signal $y_{k,t}$ of the k-th relay at the t-th time slot is given by $y_{k,t} = \sqrt{E_s}h_k x_t + n_{k,t}$, where $n_{k,t}$ is the additive white Gaussian noise and $n_{k,t} \sim \mathscr{CN}(0,\sigma_n^2)$. The k-th relay multiplies the received signal $y_{k,t}$ with an amplifying coefficient ρ_k. The value of ρ_k will be discussed in detail later.

At the third and fourth time slots, the two relays use the distributed Alamouti's code to transmit signals to the destination. Specifically, at the third time slot, the first relay transmits $\rho_1 y_{1,1}$ and the second relay transmits $-\rho_2 y_{2,2}^*$. Thus, the received signal at the destination is $y_1 = \rho_1 f_1 y_{1,1} - \rho_2 f_2 y_{2,2}^* + n_1$, where n_1 is the additive white Gaussian noise and $n_1 \sim \mathscr{CN}(0,\sigma_n^2)$. At the fourth time slot, the first relay transmits $\rho_1 y_{1,2}$ and the second relay transmits $\rho_2 y_{2,1}^*$. Consequently, the received signal at the destination is $y_2 = \rho_1 f_1 y_{1,2} + \rho_2 f_2 y_{2,1}^* + n_2$, where n_2 is the additive white Gaussian noise and $n_2 \sim \mathscr{CN}(0,\sigma_n^2)$. Due to the orthogonal structure of the distributed Alamouti's code, the maximum likelihood (ML) estimate $\hat{x}_1$ of x_1 is given by $\hat{x}_1 = \rho_1 f_1^* h_1^* y_1 + \rho_2 f_2 h_2^* y_2^*$ [29]. Thus, the instantaneous SNR $\gamma(\rho_1,\rho_2)$ of $\hat{x}_1$ is given by

$$\gamma(\rho_1,\rho_2) = \frac{E_s(\rho_1^2|f_1 h_1|^2 + \rho_2^2|f_2 h_2|^2)}{\sigma_n^2(\rho_1^2|f_1|^2 + \rho_2^2|f_2|^2 + 1)}. \tag{5.1}$$

[1] This chapter does not consider the measurement of the reference distances. This topic has been extensively studied in [44] for a variety of radio propagation environments.

Similarly, the instantaneous SNR of the ML estimate $\hat{x}_2$ of x_2 is also $\gamma(\rho_1,\rho_2)$.

If M-quadrature amplitude modulation (QAM) is used as the modulation scheme and Gray mapping is used, the conditional BER $P_b(\gamma(\rho_1,\rho_2))$, conditioned on the instantaneous channel coefficients h_k and f_k, of $\hat{x}_1$ or $\hat{x}_2$ is given by [8][2]

$$P_b\left(\gamma(\rho_1,\rho_2)\right)=\frac{2}{\sqrt{M}\log_2 M}\sum_{j=1}^{\log_2\sqrt{M}}\left[\sum_{i=0}^{\left(1-2^{-j}\right)\sqrt{M}-1}A_{j,i}(M)Q\left((2i+1)\sqrt{\frac{3\gamma(\rho_1,\rho_2)}{M-1}}\right)\right] \quad (5.2)$$

where the coefficient $A_{j,i}(M)$ is given by

$$A_{j,i}(M)=(-1)^{\left\lfloor 2^{j-1}i/M\right\rfloor}\left(2^{j-1}-\left\lfloor\frac{2^{j-1}i}{\sqrt{M}}+\frac{1}{2}\right\rfloor\right). \quad (5.3)$$

The average BER P_b can be obtained by $P_b=\mathbb{E}\left[P_b(\gamma(\rho_1,\rho_2))\right]$, i.e.

$$P_b=\frac{2}{\sqrt{M}\log_2 M}\sum_{j=1}^{\log_2\sqrt{M}}\left\{\sum_{i=0}^{\left(1-2^{-j}\right)\sqrt{M}-1}A_{j,i}(M)\mathbb{E}\left[Q\left((2i+1)\sqrt{\frac{3\gamma(\rho_1,\rho_2)}{M-1}}\right)\right]\right\}. \quad (5.4)$$

5.3 BER and Diversity Order Analysis of the Distributed Alamouti's Code

In this section, we first consider a dissimilar cooperative network with two CSI-assisted relays. The relays use the amplifying coefficient ρ_k proposed in [33] and it is given by

$$\rho_k=\sqrt{\frac{E_{rk}}{E_s|h_k|^2+\sigma_n^2}}. \quad (5.5)$$

The amplifying coefficient ρ_k ensures that the power of the transmitted signal from the k-th relay is always E_{rk}. Thus, the amplifiers at the relays will never go into saturation. Due to this reason, the amplifying coefficient ρ_k has been used in many previous publications [2, 45, 48]. In this section, we also assume that the relays adopt the amplifying coefficient

[2] If other modulation schemes are used, the conditional BER can be obtained by using [8] as well. Moreover, conditional SER can be obtained by using [42] and [52].

ρ_k. Under this assumption, we derive lower and upper bounds of the average BER of the distributed Alamouti's code. Based on the lower bound, we show that, very surprisingly, the distributed Alamouti's code only achieves diversity order one. Then we consider a general cooperative network with more than two relays. We show that the DSTBCs developed in [27] only achieve diversity order one as well when the relays use the amplifying coefficient ρ_k.

In order to facilitate the analysis of the average BER P_b, we approximate ρ_k by $\rho_k \approx \sqrt{E_{rk}/(E_s|h_k|^2)}$ as in [2,45]. Since $\sqrt{E_{rk}/(E_s|h_k|^2)}$ is a very tight approximation of ρ_k as shown in [2,45][3], the instantaneous SNR $\gamma(\rho_1,\rho_2)$ in (5.1) is tightly approximated by

$$\gamma(\rho_1,\rho_2) \approx \frac{1}{\sigma_n^2}\frac{E_{r1}|f_1|^2+E_{r2}|f_2|^2}{\frac{E_{r1}|f_1|^2}{E_s|h_1|^2}+\frac{E_{r2}|f_2|^2}{E_s|h_2|^2}+1}. \tag{5.6}$$

In the following, we will analyze the average BER P_b based on (5.6). In order to obtain the value of P_b, one needs the MGF of $\gamma(\rho_1,\rho_2)$, which is technically very hard. In the following, we try to find lower and upper bounds of P_b and show that the bounds are very tight to P_b.

5.3.1 A lower bound of P_b

We upper-bound $\gamma(\rho_1,\rho_2)$ in the following way

$$\gamma(\rho_1,\rho_2) < \gamma^U = \frac{1}{\sigma_n^2}\frac{E_{r1}|f_1|^2+E_{r2}|f_2|^2}{\max\left(\frac{E_{r1}|f_1|^2}{E_s|h_1|^2},\frac{E_{r2}|f_2|^2}{E_s|h_2|^2}\right)}. \tag{5.7}$$

In order to find a lower bound of P_b, it is desirable to obtain the MGF of γ^U. To this end, we develop the following lemma.

[3]For example, in [2], it has been demonstrated that the difference between the exact average BER and the approximate average BER, which is based on the approximation $\rho_k \approx \sqrt{E_{rk}/(E_s|h_k|^2)}$, is less than 0.2 dB.

Lemma 5.1. *Assume X_1, X_2, Y_1, and Y_2 are exponential random variables with means a_1, a_2, b_1, and b_2, respectively. The MGF $\mathscr{M}_1(s;a_1,a_2,b_1,b_2)$ of the function (Y_1+Y_2) $/\max(Y_1/X_1,Y_2/X_2)$ is given as follows:*

$$\begin{aligned}\mathscr{M}_1(s;a_1,a_2,b_1,b_2) &= \frac{b_1b_2}{a_1a_2}\left(\frac{a_1-a_2}{b_1-b_2}\mathscr{M}_1^1(s;a_1,a_2,b_1,b_2)\right.\\ &\qquad\left.+\frac{a_2b_1-a_1b_2}{b_1-b_2}\mathscr{M}_1^2(s;a_1,a_2,b_1,b_2)\right). \qquad (5.8)\end{aligned}$$

In this function, $\mathscr{M}_1^1(s;a_1,a_2,b_1,b_2)$ and $\mathscr{M}_1^2(s;a_1,a_2,b_1,b_2)$ are given by

$$\mathscr{M}_1^1(s;a_1,a_2,b_1,b_2) = \frac{a_1a_2}{a_1b_2(1-a_2s)-a_2b_1(1-a_1s)}\ln\frac{a_1b_2(1-a_2s)}{a_2b_1(1-a_1s)} \qquad (5.9)$$

$$\begin{aligned}\mathscr{M}_1^2(s;a_1,a_2,b_1,b_2) &= \frac{a_1}{b_2(b_1-b_2)(1-a_1s)}-\frac{a_2}{b_1(b_1-b_2)(1-a_2s)}\\ &\quad+\frac{a_2(a_1-a_2)}{2a_1(1-a_2s)^2(b_2-b_1)^2}\,{}_2F_1\left(1,2;3;\frac{\frac{a_2b_1-a_1b_2}{a_1(b_1-b_2)}-a_2s}{1-a_2s}\right)\\ &\quad+\frac{a_1(a_2-a_1)}{2a_2(1-a_1s)^2(b_1-b_2)^2}\,{}_2F_1\left(1,2;3;\frac{\frac{a_2b_1-a_1b_2}{a_2(b_1-b_2)}-a_1s}{1-a_1s}\right) \qquad (5.10)\end{aligned}$$

Proof: See Appendix 5-A. ■

The MGF $\mathscr{M}^U(s)$ of γ^U can be easily derived by using Lemma 5.1 and it is given by

$$\mathscr{M}^U(s) = \mathscr{M}_1\left(\frac{s}{\sigma_n^2};E_s\Omega_{h_1},E_s\Omega_{h_2},E_{r_1}\Omega_{f_1},E_{r_2}\Omega_{f_2}\right). \qquad (5.11)$$

Based on (5.11), we obtain a lower bound of P_b in the following theorem.

Theorem 5.1. *When M-QAM is used as the modulation scheme, the average BER P_b can be lower-bounded by*

$$\begin{aligned}P_b > P_b^L &= \frac{2}{\pi\sqrt{M}\log_2 M}\sum_{j=1}^{\log_2\sqrt{M}}\left\{\sum_{i=0}^{\left(1-2^{-j}\right)\sqrt{M}-1}A_{j,i}(M)\right.\\ &\quad\left.\times\int_{\theta=0}^{\frac{\pi}{2}}\mathscr{M}^U\left(-\frac{3(2i+1)^2}{2(M-1)\sin^2\theta}\right)d\theta\right\}. \qquad (5.12)\end{aligned}$$

Proof: Since $\gamma(\rho_1,\rho_2)$ is upper-bounded by γ^U and the MGF of γ^U is given by $\mathscr{M}^U(s)$ in (5.11), it follows Craig's formula that

$$\mathbb{E}\left[Q\left((2i+1)\sqrt{\frac{3\gamma(\rho_1,\rho_2)}{M-1}}\right)\right] > \frac{1}{\pi}\int_{\theta=0}^{\frac{\pi}{2}} \mathscr{M}^U\left(-\frac{3(2i+1)^2}{2(M-1)\sin^2\theta}\right)d\theta. \qquad (5.13)$$

By substituting (5.13) into (5.4), we obtain the lower bound P_b^L. ■

Although the lower bound P_b^L contains an integration, this integration is over a finite range, and hence, it is not hard to compute.[4] Numerical results will demonstrate that P_b^L is a very tight lower bound of P_b except when Ω_{h_k} is much larger than Ω_{f_k}. For this special case, the ratio $E_{rk}|f_k|^2/(E_s|h_k|^2)$ in the denominator of (5.6) is much smaller than one with a very high probability. Therefore, P_b^L loses its tightness because we neglect the constant one in the denominator of $\gamma(\rho_1,\rho_2)$ as shown in (5.7) when we derive P_b^L. This particular case will be addressed by deriving an upper bound of P_b in the next subsection.

5.3.2 An upper bound of P_b

In order to find a tight bound for P_b when Ω_{h_k} is much larger than Ω_{f_k}, we develop an upper bound of P_b in the following. We keep the constant one in the denominator of $\gamma(\rho_1,\rho_2)$; but replace $|h_1|^2$ and $|h_2|^2$ by $\min(|h_1|^2,|h_2|^2)$. This gives us a lower bound γ^L of $\gamma(\rho_1,\rho_2)$

$$\gamma(\rho_1,\rho_2) \geq \gamma^L = \frac{1}{\sigma_n^2}\frac{E_{r1}|f_1|^2+E_{r2}|f_2|^2}{\frac{E_{r1}|f_1|^2+E_{r2}|f_2|^2}{E_s\min(|h_1|^2,|h_2|^2)}+1}. \qquad (5.14)$$

In order to find an upper bound of P_b, it is desirable to obtain the MGF of γ^L. Thus, we show the following lemma.

[4] In fact, it is well-known that Q-function can be approximated by $e^{-x^2/2}/12+e^{-2x^2/3}/4$ [7]. By using this approximation, we can approximate P_b^L and express it in closed-form as shown in the proof of Lemma 5.3. This can further reduce the computational complexity with marginal loss of tightness.

Lemma 5.2. *Assume X_1, X_2, Y_1, and Y_2 are exponential random variables with means a_1, a_2, b_1, and b_2, respectively. The MGF $\mathscr{M}_2(s;a_1,a_2,b_1,b_2)$ of the function $(Y_1+Y_2)/((Y_1+Y_2)/\min(X_1,X_2)+1)$ is given as follows:*

$$\mathscr{M}_2(s;a_1,a_2,b_1,b_2)=\frac{b_1}{b_1-b_2}W\left(s,\frac{a_1a_2}{a_1+a_2},b_1\right)-\frac{b_2}{b_1-b_2}W\left(s,\frac{a_1a_2}{a_1+a_2},b_2\right), \quad (5.15)$$

where the function $W(x,y,z)$ is given by

$$\begin{aligned} W(x,y,z) &= \frac{1}{(y+z-xyz)^2-4yz}\left[(y+z)(y+z-xyz)-4yz\right. \\ &\quad \left.+\frac{4yz(-xyz)\sqrt{(y+z-xyz)^2}}{(y+z-xyz)\sqrt{4yz-(y+z-xyz)^2}}\arccos\left(\frac{y+z-xyz}{2\sqrt{yz}}\right)\right]. \quad (5.16)\end{aligned}$$

Proof: Let $T=Y_1+Y_2$ and $Z=\min(X_1,X_2)$. Thus, the function $(Y_1+Y_2)/((Y_1+Y_2)/\min(X_1,X_2)+1)$ becomes $T/((T/Z)+1)=TZ/(T+Z)$ which is actually the harmonic mean of T and Z. Moreover, it is not hard to find the PDFs $f_T(t)$ of T and $f_Z(z)$ of Z

$$f_T(t)=\frac{e^{-\frac{t}{b_1}}-e^{-\frac{t}{b_2}}}{b_1-b_2}, \qquad f_Z(z)=\left(\frac{1}{a_1}+\frac{1}{a_2}\right)e^{-\left(\frac{1}{a_1}+\frac{1}{a_2}\right)z}. \quad (5.17)$$

By using the results in [2], it is not hard to find $\mathscr{M}_2(s;a_1,a_2,b_1,b_2)$ in (5.15). ■

Based on Lemma 5.2, one can easily find the MGF $\mathscr{M}^L(s)$ of γ^L and it is given by

$$\mathscr{M}^L(s)=\mathscr{M}_2\left(\frac{s}{\sigma_n^2};E_s\Omega_{h_1},E_s\Omega_{h_2},E_{r_1}\Omega_{f_1},E_{r_2}\Omega_{f_2}\right). \quad (5.18)$$

The MGF $\mathscr{M}^L(s)$ enables us to find an upper bound of P_b as in the following theorem.

Theorem 5.2. *When M-QAM is used as the modulation scheme, the average BER P_b can be upper-bounded by*

$$\begin{aligned} P_b\le P_b^U &= \frac{2}{\pi\sqrt{M}\log_2 M}\sum_{j=1}^{\log_2\sqrt{M}}\left\{\sum_{i=0}^{(1-2^{-j})\sqrt{M}-1}A_{j,i}(M)\right. \\ &\quad \left.\times\int_{\theta=0}^{\frac{\pi}{2}}\mathscr{M}^L\left(-\frac{3(2i+1)^2}{2(M-1)\sin^2\theta}\right)d\theta\right\}. \quad (5.19)\end{aligned}$$

Proof: The proof is the same as that of Theorem 5.1, except $\mathscr{M}^L(s)$ is used in order to obtain an upper bound. ■

The upper bound P_b^U also just contains an finite integration, and hence, it is not hard to compute. Moreover, as we expected, P_b^U is a very tight bound of the average BER P_b when Ω_{h_k} is much larger than Ω_{f_k}. This is because the denominator of (5.6) is dominantly decided by the constant one for this special case. As a result, replacing $|h_1|^2$ and $|h_2|^2$ by $\min(|h_1|^2, |h_2|^2)$ in (5.14) only slightly reduces the value of $\gamma(\rho_1, \rho_2)$, and hence, P_b^U is very tight to P_b. Recall that the lower bound P_b^L is very tight to P_b except when Ω_{h_k} is much larger than Ω_{f_k}. Therefore, depending on the values of Ω_{h_k} and Ω_{f_k}, one can always use either P_b^L or P_b^U in order to tightly bound the average BER P_b.

5.3.3 Diversity order of the DSTBCs when the CSI-assisted relays use ρ_k

Note that the diversity order of the distributed Alamouti's code is based on the limit of the average SNR E_s/σ_n^2 to infinity. On the other hand, our approximation of the amplifying coefficient ρ_k is based on the fact that, when $E_s|h_k|^2$ is much larger than σ_n^2, we can ignore σ_n^2 in the denominator of (5.5) and this almost does not change the value of ρ_k. Thus, when the average SNR goes to infinity, our approximation of ρ_k becomes tighter, and hence, the lower bound P_b^L is extremely close to the exact average BER P_b, which can be seen in Figs. 5.1–5.3. Therefore, the lower bound P_b^L enables us to find the diversity order of the distributed Alamouti's code in the following lemma.

Lemma 5.3. *In a cooperative network with two CSI-assisted relays, the distributed Alamouti's code achieves diversity order one when the relays use ρ_k as the amplifying coefficient.*

Proof: We first use the following well-known approximation [7] to make the lower

bound P_b^L given in closed-form

$$Q(x) \approx \frac{1}{12}e^{-\frac{1}{2}x^2} + \frac{1}{4}e^{-\frac{2}{3}x^2}. \tag{5.20}$$

Based on this approximation and (5.4), the lower bound P_b^L can be approximated very tightly and given in closed-form as follows:

$$P_b^L \approx \Gamma_{\mathscr{M}^U} := \frac{2}{\sqrt{M}\log_2 M}\sum_{j=1}^{\log_2\sqrt{M}}\left\{\sum_{i=0}^{\left(1-2^{-j}\right)\sqrt{M}-1} A_{j,i}(M)\left[\frac{1}{12}\mathscr{M}^U\left(-\frac{3(2i+1)^2}{2(M-1)}\right)\right.\right.$$
$$\left.\left. + \frac{1}{4}\mathscr{M}^U\left(-\frac{2(2i+1)^2}{M-1}\right)\right]\right\}, \tag{5.21}$$

For simplicity, we assume $E_s = E_{r1} = E_{r2} = E$ and $\sigma_n^2 = 1$. Note that this assumption does not change the diversity order of the code. When E goes to infinity, we have

$$\lim_{E\to\infty}\mathscr{M}^U\left(-\frac{3(2i+1)^2}{2(M-1)}\right) = \frac{C_1}{E} + \mathscr{O}\left(\frac{1}{E^2}\right), \tag{5.22}$$

where C_1 is a constant. That is, $\mathscr{M}^U\left(-3(2i+1)^2/(2(M-1))\right)$ behaves like $1/E$, when E is large. This is also true for $\mathscr{M}^U(-2(2i+1)^2/(M-1))$. Thus, when E is large, the lower bound P_b^L decays with E as $1/E$. Since P_b^L is a lower bound of P_b, the average BER P_b also decays with E as $1/E$. That is, the diversity order of the distributed Alamouti's code is just one when the relays use ρ_k as the amplifying coefficient. ■

Actually, the diversity order of the distributed Alamouti's code can be seen from its instantaneous SNR $\gamma(\rho_1,\rho_2)$ in (5.6). When the channel from the source to the first relay is in deep fading, i.e. when $|h_1|^2$ is very small, the denominator of (5.6) may go to infinity, and hence, $\gamma(\rho_1,\rho_2)$ may be very small. Similarly, when $|h_2|^2$ is very small, $\gamma(\rho_1,\rho_2)$ may go to zero as well. That is, the failure of either h_1 or h_2 will make the instantaneous SNR at the destination very small, which implies the diversity order is just one. In general, when there are more than two CSI-assisted relays and every relay uses the amplifying coefficient ρ_k, the diversity order of the DSTBCs proposed in [27] is also just one as shown in the

following theorem.[5]

Theorem 5.3. *In a cooperative network with K CSI-assisted relays, the diversity order of the DSTBCs proposed in [27] is just one, when the relays use ρ_k as the amplifying coefficient.*

Proof: See Appendix 5-B. ■

We notice that, although the amplifying coefficient ρ_k was used, the cooperative networks considered in [2, 45] did not loss any diversity order and they achieved the full diversity order K. This is because the authors used the repetition-based cooperative strategy in [2, 45], which is fundamentally different from the DSTBCs considered in Theorem 5.3. Due to this reason, the instantaneous SNR at the destination was the summation of the SNRs of the K branches in the network, i.e. $\gamma = \sum_{k=1}^{K} \gamma_k$. When $|h_i|$ is very small, the SNR γ_i of the i-th branch will be very small, but the SNRs γ_k, $k \neq i$, of the other branches will not be affected. That is, the failure of any branch will not make the SNR γ very small. Only the failure of all the K branches can make the SNR γ very small, and hence, the full diversity order K was achieved in [2, 45].

5.4 A New Threshold-Based Amplifying Coefficient for the Distributed Alamouti's Code with CSI-Assisted Relays

In this section, we propose a new threshold-based amplifying coefficient. This new amplifying coefficient not only avoids saturations of the amplifiers at the relays but also makes

[5] Note that the DSTBCs proposed in [27] represent a large collection of distributed space-time block codes and they have been used in many previous publications including [28, 37, 47].

the distributed Alamouti's code achieve the full diversity order two. Furthermore, we propose three optimum and one suboptimum schemes to choose the value of the threshold used in the new amplifying coefficient.

Section 5.3 has shown that the distributed Alamouti's code only achieves diversity order one when the CSI-assisted relays use the amplifying coefficient ρ_k. In order to achieve the full diversity order, we propose a new amplifying coefficient $\tilde{\rho}_k$ as follows:

$$\tilde{\rho}_k = \sqrt{\frac{E_{rk}}{E_s \max(|h_k|^2, \alpha_k) + \sigma_n^2}}, \tag{5.23}$$

where $\alpha_k > 0$ can be seen as a threshold for $|h_k|^2$ and the choice of α_k will be discussed in detail later. It is easy to check that the power of the transmitted signal of the k-th relay is always less than or equal to E_{rk} when $\tilde{\rho}_k$ is used. Thus, the new amplifying coefficient $\tilde{\rho}_k$ avoids saturations of the amplifiers at the relays. Furthermore, we will show that the use of $\tilde{\rho}_k$ also makes the distributed Alamouti's code achieve the full diversity order.[6]

5.4.1 Diversity order of the distributed Alamouti's code when the CSI-assisted relays use $\tilde{\rho}_k$

In this subsection, we show that the distributed Alamouti's code can achieve the full diversity order when the relays use $\tilde{\rho}_k$. In this circumstance, the instantaneous SNR $\tilde{\gamma}(\alpha_1, \alpha_2)$ of $\hat{x}_1$ or $\hat{x}_2$ is given by

$$\tilde{\gamma}(\alpha_1, \alpha_2) = \gamma(\tilde{\rho}_1, \tilde{\rho}_2) = \frac{E_s \left(\frac{E_{r1}|f_1 h_1|^2}{E_s \max(|h_1|^2, \alpha_1) + \sigma_n^2} + \frac{E_{r2}|f_2 h_2|^2}{E_s \max(|h_2|^2, \alpha_2) + \sigma_n^2} \right)}{\sigma_n^2 \left(\frac{E_{r1}|f_1|^2}{E_s \max(|h_1|^2, \alpha_1) + \sigma_n^2} + \frac{E_{r2}|f_2|^2}{E_s \max(|h_2|^2, \alpha_2) + \sigma_n^2} + 1 \right)}. \tag{5.24}$$

[6] In order to avoid saturations of the amplifiers and make the code achieve the full diversity order, an alternative way is to set the amplifying coefficients as $\sqrt{E_{rk}/(E_s \Omega_{h_k} + \sigma_n^2)}$ and clip the power of the transmitted signal of the k-th relay at E_{rk}. This method has been considered in [23]. However, note that [23] only studied the repetition-based cooperative strategy, while our work focuses on the distributed Alamouti's code.

Thus, the conditional BER is given by $P_b(\tilde{\gamma}(\alpha_1,\alpha_2))$ and the average BER $\tilde{P}_b$ is given by $\tilde{P}_b = \mathbb{E}[P_b(\tilde{\gamma}(\alpha_1,\alpha_2))]$. We show the diversity order by deriving an upper bound of $\tilde{P}_b$. To this end, we develop the following lemma.

Lemma 5.4. *Assume X, Y_1, and Y_2 are exponential random variables with means a, b_1, and b_2, respectively. The MGF $\mathscr{M}_3(s;a,b_1,b_2)$ of the function $XY_1/(Y_1+Y_2+1)$ is given as follows:*

$$\mathscr{M}_3(s;a,b_1,b_2) = 1 + asH\left(\frac{b_2}{b_1}, -as, \frac{1}{b_1}\right), \tag{5.25}$$

where the function $H(x,y,z)$ is given by

$$\begin{aligned} H(x,y,z) &= \frac{1}{(x-y-1)^2(y+1)}\left[(y+1)(y+1-x) + e^{\frac{z}{x}}\mathrm{Ei}\left(\frac{z}{x}\right)x(y+1)\right. \\ &\qquad \left. + e^{\frac{z}{1+y}}\mathrm{Ei}\left(\frac{z}{1+y}\right)(xz-(x+z)(y+1))\right]. \end{aligned} \tag{5.26}$$

Proof: See Appendix 5-C. ■

Based on Lemma 5.4, an upper bound of $\tilde{P}_b$ is derived in the following lemma.

Lemma 5.5. *When M-QAM is used as the modulation scheme, the average BER $\tilde{P}_b$ can be upper-bounded by*

$$\tilde{P}_b \lesssim \tilde{P}_b^U = \Gamma_{\tilde{\mathscr{M}}^L}. \tag{5.27}$$

The function $\Gamma_{\tilde{\mathscr{M}}^L}$ is obtained from (5.21) by replacing $\mathscr{M}^U(s)$ with $\tilde{\mathscr{M}}^L(s)$ which is given by $\tilde{\mathscr{M}}^L(s) = \sum_{i=1}^4 \mathscr{M}_{\tilde{\gamma}^{L\text{-}i}}(s)$. The function $\mathscr{M}_{\tilde{\gamma}^{L\text{-}i}}(s)$ is given by

$$\mathscr{M}_{\tilde{\gamma}^{L\text{-}1}}(s) \approx \mathscr{M}_3\left(s\frac{E_s}{\sigma_n^2};\Omega_{h_1},b_1,b_2\right)\mathscr{M}_3\left(s\frac{E_s}{\sigma_n^2};\Omega_{h_2},b_2,b_1\right), \tag{5.28}$$

$$\mathscr{M}_{\tilde{\gamma}^{L\text{-}2}}(s) \lesssim \mathscr{M}_3\left(s\frac{E_s}{\sigma_n^2};\Omega_{h_1},b_1,b_2\right)\mathscr{M}_3\left(s\frac{E_s\alpha_2}{\sigma_n^2};1,b_2,b_1\right), \tag{5.29}$$

$$\mathscr{M}_{\tilde{\gamma}^{L\text{-}3}}(s) \lesssim \mathscr{M}_3\left(s\frac{E_s\alpha_1}{\sigma_n^2};1,b_1,b_2\right)\mathscr{M}_3\left(s\frac{E_s}{\sigma_n^2};\Omega_{h_2},b_2,b_1\right), \tag{5.30}$$

$$\mathscr{M}_{\tilde{\gamma}^{L\text{-}4}}(s) \lesssim \mathscr{M}_3\left(s\frac{E_s\alpha_1}{\sigma_n^2};1,b_1,b_2\right)\mathscr{M}_3\left(s\frac{E_s\alpha_2}{\sigma_n^2};1,b_2,b_1\right), \tag{5.31}$$

where $b_1 = E_{r1}\Omega_{f_1}/(E_s\alpha_1)$ and $b_2 = E_{r2}\Omega_{f_2}/(E_s\alpha_2)$.

Proof: See Appendix 5-D. ■

The upper bound $\tilde{P}_b^U$ enables us to obtain the diversity order of the distributed Alamouti's code when the relays use $\tilde{\rho}_k$ as the amplifying coefficient and it is shown in the following theorem.

Theorem 5.4. *In a cooperative network with two CSI-assisted relays, the distributed Alamouti's code achieves the full diversity order two when the relays use $\tilde{\rho}_k$ as the amplifying coefficient.*

Proof: In order to show the diversity order, we assume $E_s = E_{r1} = E_{r2} = E$ and $\sigma_n^2 = 1$. Then it can be easily shown that

$$\lim_{E\to\infty} \tilde{\mathscr{M}}^L\left(-\frac{3(2i+1)^2}{2(M-1)}\right) = \frac{C_2}{E^2} + \mathscr{O}\left(\frac{1}{E^3}\right), \tag{5.32}$$

where C_2 is a constant. That is, $\tilde{\mathscr{M}}^L\left(-3(2i+1)^2/(2(M-1))\right)$ behaves like $1/E^2$, when E is large. This is also true for $\tilde{\mathscr{M}}^L(-2(2i+1)^2/(M-1))$. Thus, when E is large, $\tilde{P}_b^U$ behaves like $1/E^2$. Since $\tilde{P}_b^U$ is an upper bound of $\tilde{P}_b$, the average BER $\tilde{P}_b$ behaves like $1/E^2$ as well when E is large. That is, the diversity order of the distributed Alamouti's code is two when the CSI-assisted relays use $\tilde{\rho}_k$ as the amplifying coefficient.[7] ■

5.4.2 Optimum and suboptimum schemes to choose the value of α_1 and α_2

The use of $\tilde{\rho}_k$ makes the distributed Alamouti's code achieve the full diversity order two as long as the threshold α_k is strictly positive. Certainly, the value of α_k can be chosen properly in order to enhance the performance. In the remaining of this subsection, we

[7] In general, when there are more than two relays, numerical results will demonstrate that the DSTBCs achieve the full diversity order when the relays use $\tilde{\rho}_k$ as the amplifying coefficient. However, it is hard to show this result analytically.

propose three optimum and one suboptimum schemes to choose the value of α_k based on different criteria.

It will be ideal to use the exact average BER $\tilde{P}_b$ to decide the value of α_k, but $\tilde{P}_b$ is too hard to obtain. Thus, we use upper bounds of $\tilde{P}_b$ to choose α_k by following similar ideas in [12, 15, 27, 70]. That is, we use the upper bound $\tilde{P}_b^U$ in (5.27) as the metric and choose α_k that minimizes the upper bound:

$$\textit{Optimum Scheme I:} \quad (\alpha_1, \alpha_2) = \arg \min_{\alpha_1>0, \alpha_2>0} \tilde{P}_b^U. \tag{5.33}$$

The scheme given in (5.33) is referred to as Optimum Scheme I in this chapter and it is optimum in the sense that it minimizes the upper bound $\tilde{P}_b^U$. Note that the upper bound $\tilde{P}_b^U$ has been averaged over the instantaneous channel gains h_k and f_k. Thus, it only depends on the channel variances Ω_{h_k} and Ω_{f_k} which change very slowly. Thus, although the minimization in Optimum Scheme I has to be solved numerically, the relays only need to conduct the minimization once in a long time and the computational loads at the relays may be negligible.

Optimum Scheme I can greatly improve the performance of the distributed Alamouti's code with very low computational loads at the relays. However, it is more desirable to propose a scheme where α_k is chosen by exploiting h_k, because the CSI-assisted relays know the exact value of h_k anyway. Furthermore, the performance may be further improved by doing so. To this end, we take the expectation of the conditional BER $P_b(\tilde{\gamma}(\alpha_1, \alpha_2))$ over f_k only and upper-bound this expectation by using the techniques developed in Lemmas 5.4 and 5.5:

$$\mathbb{E}_{f_1, f_2}\left[P_b\left(\tilde{\gamma}(\alpha_1, \alpha_2)\right)\right] \lesssim \tilde{P}_b^U(h_1, h_2) = \Gamma_{\tilde{\mathscr{M}}^U} \tag{5.34}$$

where $\tilde{\mathscr{M}}^U(s)$ is given by

$$\tilde{\mathscr{M}}^U(s) = \mathscr{M}_3\left(s\frac{E_s|h_1|^2}{\sigma_n^2}; 1, \tilde{\rho}_1^2\Omega_{f_1}, \tilde{\rho}_2^2\Omega_{f_2}\right)\mathscr{M}_3\left(s\frac{E_s|h_2|^2}{\sigma_n^2}; 1, \tilde{\rho}_2^2\Omega_{f_2}, \tilde{\rho}_1^2\Omega_{f_1}\right) \tag{5.35}$$

and $\Gamma_{\tilde{\mathscr{M}}^U}$ is obtained from (5.21) by replacing $\mathscr{M}^U(s)$ with $\tilde{\mathscr{M}}^U(s)$ in (5.35). Then a new scheme to choose α_k is as follows:

$$\textit{Optimum Scheme II:} \quad (\alpha_1, \alpha_2) = \arg \min_{\alpha_1>0, \alpha_2>0} \tilde{P}_b^U(h_1, h_2). \tag{5.36}$$

The scheme given in (5.36) is called Optimum Scheme II in this chapter and it is optimum in the sense that the upper bound $\tilde{P}_b^U(h_1, h_2)$ is minimized.[8] Numerical results will show that, compared to Optimum Scheme I, Optimum Scheme II indeed further improves the performance. This is because Optimum Scheme II takes advantage of the CSI available at the relays. However, the minimization in (5.36) must be solved numerically and it has to be done whenever the instantaneous channel gain h_k changes, because the upper bound $\tilde{P}_b^U(h_1, h_2)$ depends on h_k. Thus, Optimum Scheme II needs more computational loads at the relays than Optimum Scheme I.

In a fast-fading environment, it may be hard to numerically perform the minimization in (5.36) whenever h_k changes. Thus, we develop a suboptimum scheme which chooses α_k by exploiting h_k and requires much less computational loads than Optimum Scheme II. This is achieved by analyzing the property of the instantaneous SNR $\tilde{\gamma}(\alpha_1, \alpha_2)$ in (5.24). It can be shown that, when $0 < \alpha_1 < |h_1|^2$, $\tilde{\gamma}(\alpha_1, \alpha_2)$ is independent of α_1; while, when $\alpha_1 \geq |h_1|^2$, $\tilde{\gamma}(\alpha_1, \alpha_2)$ is decreasing with α_1 if and only if

$$E_{r2}|f_2|^2 \left(|h_2|^2 - |h_1|^2\right) - E_s|h_1|^2 \max(|h_2|^2, \alpha_2) - |h_1|^2\sigma_n^2 < 0. \tag{5.37}$$

A sufficient condition for the inequality (5.37) is $|h_1|^2 > |h_2|^2$, and hence, the first relay must set $\alpha_1 = |h_1|^2$ when $|h_1|^2 > |h_2|^2$ in order to maximize $\tilde{\gamma}(\alpha_1, \alpha_2)$.

[8] Note that the upper bounds $\tilde{P}_b^U$ and $\tilde{P}_b^U(h_1, h_2)$ are not used to evaluate the BER performance of the distributed Alamouti's code, and hence, their tightness is not of our greatest concern. Those two bounds might not be tight bounds, but they enable us to propose Optimum Schemes I and II, which can greatly improve the performance of the distributed Alamouti's code as demonstrated by numerical results.

Then we show how the second relay should decide α_2 after the first relays sets $\alpha_1 = |h_1|^2$. When $|h_1|^2 > |h_2|^2$ and $\alpha_1 = |h_1|^2$, it can be shown that, if $0 < \alpha_2 < |h_2|^2$, $\tilde{\gamma}(|h_1|^2, \alpha_2)$ is independent of α_2; while, if $\alpha_2 \geq |h_2|^2$, $\tilde{\gamma}(|h_1|^2, \alpha_2)$ is decreasing with α_2 if and only if

$$\frac{\tilde{\gamma}_{s,1}\tilde{\gamma}_{1,d}}{\tilde{\gamma}_{s,1} + \tilde{\gamma}_{1,d} + 1} < \tilde{\gamma}_{s,2}, \tag{5.38}$$

where $\tilde{\gamma}_{s,k} = E_s|h_k|^2/\sigma_n^2$ and $\tilde{\gamma}_{k,d} = E_{rk}|f_k|^2/\sigma_n^2$. That is, when the inequality (5.38) is satisfied, the maximum value of $\tilde{\gamma}(|h_1|^2, \alpha_2)$ is $\tilde{\gamma}(|h_1|^2, |h_2|^2)$ and it is achieved by setting $\alpha_2 = |h_2|^2$; while, when the inequality (5.38) is not satisfied, the maximum value of $\tilde{\gamma}(|h_1|^2, \alpha_2)$ is $\tilde{\gamma}(|h_1|^2, \infty)$ and it is achieved by setting $\alpha_2 = \infty$. However, the second relay cannot use (5.38) to decide α_2, because it requires $\tilde{\gamma}_{1,d}$ or equivalently f_1 which is not available at the second relay.

Although (5.38) cannot be directly used to decide the value of α_2, it implies that, if $\tilde{\gamma}_{s,2}$ is very large, $\tilde{\gamma}(|h_1|^2, \alpha_2)$ is decreasing with α_2 with a higher probability, and hence, we should try to make its value close to $\tilde{\gamma}(|h_1|^2, |h_2|^2)$. On the other hand, when $\tilde{\gamma}_{s,2}$ is very small, $\tilde{\gamma}(|h_1|^2, \alpha_2)$ is increasing with α_2 with a higher probability, and hence, we should try to make its value close to $\tilde{\gamma}(|h_1|^2, \infty)$. Therefore, we let $\tilde{\gamma}(|h_1|^2, \alpha_2)$ equal to a combination of $\tilde{\gamma}(|h_1|^2, |h_2|^2)$ and $\tilde{\gamma}(|h_1|^2, \infty)$ as follows:

$$\tilde{\gamma}(|h_1|^2, \alpha_2) = \left(1 - e^{-\tilde{\gamma}_{s,2}}\right) \tilde{\gamma}(|h_1|^2, |h_2|^2) + e^{-\tilde{\gamma}_{s,2}} \tilde{\gamma}(|h_1|^2, \infty). \tag{5.39}$$

It can be easily seen from (5.39) that the instantaneous SNR $\tilde{\gamma}(|h_1|^2, \alpha_2)$ will be very close to $\tilde{\gamma}(|h_1|^2, |h_2|^2)$ when $\tilde{\gamma}_{s,2}$ is very large. On the other hand, when $\tilde{\gamma}_{s,2}$ is very small, $\tilde{\gamma}(|h_1|^2, \alpha_2)$ will converge to $\tilde{\gamma}(|h_1|^2, \infty)$.[9]

[9] Instead of (5.39), one can let $\tilde{\gamma}(|h_1|^2, \alpha_2)$ equal to a combination of $\tilde{\gamma}(|h_1|^2, |h_2|^2)$ and $\tilde{\gamma}(|h_1|^2, \infty)$ in many other different ways. They may also make $\tilde{\gamma}(|h_1|^2, \alpha_2)$ very close to $\tilde{\gamma}(|h_1|^2, |h_2|^2)$, when $\tilde{\gamma}_{s,2}$ is very large, and make $\tilde{\gamma}(|h_1|^2, \alpha_2)$ converge to $\tilde{\gamma}(|h_1|^2, \infty)$, when $\tilde{\gamma}_{s,2}$ is very small. In this chapter, however, we use (5.39), because it enables us to analytically derive α_2 and its expectation in closed-form. Moreover, using (5.39) also achieves very good performance as demonstrated by numerical results.

The value of α_2 can be solved from (5.39) and it is equal to α_2^* that is given by

$$\alpha_2^* = |h_2|^2 + \frac{\sigma_n^2}{E_s(e^{\tilde{\gamma}_{s,2}}-1)}\left(1+\tilde{\gamma}_{s,2}+\frac{\tilde{\gamma}_{2,d}(1+\tilde{\gamma}_{s,1})}{\tilde{\gamma}_{s,1}+\tilde{\gamma}_{1,d}+1}\right). \tag{5.40}$$

Note that α_2^* still depends on f_k through $\tilde{\gamma}_{k,d}$. This dependence can be removed by simply taking the expectation of α_2^* over f_k and it gives us

$$\begin{aligned}\bar{\alpha}_2^* = \mathbb{E}_{f_1,f_2}[\alpha_2^*] &= |h_2|^2 + \frac{\sigma_n^2}{E_s(e^{\tilde{\gamma}_{s,2}}-1)}\left[1+\tilde{\gamma}_{s,2}\right. \\ &\quad \left. +(1+\tilde{\gamma}_{s,1})\frac{E_{r2}\Omega_{f_2}}{E_{r1}\Omega_{f_1}}e^{\frac{\sigma_n^2(1+\tilde{\gamma}_{s,1})}{E_{r1}\Omega_{f_1}}}\,\mathrm{Ei}\left(\frac{\sigma_n^2(1+\tilde{\gamma}_{s,1})}{E_{r1}\Omega_{f_1}}\right)\right].\end{aligned} \tag{5.41}$$

Therefore, our suboptimum scheme to choose α_k is as follows:

$$\textit{Suboptimum Scheme:}\quad (\alpha_1,\alpha_2) = \begin{cases} (|h_1|^2, \bar{\alpha}_2^*), & |h_1|^2 > |h_2|^2 \\ (\bar{\alpha}_1^*, |h_2|^2), & |h_2|^2 > |h_1|^2 \end{cases}, \tag{5.42}$$

where $\bar{\alpha}_1^*$ can be obtained similarly as in (5.40) and (5.41). The scheme given in (5.42) is called Suboptimum Scheme in this chapter. This scheme makes full use of the CSI available at the relays and it does not need any feedback overhead from the destination to the relays. Compared to Optimum Scheme II, the Suboptimum Scheme has similar performance; but it needs much less computational loads at the relays, because it does not require any numerical minimization.

Remarks: If f_k are known at the relays, the inequality (5.38) can be used by the relays to decide α_k. Based on (5.37) and (5.38), we have a new optimum scheme as follows:

$$\textit{Optimum Scheme III:}\quad (\alpha_1,\alpha_2) = \begin{cases} (|h_1|^2,\infty), & |h_1|^2 > |h_2|^2, \frac{\tilde{\gamma}_{s,1}\tilde{\gamma}_{1,d}}{\tilde{\gamma}_{s,1}+\tilde{\gamma}_{1,d}+1} > \tilde{\gamma}_{s,2} \\ (\infty, |h_2|^2), & |h_2|^2 > |h_1|^2, \frac{\tilde{\gamma}_{s,2}\tilde{\gamma}_{2,d}}{\tilde{\gamma}_{s,2}+\tilde{\gamma}_{2,d}+1} > \tilde{\gamma}_{s,1} \\ (|h_1|^2, |h_2|^2), & \text{otherwise} \end{cases} \tag{5.43}$$

This method is referred to as Optimum Scheme III in this chapter and it is optimum in the sense that it maximizes the instantaneous SNR $\tilde{\gamma}(\alpha_1,\alpha_2)$. Compared to Optimum Schemes

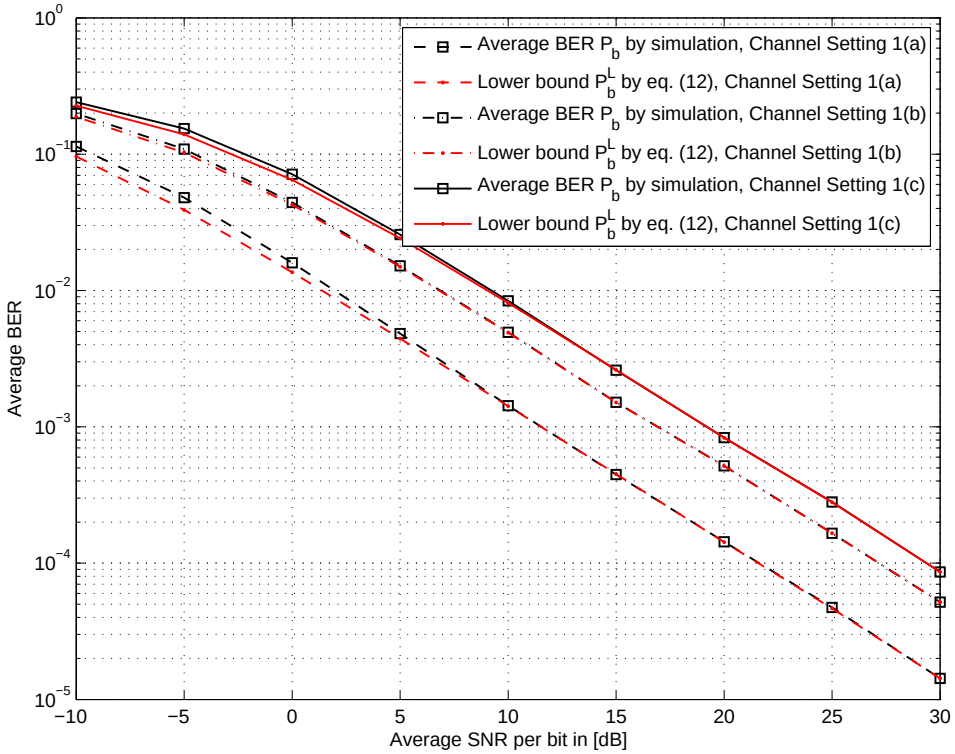

Figure 5.1. Comparison of the lower bound P_b^L of (5.12) and the average BER P_b, 4-QAM. Channel Setting 1(a): $d_{s,1} = 0.5$, $d_{s,2} = 0.5$; Channel Setting 1(b): $d_{s,1} = 0.3$, $d_{s,2} = 0.7$; Channel Setting 1(c): $d_{s,1} = 0.7$, $d_{s,2} = 0.8$.

I and II and Suboptimum Scheme, Optimum Scheme III achieves the best performance and it can be used as the performance benchmark. However, Optimum Scheme III may not be practical, because it requires a large amount of feedback overhead from the destination to the relays.

5.5 Numerical Results

We present some numerical results in this section. We use M-QAM as the modulation scheme. The source and the two relays have the same transmission powers, i.e. $E_s = E_{r1} =$

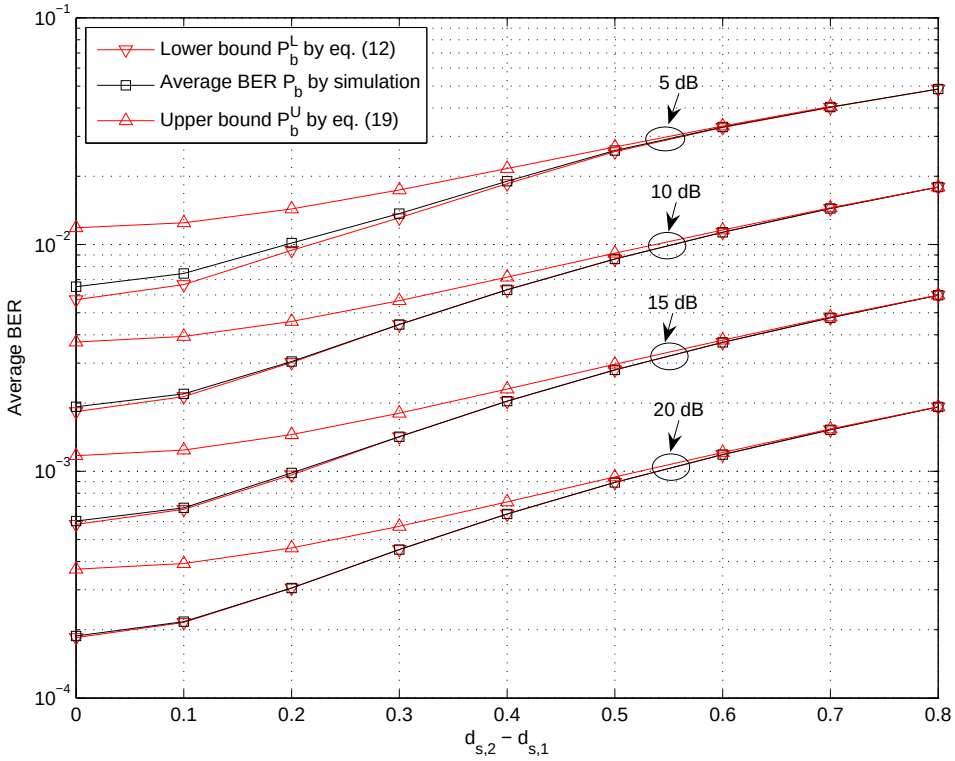

Figure 5.2. Comparison of the lower bound P_b^L of (5.12), the upper bound of P_b^U (5.19), and the average BER P_b, 8-QAM and $d_{s,1} = d_{2,d}$.

$E_{r2} = E$. Thus, the average SNR per bit is equal to $E/(\sigma_n^2 \log_2 M)$. We assume that the source, the relays, and the destination are located in a straight line. Furthermore, we let the reference distance equal to the distance from the source to the destination, and hence, $d_{s,k} = 1 - d_{k,d}$. We set the path loss exponents as $\beta_{s,k} = \beta_{k,d} = 4$ in order to model the wireless channels in an urban area. As a result, the channel variances Ω_{h_k} and Ω_{f_k} are purely decided by the locations of the relays, i.e. $\Omega_{h_k} = d_{s,k}^{-4}$ and $\Omega_{f_k} = d_{k,d}^{-4}$.

In Fig. 5.1, we compare the lower bound P_b^L in (5.12) with the average BER P_b. In order to test the tightness of P_b^L, we consider three channel settings by placing the relays at three different locations. It can be seen that P_b^L is very tight to P_b in all channel settings. In Fig. 5.2, we set $d_{s,1} = d_{2,d}$ and consider a wide range of channel settings by changing the

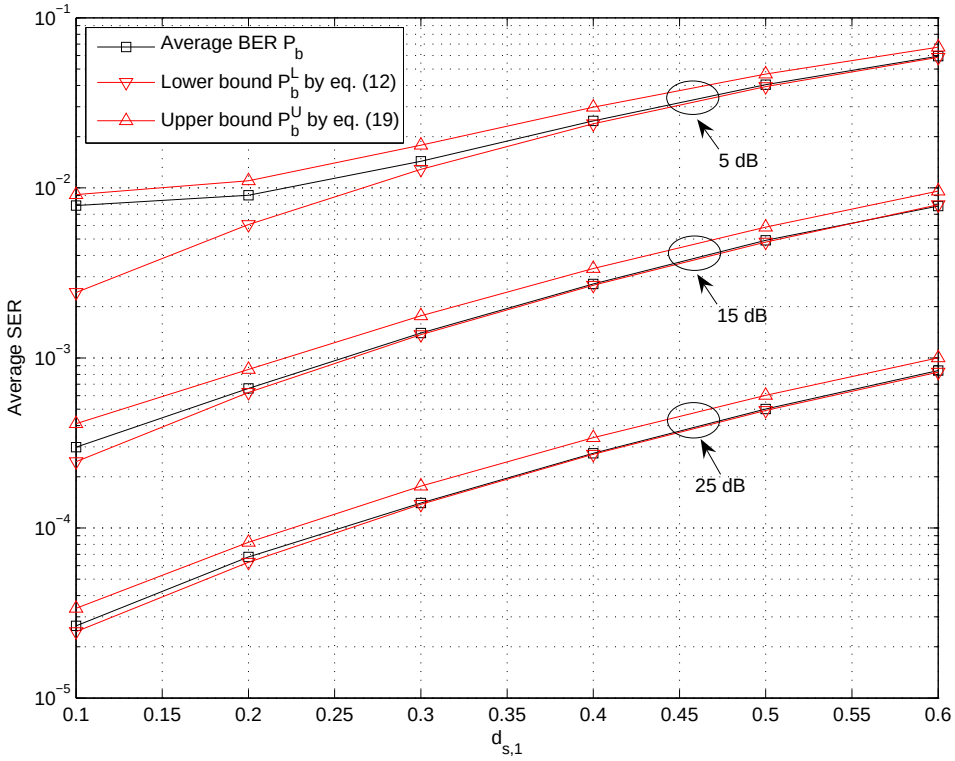

Figure 5.3. Comparison of the lower bound P_b^L of (5.12), the upper bound of P_b^U (5.19), and the average BER P_b, 16-QAM and $d_{s,2} - d_{s,1} = 0.3$.

distance $d_{s,2} - d_{s,1}$ between the two relays. One can see that P_b^L is very tight in all channel settings, but P_b^U is not very tight when the two relays are at the center of the source and the destination.

In Fig. 5.3, we fix the distance between the two relays by setting $d_{s,2} - d_{s,1} = 0.3$ and change the value of $d_{s,1}$. At high SNR range, P_b^L is still very tight. At low SNR range, P_b^L is not close to P_b when $d_{s,1}$ is small. However, P_b^U is tight to P_b for this case. Note that, when $d_{s,1}$ is small and $d_{s,2} - d_{s,1} = 0.3$, it actually implies that the value of Ω_{h_k} is much larger than that of Ω_{f_k}. Therefore, as we have discussed in Subsection 5.3.2, P_b^U is a tight bound when the value of Ω_{h_k} is much larger than that of Ω_{f_k}.

From Fig. 5.3, one may argue that, when $d_{s,1} = 0.2$, P_b^U is not very close to P_b neither.

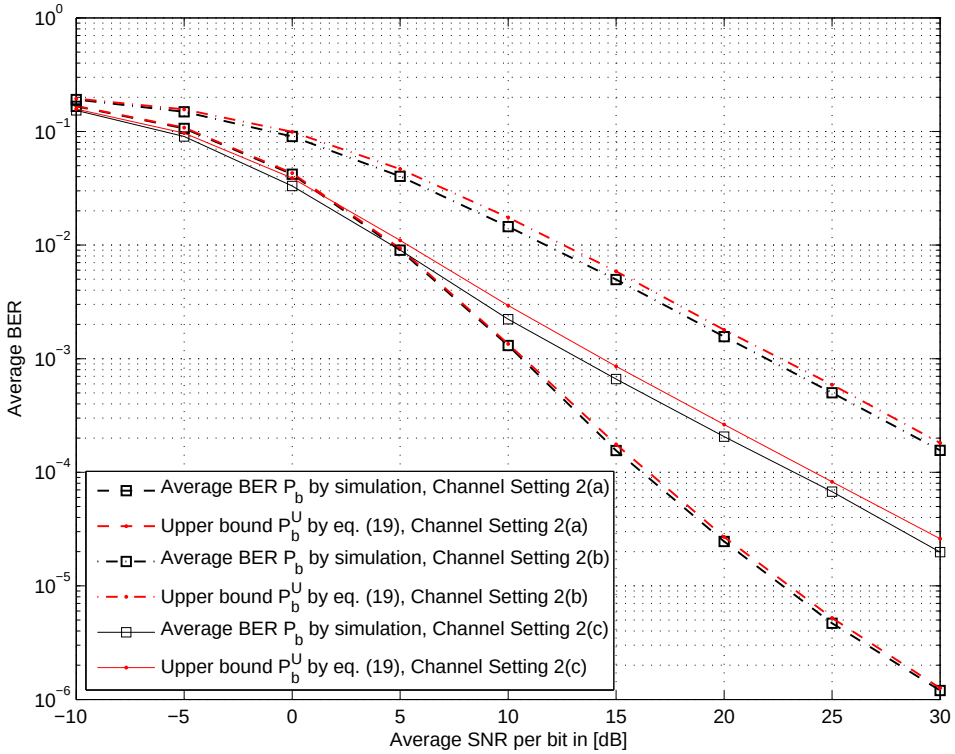

Figure 5.4. Comparison of the upper bound P_b^U of (5.19) and the average BER P_b, 16-QAM. Channel Setting 2(a): $d_{s,1} = 0.2$, $d_{s,2} = 0.2$; Channel Setting 2(b): $d_{s,1} = 0.8$, $d_{s,2} = 0.5$; Channel Setting 2(c): $d_{s,1} = 0.2$, $d_{s,2} = 0.5$.

We consider this special case as Channel Setting 2(c) in Fig. 5.4. We can see that P_b^U is at most 1 dB away from P_b, and hence, it still bounds the error performance of the distributed Alamouti's code well. Furthermore, in Channel Setting 2(a), we place the relays very close to the source, and hence, the value of Ω_{h_k} is much larger than that of Ω_{f_k}. For this special case, P_b^L may not be tight to P_b as we have discussed in Subsection 5.3.1 and seen in Fig. 5.3; but Fig. 5.4 demonstrates that P_b^U is very tight to P_b. In all, our simulation results in Figs. 5.1–5.4 demonstrate that, irrespective of the values of Ω_{h_k} and Ω_{f_k}, we can always use either P_b^L or P_b^U in order to tightly bound P_b. Furthermore, the tightness of our bounds, especially the lower bound P_b^L, increases with the value of average SNR. At high SNR

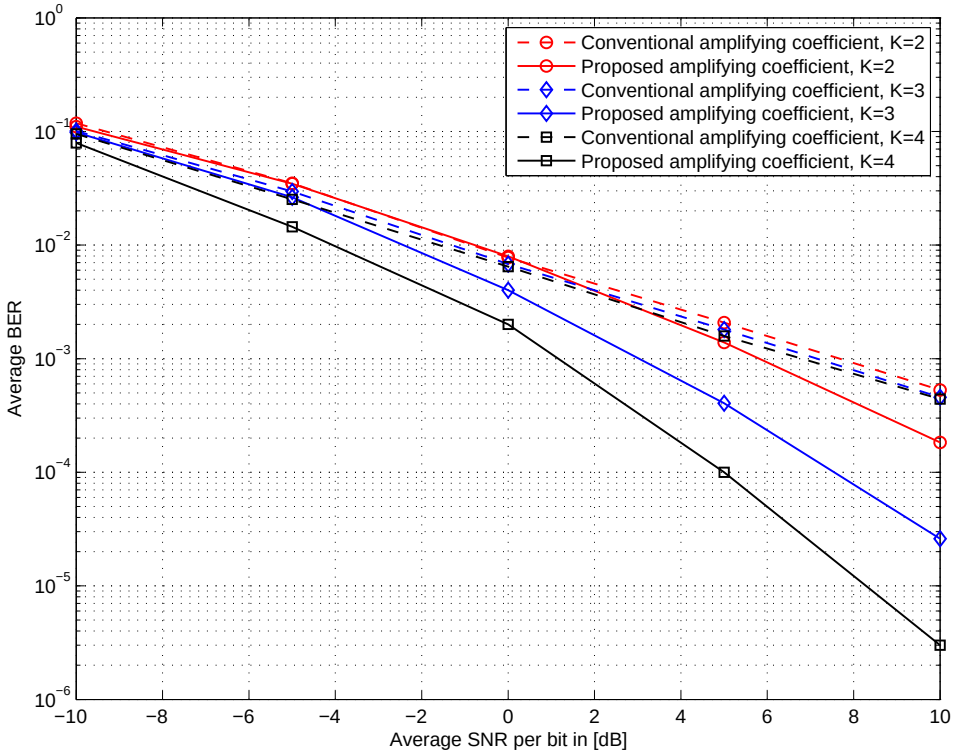

Figure 5.5. Diversity order of the DSTBCs proposed by [27], BPSK, $d_{s,k} = 0.5$, $\alpha_k = \Omega_{h_k}$.

range, P_b^L is extremely close to P_b even when the value of Ω_{h_k} is much larger than that of Ω_{f_k}. Thus, it precisely evaluates the diversity order of the distributed Alamouti's code as we have discussed in Subsection 5.3.3.

In Fig. 5.5, we examine the diversity order of the DSTBCs proposed by [27]. When the relays use the conventional amplifying coefficient ρ_k, it can be easily seen that the codes only achieve diversity order one. When the relays use our proposed amplifying coefficient $\tilde{\rho}_k$, however, the codes achieve the full diversity order in the number of relays.

Lastly, in Figs. 5.6 and 5.7, we compare the performance of the optimum and suboptimum schemes proposed in Subsection 5.4.2. As performance benchmark, we include the average BER of the distributed Alamouti's code when the relays use the conventional amplifying coefficient ρ_k. We also present the average BER of the distributed Alamouti's code

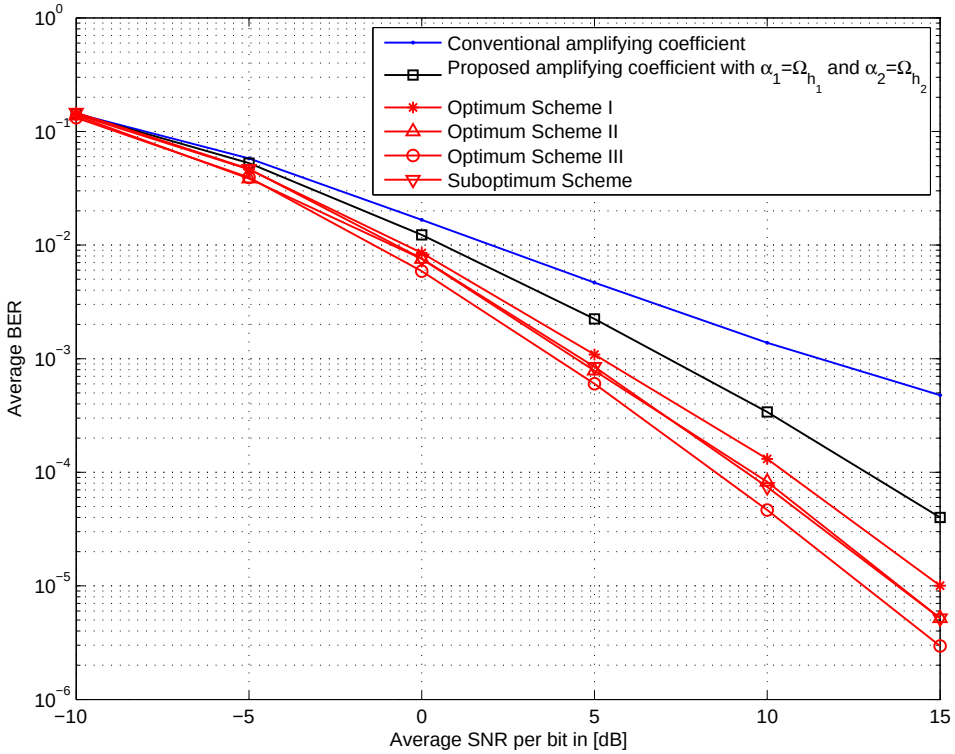

Figure 5.6. Comparison of Optimum Schemes I–III and Suboptimum Scheme, 4-QAM, $d_{s,1} = 0.5$, $d_{s,2} = 0.5$.

when the relays use the proposed amplifying coefficient $\tilde{\rho}_k$ and choose $\alpha_k = \Omega_{h_k}$. In Figs. 5.6 and 5.7, when the relays use ρ_k, the code has the worst performance, because it only achieves diversity order one. When the relays use $\tilde{\rho}_k$, the code achieves the full diversity order two even by simply letting $\alpha_k = \Omega_{h_k}$. Furthermore, Optimum Scheme I achieves much better performance compared to the case that the relays choose $\alpha_k = \Omega_{h_k}$. Optimum Scheme II further improves the performance by exploiting the CSI at the relays. Suboptimum Scheme has a similar performance as Optimum Scheme II and it has much lower computational loads. Among all the proposed schemes, Optimum Scheme III achieves the best performance; but it requires a large feedback overhead.

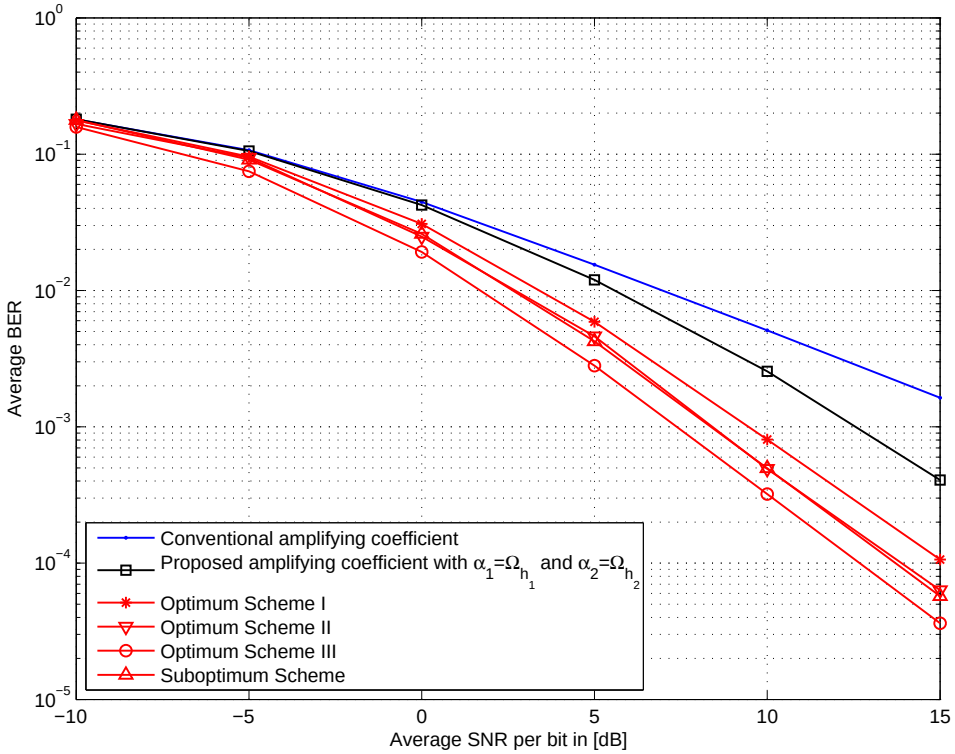

Figure 5.7. Comparison of Optimum Schemes I–III and Suboptimum Scheme, 8-QAM, $d_{s,1} = 1/3$, $d_{s,2} = 2/3$.

5.6 Conclusion

In this chapter, we analyze the average BER and the diversity order of the distributed Alamouti's code in dissimilar cooperative networks with CSI-assisted relays. We first let the relays adopt the amplifying coefficient ρ_k proposed in [33]. We derive lower and upper bounds of the average BER of the distributed Alamouti's code. The proposed bounds only contain integrations over finite range, and hence, can be easily calculated. Moreover, they can tightly bound the average BER irrespective of the values of the channel variances. Then we show that the code only achieves diversity order one when the relays use ρ_k. Moreover, in a general cooperative network with more than two relays, we show that the DSTBCs

proposed in [27] only achieve diversity order one as well when ρ_k is used at the relays. To address this problem, we propose a new threshold-based amplifying coefficient $\tilde{\rho}_k$ for the distributed Alamouti's code based on the work in [23]. This new amplifying coefficient enables the code achieve the full diversity order two. Based on three different criteria, we develop three optimum and one suboptimum schemes in order to choose the value of the threshold used in $\tilde{\rho}_k$. Numerical results demonstrate that the proposed schemes can enhance the performance of the distributed Alamouti's code substantially.

5.7 Appendix 5-A: Proof of Lemma 5.1

We start the proof by rewriting the function $(Y_1+Y_2)/\max(Y_1/X_1, Y_2/X_2)$ as

$$\frac{Y_1+Y_2}{\max\left(\frac{Y_1}{X_1},\frac{Y_2}{X_2}\right)} = \min\left(\left(1+\frac{Y_2}{Y_1}\right)X_1, \left(1+\frac{Y_1}{Y_2}\right)X_2\right). \tag{5.A-1}$$

Let $T = Y_2/Y_1$ and $Z = \min((1+T)X_1, (1+1/T)X_2)$. The probability density function (PDF) $f_T(t)$ of T is given by

$$f_T(t) = \frac{b_1 b_2}{(b_2+b_1 t)^2}. \tag{5.A-2}$$

When T is fixed, the conditional PDF $f_{(1+T)X_1|T}(x,t)$ of $(1+T)X_1$ is given by

$$f_{(1+T)X_1|T}(x,t) = \frac{1}{(1+t)a_1} e^{-\frac{x}{(1+t)a_1}}. \tag{5.A-3}$$

Similarly, the conditional PDF $f_{\left(1+\frac{1}{T}\right)X_2|T}(x,t)$ of $(1+1/T)X_2$ is given by

$$f_{\left(1+\frac{1}{T}\right)X_2|T}(x,t) = \frac{1}{\left(1+\frac{1}{t}\right)a_2} e^{-\frac{x}{\left(1+\frac{1}{t}\right)a_2}}. \tag{5.A-4}$$

Thus, the conditional PDF $f_{Z|T}(z,t)$ of Z is given by

$$f_{Z|T}(z,t) = \frac{a_2+a_1 t}{a_1 a_2 (1+t)} e^{-\frac{a_2+a_1 t}{a_1 a_2 (1+t)} z}. \tag{5.A-5}$$

By taking the expectation over T, we can obtain the unconditional PDF $f_Z(z)$ of Z

$$f_Z(z) = \mathbb{E}[f_{Z|T}(z,t)] = \frac{b_1 b_2}{a_1 a_2}\left[\frac{a_1-a_2}{b_1-b_2} f_Z^1(z) + \frac{a_2 b_1 - a_1 b_2}{b_1-b_2} f_Z^2(z)\right]. \tag{5.A-6}$$

By using [19, pp. 337, 3.352.3], we obtain $f_Z^1(z)$ as follows:

$$f_Z^1(z) = \frac{e^{\frac{a_1 b_2 - a_2 b_1}{a_1 a_2 (b_1-b_2)} z}}{b_1-b_2}\left[\mathrm{Ei}\left(\frac{b_2(a_1-a_2)}{a_1 a_2 (b_1-b_2)} z\right) - \mathrm{Ei}\left(\frac{b_1(a_1-a_2)}{a_1 a_2 (b_1-b_2)} z\right)\right]. \tag{5.A-7}$$

By integration by parts and using [19, pp. 337, 3.352.1], the function $f_Z^2(z)$ is given by

$$\begin{aligned} f_Z^2(z) = {} & \frac{e^{-\frac{z}{a_1}}}{b_2(b_1-b_2)} - \frac{e^{-\frac{z}{a_2}}}{b_1(b_1-b_2)} \\ & + \left(\frac{1}{a_2} - \frac{1}{a_1}\right) \frac{z}{(b_2-b_1)^2} e^{\frac{a_1 b_2 - a_2 b_1}{a_1 a_2 (b_1-b_2)} z} \mathrm{Ei}\left(\frac{b_1(a_1-a_2)}{a_1 a_2 (b_1-b_2)} z\right) \\ & + \left(\frac{1}{a_1} - \frac{1}{a_2}\right) \frac{z}{(b_2-b_1)^2} e^{\frac{a_1 b_2 - a_2 b_1}{a_1 a_2 (b_1-b_2)} z} \mathrm{Ei}\left(\frac{b_2(a_1-a_2)}{a_1 a_2 (b_1-b_2)} z\right). \end{aligned} \tag{5.A-8}$$

By definition, the MGF $\mathscr{M}_1(s; a_1, a_2, b_1, b_2)$ is given by

$$\mathscr{M}_1(s; a_1, a_2, b_1, b_2) = \frac{b_1 b_2}{a_1 a_2}\left[\frac{a_1-a_2}{b_1-b_2}\int_0^\infty e^{sz} f_Z^1(z) dz + \frac{a_2 b_1 - a_1 b_2}{b_1-b_2}\int_0^\infty e^{sz} f_Z^2(z) dz\right]. \tag{5.A-9}$$

With the help of [19, pp. 632, 6.227.1] and [19, pp. 633, 6.228], the integration involved in (5.A-9) can be solved and the final expression of $\mathscr{M}_1(s; a_1, a_2, b_1, b_2)$ is given by (5.8).

5.8 Appendix 5-B: Proof of Theorem 5.3

In order to show the diversity order, we assume $E_s = E_{r1} = E_{r2} = E$ and $\sigma_n^2 = 1$. Based on the results in [27], it can be shown that the conditional pairwise error probability (PEP) of two distinct code matrices $\boldsymbol{X}_1$ and $\boldsymbol{X}_2$ is given by

$$\Pr(\boldsymbol{X}_1 \to \boldsymbol{X}_2 | \boldsymbol{w}) = Q\left(\sqrt{\frac{E}{2(\sum_{k=1}^K \rho_k^2 |f_k|^2 + 1)} \boldsymbol{w} \Delta \boldsymbol{X} \Delta \boldsymbol{X}^H \boldsymbol{w}^H}\right) \tag{5.B-1}$$

$$\geq Q\left(\sqrt{\frac{E\lambda}{2\sum_{k=1}^K \rho_k^2 |f_k|^2} \boldsymbol{w}\boldsymbol{w}^H}\right) \tag{5.B-2}$$

$$\approx \quad Q\left(\sqrt{\frac{\lambda E\sum_{k=1}^{K}|f_k|^2}{2\sum_{k=1}^{K}\frac{|f_k|^2}{|h_k|^2}}}\right) \tag{5.B-3}$$

where $\boldsymbol{w} = [\rho_1 f_1|h_1|, \cdots, \rho_K f_K|h_K|]$, $\Delta\boldsymbol{X} = \boldsymbol{X}_1 - \boldsymbol{X}_2$, and λ is the largest eigenvalue of $\Delta\boldsymbol{X}\Delta\boldsymbol{X}^H$. The last approximation is by $\rho_k \approx \sqrt{1/|h_k|^2}$ which has been used in [2, 45].

It is very hard to obtain the average PEP by averaging (5.B-3). However, we notice that $\sum_{k=1}^{K}|f_k|^2$ can be approximated by its mean $\sum_{k=1}^{K}\Omega_{f_k}$ and this approximation does not affect the diversity order of the code as shown in [27]. Thus, the average PEP is lower-bounded by

$$\mathbb{E}\left[\Pr(\boldsymbol{X}_1 \to \boldsymbol{X}_2|\boldsymbol{w})\right] \gtrsim \mathbb{E}\left[Q\left(\sqrt{\frac{\lambda E\sum_{k=1}^{K}\Omega_{f_k}}{2\sum_{k=1}^{K}\frac{|f_k|^2}{|h_k|^2}}}\right)\right]. \tag{5.B-4}$$

It is still very difficult to solve the expectation in (5.B-4). In order to show the diversity order, however, it is sufficient to analyze the PDF of $1/(\sum_{k=1}^{K}|f_k|^2/|h_k|^2)$ [45].

To this end, we let X_k denote $|h_k|^2$ and Y_k denote $|f_k|^2$. Define two new random variables Z_k and W as $Z_k = X_k/Y_k$ and $W = g(Z_1, \cdots, Z_K) = 1/(\sum_{k=1}^{K}(1/Z_k))$, respectively. Furthermore, let $P_W(w)$ and $P_{Z_k}(z_k)$ denote the PDFs of W and Z_k, respectively. Then, we can evaluate the value of $P_W(w)$ at the point of $w = 0$ as follows [42, Section 2.1.2]:

$$p_W(0) = \sum_{k=1}^{K} p_{Z_k}(0)\int \frac{\Pi_{i=1,i\neq k}^{K} p_{Z_i}(z_i)dz_i}{|\bigtriangledown g(z_1, \cdots, z_{k-1}, 0, z_{k+1}, \cdots, z_K)|} \tag{5.B-5}$$

$$= \sum_{k=1}^{K} p_{Z_k}(0) \tag{5.B-6}$$

$$= \sum_{k=1}^{K}\frac{\Omega_{f_k}}{\Omega_{h_k}}, \tag{5.B-7}$$

where $|\bigtriangledown g(z_1, \cdots, z_K)|$ is the modulus of the gradient of $g(z_1, \cdots, z_K)$. The equality in (5.B-6) is due to $|\bigtriangledown g(z_1, \cdots, z_{k-1}, 0, z_{k+1}, \cdots, z_K)| = 1$. Based on (5.B-7) and [45, eq. 10], it is easy to show that

$$\lim_{E\to\infty}\mathbb{E}\left[Q\left(\sqrt{\frac{\lambda E\sum_{k=1}^{K}\Omega_{f_k}}{2\sum_{k=1}^{K}\frac{|f_k|^2}{|h_k|^2}}}\right)\right] = \frac{1}{\lambda E\sum_{k=1}^{K}\Omega_{f_k}}\sum_{k=1}^{K}\frac{\Omega_{f_k}}{\Omega_{h_k}}. \tag{5.B-8}$$

By using (5.B-4) and (5.B-8), we notice that the average PEP $\mathbb{E}\left[\Pr(\boldsymbol{X}_1 \to \boldsymbol{X}_2|\boldsymbol{w})\right]$ decays with E in an order of one. That is, the DSTBC only achieves a diversity order one.

5.9 Appendix 5-C: Proof of Lemma 5.4

Let $T = Y_1/(Y_1+Y_2+1)$ and the cumulative density function (CDF) $F_T(t)$ of T is given by

$$F_T(t) = \begin{cases} 1 - \frac{e^{-\frac{t}{b_1(1-t)}}}{\frac{b_2 t}{b_1(1-t)}+1}, & 0 \le t \le 1 \\ 1, & t \ge 1 \end{cases}. \tag{5.C-1}$$

Furthermore, we find the following integration

$$\int_0^1 \frac{e^{-z\frac{t}{(1-t)}}}{\frac{xt}{(1-t)}+1}\frac{1}{(1-yt)^2}dt \overset{\frac{t}{1-t}=w}{=} \int_0^\infty \frac{e^{-zw}}{(xw+1)((1+y)w+1)^2}dw \tag{5.C-2}$$

$$= H(x,y,z), \tag{5.C-3}$$

where the last step is done by partial fraction and using [19, pp. 337, 3.352.4, 3.353.3]. Let $f_T(t)$ denote the PDF of T, then $\mathscr{M}_3(s;a,b_1,b_2)$ is given by

$$\mathscr{M}_3(s;a,b_1,b_2) = \int_0^1\int_0^\infty e^{sxt}\frac{1}{a}e^{-\frac{x}{a}}f_T(t)dxdt \tag{5.C-4}$$

$$= \int_0^1 \frac{1}{1-ast}dF_T(t) \tag{5.C-5}$$

$$= 1 + asH\left(\frac{b_2}{b_1}, -as, \frac{1}{b_1}\right), \tag{5.C-6}$$

where the last step is done by integration by parts and using (5.C-3).

5.10 Appendix 5-D: Proof of Lemma 5.5

We lower-bound the instantaneous SNR $\tilde{\gamma}(\alpha_1,\alpha_2)$ in the following way

$$\tilde{\gamma}(\alpha_1,\alpha_2) > \frac{E_s\left(\frac{E_{r1}|f_1h_1|^2}{E_s\max(|h_1|^2,\alpha_1)} + \frac{E_{r2}|f_2h_2|^2}{E_s\max(|h_2|^2,\alpha_2)}\right)}{\sigma_n^2\left(\frac{E_{r1}|f_1|^2}{E_s\alpha_1} + \frac{E_{r2}|f_2|^2}{E_s\alpha_2} + 1\right)} =: \tilde{\gamma}^L. \tag{5.D-1}$$

As a result, the average BER $\tilde{P}_b$ is upper-bounded by $\mathbb{E}\left[P_b(\tilde{\gamma}^L)\right]$. It is hard to obtain the exact value of $\mathbb{E}\left[P_b(\tilde{\gamma}^L)\right]$; but, in order to show the diversity order, it is sufficient to derive an upper bound of this expectation. To this end, we first develop the following inequality

$$\begin{aligned}\mathbb{E}\left[Q\left(g\sqrt{\tilde{\gamma}^L}\right)\right] \;<\; & \mathbb{E}\left[Q\left(g\sqrt{\tilde{\gamma}^{L\text{-}1}}\right)\right]+\mathbb{E}\left[Q\left(g\sqrt{\tilde{\gamma}^{L\text{-}2}}\right)\right] \\ & +\mathbb{E}\left[Q\left(g\sqrt{\tilde{\gamma}^{L\text{-}3}}\right)\right]+\mathbb{E}\left[Q\left(g\sqrt{\tilde{\gamma}^{L\text{-}4}}\right)\right], \qquad \text{(5.D-2)}\end{aligned}$$

where g can be any positive constant. The inequality in (5.D-2) is obtained by making all the integration limits from zero to ∞. Moreover, $\tilde{\gamma}^{L\text{-}i}$ is given by

$$\tilde{\gamma}^{L\text{-}1}=\frac{E_s\left(\frac{E_{r1}|f_1h_1|^2}{E_s\alpha_1}+\frac{E_{r2}|f_2h_2|^2}{E_s\alpha_2}\right)}{\sigma_n^2\left(\frac{E_{r1}|f_1|^2}{E_s\alpha_1}+\frac{E_{r2}|f_2|^2}{E_s\alpha_2}+1\right)}, \qquad \tilde{\gamma}^{L\text{-}2}=\frac{E_s\left(\frac{E_{r1}|f_1h_1|^2}{E_s\alpha_1}+\frac{E_{r2}|f_2|^2}{E_s}\right)}{\sigma_n^2\left(\frac{E_{r1}|f_1|^2}{E_s\alpha_1}+\frac{E_{r2}|f_2|^2}{E_s\alpha_2}+1\right)},$$

$$\tilde{\gamma}^{L\text{-}3}=\frac{E_s\left(\frac{E_{r1}|f_1|^2}{E_s}+\frac{E_{r2}|f_2h_2|^2}{E_s\alpha_2}\right)}{\sigma_n^2\left(\frac{E_{r1}|f_1|^2}{E_s\alpha_1}+\frac{E_{r2}|f_2|^2}{E_s\alpha_2}+1\right)}, \qquad \tilde{\gamma}^{L\text{-}4}=\frac{E_s\left(\frac{E_{r1}|f_1|^2}{E_s}+\frac{E_{r2}|f_2|^2}{E_s}\right)}{\sigma_n^2\left(\frac{E_{r1}|f_1|^2}{E_s\alpha_1}+\frac{E_{r2}|f_2|^2}{E_s\alpha_2}+1\right)}.$$

Secondly, we solve the expectations in (5.D-2) by analyzing the MGF of $\tilde{\gamma}^{L-i}$. We rewrite $\tilde{\gamma}^{L\text{-}1}$ as

$$\tilde{\gamma}^{L\text{-}1}=\frac{E_s}{\sigma_n^2}\left(\frac{\frac{E_{r1}|f_1h_1|^2}{E_s\alpha_1}}{\frac{E_{r1}|f_1|^2}{E_s\alpha_1}+\frac{E_{r2}|f_2|^2}{E_s\alpha_2}+1}+\frac{\frac{E_{r2}|f_2h_2|^2}{E_s\alpha_2}}{\frac{E_{r1}|f_1|^2}{E_s\alpha_1}+\frac{E_{r2}|f_2|^2}{E_s\alpha_2}+1}\right)=:\tilde{\gamma}^{L\text{-}1a}+\tilde{\gamma}^{L\text{-}1b}. \quad \text{(5.D-3)}$$

The MGFs of $\tilde{\gamma}^{L\text{-}1a}$ and $\tilde{\gamma}^{L\text{-}1b}$ can be easily obtained by using Lemma 5.4. Although $\tilde{\gamma}^{L\text{-}1a}$ and $\tilde{\gamma}^{L\text{-}1b}$ are dependent with each other, we ignore this dependency in this chapter. Thus, the MGF $\mathscr{M}_{\tilde{\gamma}^{L\text{-}1}}(s)$ of $\tilde{\gamma}^{L\text{-}1}$ is approximated by the product of the MGFs of $\tilde{\gamma}^{L\text{-}1a}$ and $\tilde{\gamma}^{L\text{-}1b}$ as in (5.28).[10]

Then we rewrite $\tilde{\gamma}^{L\text{-}2}$ in the following way

$$\tilde{\gamma}^{L\text{-}2}=\frac{E_s}{\sigma_n^2}\left(\frac{\frac{E_{r1}|f_1h_1|^2}{E_s\alpha_1}}{\frac{E_{r1}|f_1|^2}{E_s\alpha_1}+\frac{E_{r2}|f_2|^2}{E_s\alpha_2}+1}+\frac{\frac{E_{r2}|f_2|^2}{E_s}}{\frac{E_{r1}|f_1|^2}{E_s\alpha_1}+\frac{E_{r2}|f_2|^2}{E_s\alpha_2}+1}\right)=:\tilde{\gamma}^{L\text{-}2a}+\tilde{\gamma}^{L\text{-}2b}. \quad \text{(5.D-4)}$$

[10] In Chapter 4, we have shown that (5.28) is a very tight approximation of $\mathscr{M}_{\tilde{\gamma}^{L\text{-}1}}(s)$. Furthermore, this approximation does not affect the diversity order of the code as shown in Chapter 4.

The MGF of $\tilde{\gamma}^{L\text{-}2a}$ can be easily obtained by using Lemma 5.4. The MGF $\mathscr{M}_{\tilde{\gamma}^{L\text{-}2b}}(s)$ of $\tilde{\gamma}^{L\text{-}2b}$ can be upper-bounded by

$$\mathscr{M}_{\tilde{\gamma}^{L\text{-}2b}}(s) = \int_0^1 e^{sx} f(x)dx < \int_0^1 \frac{1}{1-sx} dF(x) = \mathscr{M}_3\left(s\frac{E_s\alpha_2}{\sigma_n^2}; 1, b_2, b_1\right), \qquad \text{(5.D-5)}$$

where $f(x)$ and $F(x)$ are the PDF and CDF of $\tilde{\gamma}^{L\text{-}2b}$, respectively. In (5.D-5), the inequality is due to $e^{sx} < 1/(1-sx)$ when $s < 0$ and the last step is by using Lemma 5.4. We still ignore the dependency between $\tilde{\gamma}^{L\text{-}2a}$ and $\tilde{\gamma}^{L\text{-}2b}$. Thus, the MGF $\mathscr{M}_{\tilde{\gamma}^{L\text{-}2}}(s)$ of $\tilde{\gamma}^{L\text{-}2}$ is upper-bounded by (5.29). By following a similar way, the MGFs $\mathscr{M}_{\tilde{\gamma}^{L\text{-}3}}(s)$ and $\mathscr{M}_{\tilde{\gamma}^{L\text{-}4}}(s)$ of $\tilde{\gamma}^{L\text{-}3}$ and $\tilde{\gamma}^{L\text{-}3}$ are upper-bounded by (5.30) and (5.31), respectively.

Lastly, based on (5.20), (5.D-2), and (5.28)–(5.31), the expectation $\mathbb{E}\left[Q\left(g\sqrt{\tilde{\gamma}^L}\right)\right]$ can be upper-bounded as follows:

$$\mathbb{E}\left[Q\left(g\sqrt{\tilde{\gamma}^L}\right)\right] \lesssim \frac{1}{12}\tilde{\mathscr{M}}^L\left(-\frac{1}{2}g^2\right) + \frac{1}{4}\tilde{\mathscr{M}}^L\left(-\frac{2}{3}g^2\right), \qquad \text{(5.D-6)}$$

where $\tilde{\mathscr{M}}^L(s)$ is given by $\tilde{\mathscr{M}}^L(s) = \sum_{i=1}^4 \mathscr{M}_{\tilde{\gamma}^{L\text{-}i}}(s)$. Based on (5.2)–(5.4), (5.D-6), and Craig's formula, the expectation $\mathbb{E}\left[P_b(\tilde{\gamma}^L)\right]$ can be upper-bounded by $\mathbb{E}\left[P_b(\tilde{\gamma}^L)\right] \lesssim \Gamma_{\tilde{\mathscr{M}}^L}$, where $\Gamma_{\tilde{\mathscr{M}}^L}$ is obtained from (5.21) by replacing $\mathscr{M}^U(s)$ with $\tilde{\mathscr{M}}^L(s)$. Moreover, since $\tilde{P}_b$ is upper-bounded by $\mathbb{E}\left[P_b(\tilde{\gamma}^L)\right]$, we conclude that the average BER $\tilde{P}_b$ is upper-bounded by $\Gamma_{\tilde{\mathscr{M}}^L}$ as well.

Chapter 6

Conclusion and Future Work

6.1 Conclusion

Diversity techniques are effective means to combat the fading phenomenon in wireless communications. In particular, spatial diversity is achieved by deploying multiple antennas at the wireless terminals and providing the receiver with multiple independent replica of the same information-bearing symbols. The antennas must be spaced sufficiently far apart in order to eliminate the correlations between the signals. When the wireless terminals cannot employ multiple antennas due to size or complexity constraints, cooperative diversity is proposed by exploiting the broadcast nature of wireless channels.

Cooperative diversity is achieved by making several single-antenna terminals cooperate to form a distributed multiple-antenna system. Specifically, the relays help the source transmit the information-bearing symbols to the destination. The coordination of the transmissions from the relays is critical to a cooperative network and it has a large impact on the performance and complexity of the network. A simple cooperative strategy is the repetition-based cooperative strategy, where only one relay is allowed to transmit the signal to the destination at each time slot. At a price of very poor bandwidth efficiency, the

repetition-based strategy makes the decoding at the destination very simple and it achieves the full diversity order. In order to improve the bandwidth efficiency, many schemes, such as DSTBCs, cooperative beamforming, and relay selection scheme, are proposed. Among them, the DSTBCs are very attractive because no feedback overhead is required.

When the relays works in the DF mode, they can perform CRC, and hence, existing STBCs designed for the co-located multiple-antenna system can be used in the cooperative networks without any modifications. Currently, DSTBCs are proposed for asynchronous cooperative networks and cooperative networks without any centralized control terminal. On the other hand, the analysis and construction of DSTBCs in the AF cooperative networks is much harder. Most of the works focus on constructing the optimum DSTBCs by minimizing the average error probability or outage probability.

Among all the DSTBCs proposed for the AF cooperative networks, the codes achieving the single-symbol ML decodability are the focus of this thesis. We first notice that orthogonal STBCs, which are single-symbol ML decodable in co-located multiple-antenna systems, lose the single-symbol ML decodability when they are directly used in the AF cooperative networks. Thus, we propose the DOSTBCs for the AF cooperative networks. Those codes are single-symbol ML decodable and they achieve the full diversity order in any constellations. Then we do further investigations on the row-monomial DOSTBCs, which are some special DOSTBCs generating uncorrelated noises at the destination. An upper bound of the data-rate of the row-monomial DOSTBC is presented and it shows that the row-monomial DOSTBCs can achieve approximately twice higher bandwidth efficiency than the repetition-based cooperative strategy. The row-monomial DOSTBCs achieving the upper bound are constructed systematically as well.

Then, we derive the upper bound of the data-rate of the DOSTBC. This upper bound

shows that the data-rate cannot be substantially improved from the row-monomial DOST-BCs by removing the row-monomial limitation. We also notice that the data-rates of the DOSTBC and row-monomial DOSTBC decrease with the number of relays, which makes them not suitable for cooperative networks with many relays. In order to further improve the data-rate, row-monomial DOSTBCs-CPI are developed and those code exploit the CPI of the first-hop channels. We derive the upper bound of the data-rate of the row-monomial DOSTBC-CPI. This upper bound shows that the data-rate of the row-monomial DOSTBC-CPI is much higher than those of DOSTBC and row-monomial DOSTBC. Furthermore, it also indicates that the data-rate of the row-monomial DOSTBC-CPI is independent of the number of relays, and hence, those codes are suitable for cooperative networks with many relays.

In the second half of this thesis, we conduct error performance analysis of single-symbol ML decodable DSTBCs in dissimilar cooperative networks. In particular, we focus on the distributed Alamouti's code in order to make analysis possible. When the relays are blind relays in the cooperative networks, two closed-form approximate expressions of the exact BER of the distributed Alamouti's code are derived. Irrespective of the values of the channel variances, we can always use one of the two proposed approximate BER expressions and accurately evaluate the BER of the distributed Alamouti's code. Furthermore, those approximate BER expressions demonstrate that the distributed Alamouti's code achieve the full diversity order two in a cooperative network with two blind relays.

Then we study the cooperative networks where the relays are CSI-assisted relays. For this case, we first assume that the relays adopt the amplifying coefficient proposed in [33]. A tight lower and an upper bounds of the average BER of the distributed Alamouti's code are derived. Very surprisingly, the lower bound shows that the distributed Alamouti's code only achieves diversity order one when the relays use the amplifying coefficient proposed

in [33]. Furthermore, in a general cooperative network with more than two relays, the DSTBCs proposed in [27] only achieve diversity order one as well when the amplifying coefficient proposed in [33] is used at the relays. Thus, we propose a new threshold-based amplifying coefficient for the distributed Alamouti's code. This new amplifying coefficient makes the code achieve the full diversity order two. Moreover, based on three different criteria, three optimum and one suboptimum schemes are developed in order to choose the value of the threshold used in the new amplifying coefficient. Those schemes improve the performance of the cooperative networks considerably.

6.2 Future Work

The work in this thesis may be extended in many different ways. For example, in Chapter 3, we proposed the row-monomial DOSTBCs-CPI and those codes always have correlated noises at the destination. One may remove this constraint by dropping the row-monomiality condition and investigate if the data-rate can be improved by doing so. Furthermore, one can also design new codes under that assumption that the relays have full CSI including the phase and the magnitude of h_k. It will not be surprising that such codes have higher data-rates than the codes presented in this thesis, because more CSI are exploited to construct such codes. However, as we have shown Chapter 5, it should be very careful to exploit full CSI at the relays, otherwise full diversity order might be lost at the destination.

Furthermore, it will be very interesting to combe DSTBCs with other transmission techniques. For example, one can combine DSTBCs with optimum power allocation across the relays. One can also combine DSTBCs with relay selection. For example, two relays with the best channel conditions can be chosen to transmit signals by using distributed Alamouti's code at every two time slots. The combination of DSTBCs with other transmission

techniques can certainly improve the performance of the network. However, such combination may also induce more signaling or feedback overhead, which eventually increases the complexity of the cooperative networks. Thus, the trade-off between system complexity and performance should be addressed always.

Lastly, the work in this thesis can be extended to bidirectional cooperative networks. The cooperative networks studied in this thesis is unidirectional cooperative networks where a source transmits information to a destination. In a bidirectional cooperative networks, on the other hand, two sources exchange information with the help of relays. In such networks, the design of new cooperative strategy becomes a new challenge. The codes proposed in this thesis may loss single-symbol ML decodability in bidirectional cooperative networks. If that is the case, one may need to design new single-symbol ML decodable codes for bidirectional cooperative networks. After that, performance analysis of such codes are necessary.

Bibliography

[1] S. Alamouti, “A simple transmit diversity technique for wireless communications,” *IEEE J. Sel. Areas Commun.*, vol. 16, pp. 1451–1458, Aug. 1998.

[2] P. A. Anghel and M. Kaveh, “Exact symbol error probability of a cooperative network in a Rayleigh-fading environment,” *IEEE Trans. Wireless Commun.*, vol. 3, pp. 1416–1421, Sept. 2004.

[3] P. A. Anghel and M. Kaveh, “On the performance of distributed space-time coding systems with one and two non-generative relays,” *IEEE Trans. Wireless Commun.*, vol. 5, pp. 682–692, Mar. 2006.

[4] A. Bletsas, A. Khisti, D. P. Reed, and A. Lippman, “A simple cooperative diversity method based on network path selection,” *IEEE J. Sel. Areas Commun.*, vol. 24, pp. 659–672, Mar. 2006.

[5] Y. Chang and Y. Hua, “Diversity analysis of orthogonal space-time modulation for distributed wireless relays,” in *Proc. IEEE ICASSP2004*, May 2004, pp. 561–564.

[6] D. Chen and J. N. Laneman, “Modulation and demodulation for cooperative diversity in wireless systems,” *IEEE Trans. Wireless Commun.*, vol. 5, pp. 1785–1794, July 2006.

[7] M. Chiani, D. Dardari, and M. K. Simon, "New exponential bounds and approximations for the compuation of error probability in fading channels," *IEEE Trans. Wireless Commun.*, vol. 2, pp. 840–845, July 2003.

[8] K. Cho and D. Yoon, "On the general BER expression of one and two dimensional amplitude modulations," *IEEE Trans. Commun.*, vol. 50, pp. 1074–1080, July 2002.

[9] Y. E. Dallal and S. Shamai, "Time diversity in DPSK noisy phase channels," *IEEE Trans. Commun.*, vol. 40, pp. 1703–1715, Nov. 1992.

[10] M. O. Damen and A. R. Hammons, "On distributed space-time coding," in *Proc. IEEE WCNC'07*, Mar. 2007, pp. 552–557.

[11] M. O. Damen and A. R. Hammons, "Delay-tolerant distributed TAST codes for cooperative diversity," *IEEE Trans. Inform. Theory*, vol. 53, pp. 3755–3773, Oct. 2007.

[12] X. Deng and A. M. Haimovich, "Power allocation for cooperative relaying in wireless networks," *IEEE Commun. Lett.*, vol. 9, pp. 994–996, Nov. 2005.

[13] Y. Ding, J.-K. Zhang, and K. M. Wong, "The amplify-and-forward half-duplex cooperative system: Pairwise error probability and precoder design," *IEEE Trans. on Sig. Proc.*, vol. 55, pp. 605–617, Feb. 2007.

[14] P. Elia and P. V. Kumar, "Approximately universal optimality over several dynamic and non-dynamic cooperative diversity schemes for wireless networks," *IEEE Trans. Inform. Theory*, submitted for publication, Dec. 2005.

[15] M. M. Fareed and M. Uysal, "BER-optimized power allocation for fading relay channels," *IEEE Trans. Wireless Commun.*, vol. 7, pp. 2350–2359, June 2008.

[16] H. El Gamal and D. Aktas, "Distributed space-time filtering for cooperative wireless networks," in *Proc. IEEE GLOBECOM'03,* Dec. 2003, pp. 1826–1830.

[17] L. C. Godara, "Applications of antenna arrays to mobile communications, Part I: Performance improvement, feasibility, and system considerations," in *Proc. IEEE,* vol. 85, pp. 1031–1060, July 1997.

[18] L. C. Godara, "Applications of antenna arrays to mobile communications, Part II: Beamforming and direction-of-arrival considerations," in *Proc. IEEE,* vol. 85, pp. 1195–1245, Aug. 1997.

[19] I. S. Gradshteyn and I. M. Ryzhik, *Table of integrals, series, and products*, 6th edition, San Diego, CA: Academic Press, 2000.

[20] I. Hammerström, M. Kuhn and A. Wittneben, "Impact of relay gain allocation on the performance of cooperative diversity networks," in *Proc. IEEE VTC'04*, Sept. 2004, pp. 1815–1819.

[21] M. O. Hasna and M. S. Alouini, "End-to-end performance of transmission systems with relays over rayleigh– fading channels," *IEEE Trans. Wireless Commun.*, vol. 2, pp. 1126–1131, Nov. 2003.

[22] M. O. Hasna and M. S. Alouini, "Harmonic mean and end-to-end performance of transmission systems with relays," *IEEE Trans. Commun.*, vol. 52, pp. 130–135, Jan. 2004.

[23] M. O. Hasna and M. S. Alouini, "A performance study of dual-hop transmissions with fixed gain relays," *IEEE Trans. Wireless Commun.*, vol. 3, pp. 1963–1968, Nov. 2004.

[24] P. Herhold, E. Zimmermann, and G. Fettweis, “A simple cooperative extension to wireless relaying,” in *Proc. International Zurich Seminar on Communications*, Feb. 2004, pp. 36–39.

[25] Y. Hua, Y. Mei, and Y. Cheng, “Wireless antennas-making wireless communications perform like wireline communications,” in *Proc. IEEE AP-S Topical Conference on Wireless Communication Technology*, Oct. 2003, pp. 47–73.

[26] R. A. Horn and C. R. Johnson, Matrix Analysis. New York: Cambridge Univ. Press, 1988.

[27] Y. Jing and B. Hassibi, “Distributed space-time coding in wireless relay networks,” *IEEE Trans. Wireless Commun.*, vol. 5, pp. 3524–3536, Dec. 2006.

[28] Y. Jing and H. Jafarkhani, “Using orthogonal and quasi-orthogonal designs in wireless relay networks,” *IEEE Trans. Inform. Theory*, vol. 53, pp. 4106–4118, Nov. 2007.

[29] M.-C. Ju, H.-K. Song, and I.-M. Kim, “BER analysis of distributed Alamouti’s code for cooperative diversity networks,” *IEEE Trans. Commun.*, accepted for publication, Dec. 2008.

[30] G. K. Kaleh, “Frequency-diversity spread-spectrum communication system to counter bandlimited gaussian interference,” *IEEE Trans. Commun.*, vol. 44, pp. 886–893, July 1996.

[31] Md. Z. A. Khan and B. S. Rajan, “Single-symbol maximum likelihood decodable linear STBCs,” *IEEE Trans. Inform. Theory*, vol. 52, pp. 2062–2091, May 2006.

[32] T. Kiran and B. S. Rajan, "Partially-coherent distributed space-time codes with differential encoder and decoder," *IEEE J. Sel. Areas Commun.*, vol. 25, pp. 426–433, Feb. 2007.

[33] J. N. Laneman, D. N. C. Tse, and G. W. Wornell, "Cooperative diversity in wireless networks: Efficient protocols and outage behavior," *IEEE Trans. Inform. Theory*, vol. 50, pp. 3062–3080, Dec. 2004.

[34] J. N. Laneman and G. W. Wornell, "Energy-efficient antenna sharing and relaying for wireless networks," in *Proc. IEEE WCNC 2000*, Sept. 2000, pp. 7–12.

[35] J. N. Laneman and G. W. Wornell, "Distributed space-time-coded protocols for exploiting cooperative diversity in wireless networks," *IEEE Trans. Inform. Theory*, vol. 49, pp. 2415–2425, Oct. 2003.

[36] Y. Li and X.-G. Xia, "A family of distributed space-time trellis codes with asynchronous cooperative diversity," *IEEE Trans. Commun.*, vol. 55, pp. 790–800, April 2007.

[37] K.-C. Liang, X. Wang, and I. Berenguer, "Minimum error rate linear dispersion codes for cooperative relays," *IEEE Trans. Veh. Technol.*, vol. 56, pp. 2143–2157, July 2007.

[38] X.-B. Liang and X.-G. Xia, "On the nonexistence of rate-one generalized complex orthogonal designs," *IEEE Trans. Inform. Theory*, vol. 49, pp. 2984–2989, Nov. 2003.

[39] H. Mheidat and M. Uysal, "Non-coherent and mismatched-coherent receivers for distributed STBCs with amplify-and-forward relaying," *IEEE Trans. Wireless Commun.* vol. 6, pp. 4060–4070, Nov. 2007.

[40] A. Murugan, K. Azarian and H. El Gamal, “Cooperative lattice coding and decoding,” *IEEE J. Sel. Areas Commun.*, vol. 25, pp. 268–279, Feb. 2007.

[41] R. U. Nabar, H. Bölcskei, and F. W. Kneubühler, “Fading relay channels: Performance limits and space-time signal designs,” *IEEE J. Sel. Areas Commun.*, vol. 22, pp. 1099–1109, Aug. 2004.

[42] J. G. Proakis, *Digital Communications*, 4th edition, New York: McGraw-Hill, 2001.

[43] G. S. Rajan and B. S. Rajan, “Distributed space-time codes for cooperative networks with partial CSI,” in *Proc. IEEE WCNC’07*, Mar. 2007, pp. 902–906.

[44] T. S. Rappaport, *Wireless Communications: Principles and Practice*, Upper Saddle River, NJ: Prentice Hall, 2002.

[45] A. Ribeiro, X. Cai, and G. B. Giannakis, “Symbol error probabilities for general cooperative links,” *IEEE Trans. Wireless Commun.*, vol. 4, pp. 1264–1273, May 2005.

[46] S. Savazzi and U. Spagnolini, “Distributed orthogonal space time coding: Design and outage analysis for randomized cooperation,“ *IEEE Trans. on Sig. Proc.*, vol. 6, pp. 4546–4557, Dec. 2007.

[47] K. G. Seddik, A. K. Sadek, A. S. Ibrahim, and K. J. R. Liu, “Design criteria and performance analysis for distributed space-time coding,” *IEEE Trans. Veh. Technol.*, vol. 57, pp. 2280–2292, July 2008.

[48] K. G. Seddik, A. K. Sadek, W. Su, and K. J. R. Liu, “Outage analysis and optimal power allocation for multi-node amplify-and-forward relay networks,” *IEEE Signal Process. Lett.*, vol. 14, pp. 377–380, Jun. 2007.

[49] A. Sendonaris, E. Erkip, and B. Aazhang, "User cooperation diversity–Part I: System description," *IEEE Trans. Commun.*, vol. 51, pp. 1927–1938, Nov. 2003.

[50] A. Sendonaris, E. Erkip, and B. Aazhang, "User cooperation diversity–Part II: Implementation aspects and performance analysis," *IEEE Trans. Commun.*, vol. 51, pp. 1939–1948, Nov. 2003.

[51] Y. Shang and X.-G. Xia, "Shift-full-rank matrices and applications in space-time trellis codes for relay networks with asynchronous cooperative diversity," *IEEE Trans. Inform. Theory*, vol. 52, pp. 3153–3167 , July 2006.

[52] M. K. Simon and M. S. Alouini, *Digital Communication Over Fading Channels: A Unified Approach to Performance Analysis*. New York: Wiley-Interscience, 2000.

[53] B. Sirkeci-Mergen and A. Scaglione, "Randomized space-time coding for distributed cooperative communication," *IEEE Trans. on Sig. Proc.*, vol. 55, pp. 5003–5017, Oct. 2007.

[54] D. Sreedhar, A. Chockalingam, and B. S. Rajan, "Single-symbol ML decodable distributed STBCs for partially-coherent cooperative networks," *IEEE ICC'08*, May 2008, pp. 1029–1033 .

[55] W. Su and X.-G. Xia, "On space-time block codes from complex orthogonal designs," *Wireless Personal Commun.*, vol. 25, pp. 1–26, Apr. 2003.

[56] V. Tarokh, H. Jafarkhani, and A. R. Calderbank, "Space-time block codes from orthogonal designs," *IEEE Trans. Inform. Theory,* vol. 45, pp. 1456–1467, July 1999.

[57] V. Tarokh, N. Seshadri, and A. R. Calderbank, "Space-time codes for high data rate wireless communication: performance criterion and code construction," *IEEE Trans. Inform. Theory,* vol. 44, pp. 744–765, Mar. 1998.

[58] R. Vaughan and W. Venables, "Permanent expressions for order statistic densities," *J. Royal Statistical Society*, vol. 34, pp. 308–310, 1972.

[59] T. Wang, A. Cano, G. B. Giannakis, and J. N. Laneman, "High-performance cooperative demodulation with decode-and-forward relays," *IEEE Trans. Commun.*, vol. 55, pp. 1427–1438, July 2007.

[60] T. Wang, R. Wang, and G. B. Giannakis, "Smart regenerative relays for link-adaptive cooperative communications," *IEEE Trans. Commun.*, vol. 56, pp. 1950–1960 , Nov. 2008.

[61] H. Wang and X.-G. Xia, "Upper bounds of rates of complex orthogonal space-time block codes," *IEEE Trans. Inform. Theory*, vol. 49. pp. 2788–2796, Oct. 2003.

[62] J. H. Winters, "Smart antennas for wireless systems," *IEEE Personal Commun.*, vol. 5, pp. 23–27, Feb. 1998.

[63] S. Yang and J.-C. Belfiore, "Optimal space-time codes for the MIMO amplify-and-forward cooperative channel," *IEEE Trans. Inform. Theory*, vol. 53, pp. 647–663, Feb. 2007.

[64] Z. Yi and I.-M. Kim, "Joint optimization of relay-precoders and decoders with partial channel side information in cooperative networks," *IEEE J. Sel. Areas Commun.*, vol. 25, pp. 447–458, Feb. 2007.

[65] Z. Yi and I.-M. Kim, "Single-symbol ML decodable distributed STBCs for cooperative networks," *IEEE Trans. Inform. Theory*, vol. 53, pp. 2977–2985, Aug. 2007.

[66] Z. Yi and I.-M. Kim, "Diversity order analysis of the decode-and-forward cooperative networks with relay selection," *IEEE Trans. Wireless Commun.*, vol. 7, pp. 1792–1799, May 2008.

[67] Z. Yi and I.-M. Kim, “Approximate BER expressions of distributed Alamouti’s code in dissimilar cooperative networks with blind relays,” *IEEE Trans. Commun.*, accepted for publication, Apr. 2009.

[68] S. Yiu, R. Schober, and L. Lampe, “Distributed space-time block coding,” *IEEE Trans. Commun.*, vol. 54, pp. 1195–1206, July 2006.

[69] Y. Zhao, R. Adve, and T. J. Lim, “Symbol error rate of selection amplify-and-forward relay systems,” *IEEE Commun. Lett.*, vol. 10, pp. 757–759, Nov. 2006.

[70] Y. Zhao, R. Adve, and L. T. Lim, “Improving amplify-and-forward relay netwroks: Optimal power allocation versus selection,” *IEEE Trans. Wireless Commun.*, vol. 6, pp. 3114–3123, Aug. 2007.

[71] L. Zheng and D. N. Tse, “Diversity and multiplexing: A fundamental tradeoff in multipleantenna channels,” *IEEE Trans. Inform. Theory*, vol. 49, pp. 1073–1096, May 2003.